TECHNO-ECONOMIC ANALYSIS OF A REVERSIBLE SOLID OXIDE CELL AND HYDROGEN GAS STORAGE SYSTEM

Oscar Lindholm

Faculty of Science and Engineering

Åbo Akademi University

2019

Supervisors:

D.Sc. (Tech.) Frank Pettersson

Laboratory of Process and Systems Technology

Åbo Akademi University

Turku, Finland

Lic.Sc. (Tech.) Robert Weiss

VTT Technical Research Center of Finland

Espoo, Finland

ACKNOWLEDGEMENTS

This Master's thesis in process and systems technology is written for VTT Technical Research Centre of Finland. The work behind it has been interesting and inspiring, and I would like to thank everyone who has supported me during my time at VTT. First I would like to thank Robert Weiss and Jari Shemeikka at VTT, who made this thesis work possible and supported me throughout the project. I would also like to thank my supervisor Frank Pettersson at Åbo Akademi who has also helped me along the way and proposed ideas for the thesis.

I would like to thank my friends and family, and last but not least I would like to thank my partner for the encouragement she has given me and for the advice she has offered me regarding the thesis.

Espoo 16.9.2019

Oscar Lindholm

ABSTRACT

As the share of intermitted renewable energy increases, there will be a growing demand of grid balancing energy storage solutions. A new type of energy storage is using hydrogen gas as an energy carrier and reversible solid oxide cell (RSOC) technology to convert electricity to hydrogen and vice-versa.

This study aims to investigate the technical and economic performance of an RSOC and hydrogen gas storage system for grid balancing applications in office buildings. The optimal system configuration and operation is determined and the competitiveness of the system is analyzed. The results are based on a bilevel optimization model, which minimizes the life cycle costs (LCC) of the RSOC and hydrogen storage system.

The results of the study show that the RSOC and hydrogen storage system cannot compete with alternative energy systems when connected to the grid and district heating network. The major drawbacks of the system are its high investment costs and mediocre performance.

Keywords: Reversible solid oxide cell, RSOC, hydrogen, energy, storage, time-series, optimization, mixed integer linear progremming, MILP, bilevel optimization, 2030, 2050

TABLE OF CONTENTS

ABBREVIATIONS

CAPEX	Capital expenditures
COP	Coefficient of performance
HP	Heat pump
LCC	Lifecycle cost
NPV	Net present value
NPV_{LCC}	Net present value of lifecycle cost
OPEX	Operating expenditures
PCM	Phase change material
PV[1)]	Present value
PV[2)]	Photovoltaic
RSOC	Reversible solid oxide cell
SOEC	Solid oxide electrolysis cell
SOFC	Solid oxide fuel cell
TES	Thermal energy storage
TCS	Thermo-chemical storage
WACC	Weighted average cost of capital

Variables and parameters

Variables for the lower level optimization

$P_{EC,in,i}$	Electrolysis mode input power in time step i
$P_{FC,out,i}$	Fuel cell mode output power in time step i
$P_{HP,i}$	HP input power in time step i
$\dot{Q}_{comb,i}$	Heat generated by combustion of hydrogen in time step i
$E_{H2S,0}$	Initial stored energy in the hydrogen storage
$Q_{QS,0}$	Initial stored energy in the TES
$E_{B,0}$	Initial stored energy in the battery storage
$\dot{Q}_{QS,i}$	Heat from heat storage (or to heat storage if negative) in time step i
$P_{B,i}$	Power from battery storage (or to battery storage if negative) in time step i
$\dot{Q}_{DH,i}$	Heat imported from the district heating network in time step i
$\dot{Q}_{exp,i}$	Heat exported to the district heating network in time step i
$P_{grid,i}$	Power imported from the grid in time step i
$P_{exp,i}$	Power exported to the grid in time step i
b_i	Binary decision variable for time step i (if $b_i = 1$ the RSOC runs in electrolysis mode and if $b_i = 0$ it runs in fuel cell mode)

Parameters for the lower level optimization

N	Number of time steps
t	Size of the time step (8 760 h/N)
$\dot{Q}_{d,i}$	Heat demand of the building in time step i
$P_{d,i}$	Electrical power demand of the building in time step i
$P_{PV,i}$	Power generated by photovoltaic cells in time step i
LHV	Lower heating value of hydrogen gas (119 MJ/kg)

$h_{comp,in}$	Specific enthalpy of hydrogen gas entering the compressor (3575.3 kJ/kg at 0°C and 1 bar)
$h_{comp,out}$	Specific enthalpy of hydrogen gas exiting the compressor (3670.5 kJ/kg at 0°C and 200 bar)
COP	Coefficient of performance for the HP
η_{comp}	Hydrogen compressor efficiency
η_{QS}	TES round-trip efficiency
η_B	Battery round-trip efficiency
$P_{FC,out,min}$	Minimum RSOC output power in fuel cell mode
$P_{FC,out,max}$	RSOC output power for maximal electrical efficiency in fuel cell mode
$P_{EC,in,min}$	Minimum RSOC input power in electrolysis mode
$P_{EC,in,max}$	Maximum RSOC input power in electrolysis mode
$E_{H2S,c}$	Hydrogen storage capacity
$Q_{QS,c}$	TES capacity
$E_{B,c}$	Battery storage capacity
$\dot{Q}_{HP,c}$	HP output heating power capacity
$\dot{Q}_{DH,c}$	District heating capacity
$P_{grid,c}$	Grid power capacity

1 INTRODUCTION

Variable energy generation, such as solar and wind energy, has increased remarkably in Finland in recent years (Tilastokeskus 2018). So has the price of pollution permits within the European Union (Energiauutiset 2018). According to electricity market simulations by Helistö et al. 2017, a larger share of variable energy generation and higher CO_2 prices might lead to more hours of high electricity spot prices and more hours of low electricity spot prices.

This phenomenon presents an opportunity for companies to invest in energy storage systems for large commercial real estate, like offices, warehouses and retail store buildings. By installing energy storage units, companies can take advantage of low electricity prices by storing electricity, and avoid high electricity prices by consuming stored electricity.

Existing battery storage technologies, such as lithium-ion (Li-ion), lead-acid and sodium sulfur (NaS) batteries, are expensive for large-scale implementations. Large-scale energy storage technologies such as compressed air energy storage (CAES) and pumped hydro can, however, not be implemented everywhere, since CAES is dependent on available large storage caverns and pumped hydro requires geographical height differences and storage reservoirs for large volumes of water. (IRENA 2017)

Hydrogen gas production via electrolysis and the use of hydrogen gas as an energy carrier has been widely debated. According to the World Energy Council, the main drawback with hydrogen electrolysis as a power-to-x (P2X) approach, is the high cost and limited performance of current electrolysers. As a result of continuous technological development, however, the price of electrolysis technology is falling and the performance is improving. (World Energy Council 2019)

Recently developed reversible solid oxide cell (RSOC) technology could be used to develop a suitable electricity storage system for large commercial real estate. An RSOC device can either operate as an electrolyser, using electricity to produce hydrogen gas, or operate as a fuel cell, using hydrogen gas to generate electricity. An RSOC connected to a hydrogen gas storage can be used as an energy storage system which can store electricity in the form of hydrogen gas.

The big question is, however, if the RSOC and hydrogen storage system is lucrative or not. In this thesis work, the economic aspects of the RSOC and hydrogen storage system are analyzed. The configuration and operation of the system are optimized in order to generate the best possible preconditions for the system.

2 THEORY

2.1 Reversible solid oxide cell

A reversible solid oxide cell (RSOC) is an electrochemical device, which can operate either as a solid oxide electrolysis cell (SOEC) or as a solid oxide fuel cell (SOFC). When the RSOC runs in electrolysis mode, it consumes electricity and produces a fuel like hydrogen gas or methane. In fuel cell mode the process is run in reverse, so that a fuel is used to produce electricity. Different fuels can be utilized or produced by the RSOC, but since this work focuses on hydrogen storage by means of RSOC technology, the focus is laid on hydrogen gas as fuel.

The RSOC operates at high temperatures, typically 600-1000°C, depending on operating mode and load. Each cell in the RSOC device consists of an oxygen electrode and a fuel electrode, which are separated by a solid electrolyte (Wendel et al. 2015). The state-of-the-art material for the oxygen electrode is lanthanum strontium-doped manganite (LSM) or lanthanum strontium cobalt ferrite (LSCF) (Wendel et al. 2015, Gómez & Hotza 2016, Laguna-Bercero et al. 2011). Nickel-impregnated yttria-stabilized zirconia (Ni-YSZ) is usually used for the fuel electrode (Wendel et al. 2015, Gómez & Hotza 2016).

The solid electrolyte used in the RSOC is thin, dense and strong with a high ionic conductivity and a low electric conductivity. The ionic conductivity increases with temperature; therefore, high operating temperatures are desirable (Gómez & Hotza 2016). The most used electrolyte material in the SOFC is yttria-stabilized zirconia (YSZ) (Wendel et al. 2015, Gómez & Hotza 2016).

One layer of each component (oxygen electrode, electrolyte and fuel electrolyte) forms an individual cell. A stack is comprised of several cells connected in series (Wendel et al. 2015) and an RSOC device, in turn, can contain one or several stacks.

2.1.1 Electrochemical reactions

Both electrolysis and fuel cell mode involve reduction-oxidation reactions. The difference between the electrolysis and fuel cell mode is that the electrochemical reactions involved in the electrolysis process are highly endothermic and require an electrical current, while the electrochemical reactions in fuel cell mode are highly exothermic and generate an electrical current and thermal energy. (Wendel et al. 2015, Reznicek & Braun 2018)

2.1.1.1 Solid oxide electrolysis cell (SOEC) mode

In SOEC mode, the RSOC can produce hydrogen through different electrochemical reactions involving different gases. If steam is fed to the RSOC, hydrogen can be produced through water electrolysis.

Water electrolysis is an electrochemical process where electricity is used to split water into oxygen and hydrogen (Buttler & Spliethoff 2018). The process involves a reduction reaction and an oxidation reaction. The reduction reaction takes place at the fuel electrode, which operates as cathode, and the oxidation reaction takes place at the oxygen electrode, which operates as anode. In the reduction reaction, electrons are donated to water that enters the cathode through the fuel channel. The water molecules then split into hydrogen gas molecules and oxygen ions (Götz et al. 2016, Wendel et al. 2015):

$$H_2O + 2e^- \rightarrow H_2 + O^{2-} \quad \text{(R1)}$$

The hydrogen gas, H_2, exits the cell through the fuel channel and is further transported to the hydrogen storage, while the oxygen ions, O^{2-}, work as charge carriers between the cathode and the anode. Oxygen ions are thus transported through the electrolyte to the anode where the oxidation reaction takes place. In the oxidation reaction, negatively charged oxygen ions donate electrons to the positively charged anode and form oxygen gas (Götz et al. 2016, Wendel et al. 2015):

$$O^{2-} \rightarrow \frac{1}{2}O_2 + 2e^- \quad \text{(R2)}$$

The oxygen gas exits the cell through the oxygen channel on the oxygen electrode side (Wendel et al. 2015). The whole electrolysis process is depicted in figure 1.

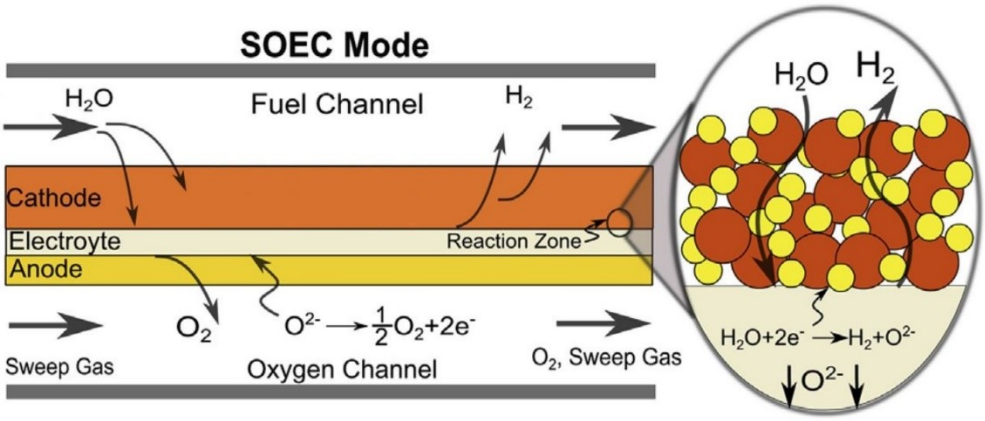

Figure 1: Electrochemical process in SOEC mode. (Wendel et al. 2015)

2.1.1.2 Solid oxide fuel cell (SOFC) mode

When the RSOC runs in SOFC mode, the chemical energy of the fuel is directly converted to electrical energy through a reduction-oxidation reaction. In fuel cell mode the fuel electrode works as anode and the oxygen electrode works as cathode, which is the opposite way compared to the

electrolysis mode. In a hydrogen/oxygen fuel cell, hydrogen enters the anode through the fuel channel, where an oxidation reaction takes place:

$$H_2 \rightarrow 2H^+ + 2e^- \quad \text{(R3)}$$

Oxygen gas is supplied through the oxygen channel to the cathode, where the reduction reaction takes place. The oxygen molecules absorb electrons from the negatively loaded cathode and negative oxygen ions are produced:

$$O_2 + 4e^- \rightarrow 2O^{2-} \quad \text{(R4)}$$

The oxygen ions from the reduction reaction are transported from the cathode through the electrolyte to the anode, where they react with the positively charged hydrogen ions from the oxidation reaction and form water:

$$O^{2-} + 2H^+ \rightarrow H_2O \quad \text{(R5)}$$

The water then exits the cell through the fuel channel on the fuel electrode side (Carette et al. 2002, Wendel et al. 2015). The whole SOFC mode process is depicted in figure 2.

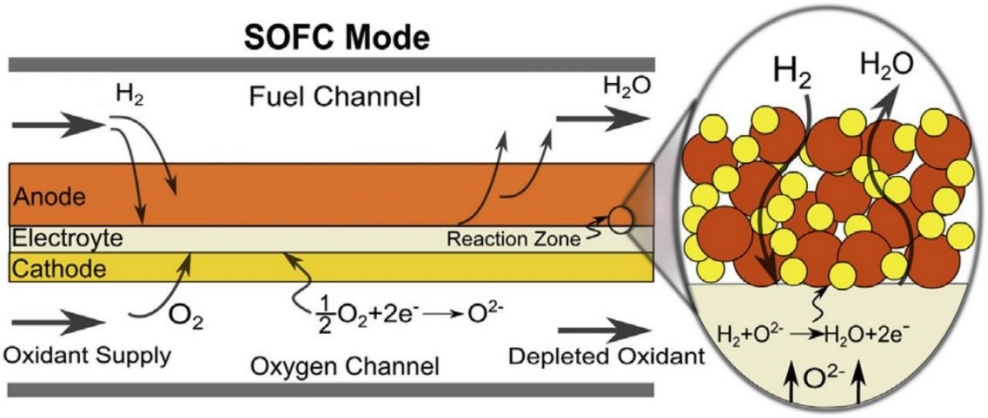

Figure 2: Electrochemical process in SOFC mode. (Wendel et al. 2015)

2.1.2 Operation of the RSOC

The performance of the RSOC depends on the electrical input/output power, since the cell voltage is directly dependent on the current density (Hauck et al. 2017). The operational temperature does also affect the RSOC performance. These dependencies were simulated with an Aspen Plus model by Hauck et al. at Technische Universität München. In the simulation, pure oxygen was provided to the oxygen electrode, while a mixture of hydrogen and steam was provided to the fuel electrode. The simulated dependencies are shown in figure 3.

The dependence between cell voltage and current density is caused by ohmic losses, which increase linearly with current density (Wendel et al. 2015). Ohmic losses mainly consist of resistance for charge carriers that travel through the electrolyte (Hauck et al. 2017).

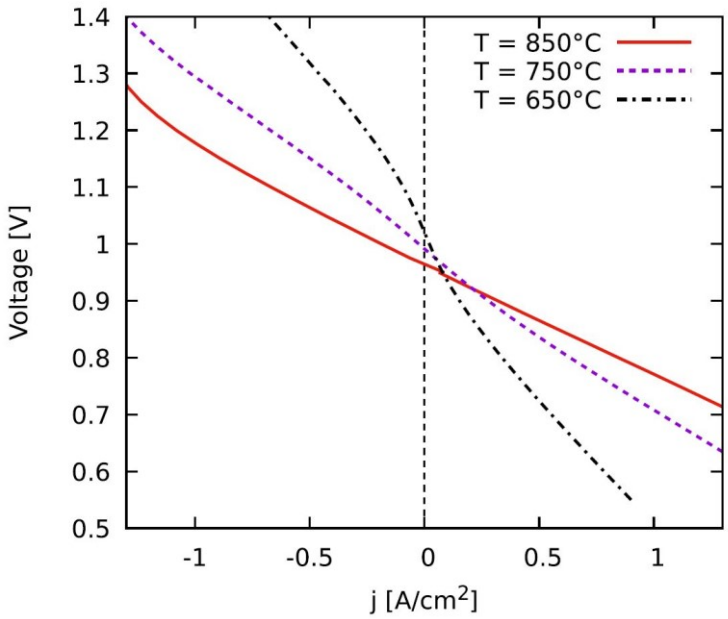

Figure 3: Temperature and current density dependency of the cell voltage. Negative current densities represent SOEC mode and positive represent SOFC mode. (Hauck et al. 2017)

The inlet compositions for the SOEC and SOFC mode are often significantly different in real operating conditions. Pure oxygen is seldom supplied to the RSOC, like in the simulation by Hauck et al. In reality, the RSOC also operates with a constant fuel flow, instead of constant reactant utilization. Hence, the current density dependency of the cell voltage in real operating conditions, depicted in figure 4, looks slightly different than the simulated curves in figure 3. (Reznicek & Braun 2018)

Figure 4 also shows the current density dependency of the thermoneutral voltage and the Nernst voltage. The thermoneutral voltage is the voltage above which the stack produces more energy than it consumes (Reznicek & Braun 2018), and the Nernst voltage is the open circuit voltage of the stack (Hauck et al. 2017).

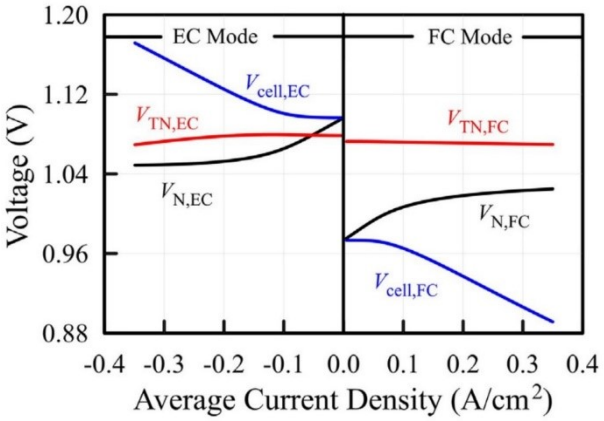

Figure 4: Cell, thermoneutral (TN) and Nernst (N) voltages for different operating loads in both SOEC and SOFC mode. Negative current densities represent SOEC mode and positive represent SOFC mode. The operating temperature of the RSOC is 600 °C. (Reznicek & Braun 2018)

The performance of the RSOC can be measured with the electrical power efficiency for the SOEC and SOFC modes. These efficiencies can be calculated with the following equations (Reznicek & Braun 2018):

$$\eta_{SOFC} = \frac{P_{sys,AC}}{\dot{m}_{fuel}\mathrm{LHV}_{fuel} - \dot{m}_{exh}\mathrm{LHV}_{exh}} \quad (1)$$

$$\eta_{SOEC} = \frac{\dot{m}_{fuel}\mathrm{LHV}_{fuel} - \dot{m}_{exh}\mathrm{LHV}_{exh}}{P_{sys,AC}} \quad (2)$$

where $P_{sys,AC}$ is the electrical output power in SOFC mode and the electrical input power in SOEC mode. $\dot{m}_{fuel}$ and $\dot{m}_{exh}$ are mass flow rates, while LHV_{fuel} and LHV_{exh} are lower heating values for the fuel gas and the exhaust gas.

Figure 5 shows the power load dependency of the efficiencies for the stack and the whole RSOC system. In SOFC mode the stack efficiency is proportional to the cell voltage, while in SOEC mode it is proportional to the inverse of the cell voltage.

The RSOC system efficiency includes the efficiencies for process equipment, e.g. heaters, motors and compressors. At low power loads the compressors and motors are very inefficient, which results in a low total efficiency for the system (Reznicek & Braun 2018). This phenomenon can be observed in figure 5 for both the SOFC mode and the SOEC mode.

In SOFC mode, the system will reach a maximum efficiency somewhere in the middle of the operation interval. When the operational load exceeds the point of maximum efficiency, the electrical power efficiency will decrease as a result of higher ohmic overpotential (Wendel et al. 2015).

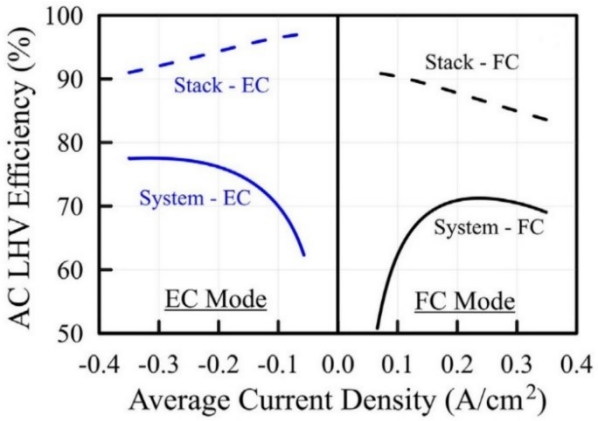

Figure 5: Stack and system efficiency for different operation loads in both SOEC and SOFC mode. The operating temperature of the RSOC is 600°C. (Reznicek & Braun 2018)

Since the electrochemical process in SOEC mode is highly endothermic, the performance of the system is dependent on waste heat and external heat generation. When the system power load is higher than the thermoneutral point of the system, the heat demand can be satisfied by waste heat alone (Reznicek & Braun 2018). Thus, the efficiency increases although the ohmic losses increase.

2.2 Hydrogen storage methods

Storage of hydrogen is challenging because of its low density in gaseous form; the density of hydrogen is namely 0.09 kg/m^3 at 1 bar and 20°C. To put this into perspective, the densities of methane and gasoline in gaseous form at 1 bar and 20°C are 0.65 and 4.4 kg/m^3, respectively. (Makridis 2016)

There are two categories of hydrogen storage: physical-based and material-based storage. Physical-based storage can either be achieved by compressing hydrogen gas and storing the pressurized gas at ambient temperature, or by cooling hydrogen gas below its boiling point and storing liquid hydrogen at low temperatures and ambient pressure. Material-based storage involves letting hydrogen interact with other materials, such as carbon or metals, in order to reduce the repelling forces between hydrogen gas molecules. (Office of Energy Efficiency and Renewable Energy 2015, Züttel 2004)

2.2.1 Compressed hydrogen gas storage

The most common way to store hydrogen is to compress hydrogen gas and store it at ambient temperature. Although the energy density for compressed hydrogen gas storage is lower than energy

densities for other storage methods, it is still one of the most cost effective methods to store hydrogen (Mazloomi & Gomes 2012, Office of Energy Efficiency and Renewable Energy 2015).

Compressed hydrogen gas can either be stored in underground caverns or in pressure vessels above ground (Zakeri & Syri 2015). Underground compressed hydrogen storage in salt caverns is already used for large-scale energy storage in Teesside, UK, and in Texas, USA. The volume of the 83.3 GWh salt cavern hydrogen storage in Texas is 580 000 m^3 and pressure varies from 70 to 135 bar (Ozarslan 2012). Hydrogen storage in underground caverns is significantly cheaper than above ground storage (Schoenung 2011). Underground storage is, however, highly dependent on available salt caverns or depleted oil/gas reservoirs (Ozarslan 2012, Schoenung 2011).

The absence of salt caverns and depleted oil/gas reservoirs makes above ground pressure vessels the go-to solution for pressurized hydrogen storage in Finland (Donadei & Schneider 2016, O'Callaghan-Gordo et al. 2016). The storage pressure for compressed hydrogen gas storages ranges up to 700 bar (Nistor et al. 2016, Office of energy efficiency and renewable energy 2015). For a 700 bar hydrogen gas storage, the energy density is 800 kWh/m^3 and the mass density is 24 kg/m^3 (Office of Energy Efficiency and Renewable Energy 2015).

There are a few drawbacks with compressed hydrogen gas storage. The foremost problem is the energy required for the compression of hydrogen gas. The energy losses of the compressor does also affect the overall efficiency of the storage.

Another problem that applies for above ground storage vessels is that materials that are in direct contact with hydrogen tend to become brittle over time. This phenomenon is caused by hydrogen atoms that diffuse into the material and create pressure from within the material when they recombine to form hydrogen molecules. To avoid cracks in a hydrogen pressure vessel, constant maintenance is required, which in turn leads to higher maintenance costs (Mazloomi & Gomes 2012).

Even though there are some drawbacks with compressed hydrogen gas storage, it is still the most used hydrogen gas storage method today (Züttel 2004). The advantage with compression of hydrogen gas is that it can be done at ambient temperature and that the material costs are lower than for hydride storage methods (Züttel 2004, Office of Energy Efficiency and Renewable Energy 2015).

2.2.2 Cryogenic liquid hydrogen storage

Hydrogen gas can also be cooled down below its boiling point (21.2 K at 1 atm) at ambient pressure, and thereby be stored as a liquid in insulated tanks. Liquid hydrogen has a volumetric density of 70.8 kg/m^3, which is almost three times more than hydrogen stored in 700 bar pressure vessels. The challenge with liquid hydrogen is the energy-intense liquefaction process and keeping heat losses from the storage tank at a low level in order to avoid boil-off gas generation. (Züttel 2004)

The boil-off gas rate is dependent on the shape and size of the storage tank (Züttel 2004). A spherical tank, with the minimum surface area to volume ratio, has lower heat losses than a cylindrical tank, and thus also a lower boil-off gas rate. A large volume of liquid hydrogen, which warms up slowly, also has a lower boil-off gas rate than a small volume of liquid hydrogen, which warms up quickly. The amount of thermal insulation also affects the boil-off gas rate (Züttel 2004).

Due to the high energy demand for the liquefaction of hydrogen as well as the boil-off gas issues in the cryogenic tanks, liquid hydrogen storage becomes a costly hydrogen gas storage method. The cryogenic conditions also require specific material properties for the storage unit (Linde AG).

2.2.3 Interaction with other materials

The third way to increase the density of hydrogen in order to make storage more efficient is letting hydrogen gas interact with other materials to reduce repulsive forces between hydrogen molecules. This can either be done through creation of metal hydrides or through physisorption.

Metal hydrides are formed by letting hydrogen react with metals or alloys. The reaction is endothermic, which means that thermal energy is required for the reaction (Züttel 2004). Metal hydrides often have a metallic or graphite-like structure, which means that hydrogen can be stored in a dense format (Züttel 2004). The major benefit with this method is that hydrogen densities up to 150 kg/m^3 can be reached, but for large-scale purposes the method is still too expensive (Office of Energy Efficiency and Renewable Energy 2015).

In physisorption, hydrogen molecules are attracted to a solid surface by Van der Waals interactions or dispersive interactions caused by fluctuating charge distribution in the solid material. Van der Waals interactions are substantially weaker than ionic and covalent bonds, which means that molecules bound by Van der Waals interactions require less energy to be separated. Hence, physisorption of hydrogen only occurs at low temperatures, when the kinetic energy of the molecules is lower. Different kinds of carbon nanostructures have been investigated as adsorbent material for the physisorption method. It has been proven that the adsorption potential for carbon nanotubes is 25% higher than for a flat surface of graphite. Although the operation pressure and the material costs of the physisorption are relatively low, the low storage temperature and low volumetric density of stored hydrogen makes the method less efficient. (Züttel 2004)

2.3 Thermal energy storage

A thermal energy storage (TES) can store energy by heating and cooling a storage medium. There are three types of TES: sensible heat storage, phase change material based TES and thermo-chemical storage (TCS). (IEA-ETSAP 2013)

2.3.1 Sensible heat storage

A sensible heat storage stores thermal energy by increasing or decreasing the temperature of a liquid or solid storage medium. Materials, such as water, sand and brick with high heat capacities and densities are commonly used as storage medium. (IEA-ETSAP 2013, Xu et al. 2014)

Hot water TES is the cheapest of the sensible heat storage methods and is often applied in building heating systems. Compared to other storage media, water has a high heat capacity. Hot water TES systems are also efficient and fast to charge and discharge. The operation temperature range of a hot water TES is dependent on the hot water temperature demand. A wide operating temperature range (10°C to 90°C) is allowed if a heat pump is used to extract thermal energy from the TES. (IEA-ETSAP 2013, Xu et al. 2014)

The advantage with sensible heat storage methods, such as hot water TES, is that they are significantly cheaper than other TES methods (IEA-ETSAP 2013). An additional benefit with a hot water TES in an RSOC and hydrogen gas storage system is that it can serve as a water reserve for the RSOC device. A drawback for sensible heat storage systems is their fluctuating discharge temperature, which makes the system control more challenging (IEA-ETSAP 2013). Another downside with sensible heat storage systems is their low energy density, which is a problem if space is limited (IEA-ETSAP 2013). This problem can, however, be solved by implementing bore hole sensible heat storage solutions (Xu et al. 2014).

2.3.2 Phase change material based thermal energy storage

The idea of a PCM-based TES is to store heat via a phase change process. A PCM-based TES can, for example, be loaded by changing the storage medium from solid state to liquid state and unloaded by changing the storage medium from liquid state to solid state. (IEA-ETSAP 2013)

By using PCM-based TES methods, it is possible to obtain a constant discharge temperature. PCM-based TES systems also have higher energy densities than sensible heat storage systems. The higher cost does, however, make it more difficult for PCM-based TES systems to compete with hot water TES systems. (IEA-ETSAP 2013)

2.3.3 Thermo-chemical storage

A TCS stores thermal energy by means of chemical reactions. A common TCS method is to let water be adsorbed by silica gel or zeolites. TCS systems are mainly used when high energy density is a priority, like in mobile applications and thermal energy transportation. The cost of TCS systems is even higher than the cost for PCM-based TES systems, and therefore it is not feasible to invest in a TCS system for large-scale stationary applications. (IEA-ETSAP 2013)

2.4 Electricity spot prices

2.4.1 Electricity spot prices today

The average spot prices for 2013 to 2018 are depicted in figure 6. The red line is the average spot price for the whole period 2013 to 2018. As can be observed in the figure, the average spot price of 2017 is closest to the average spot price for the whole period. The spot price of 2017 as a function of time is presented in figure 7.

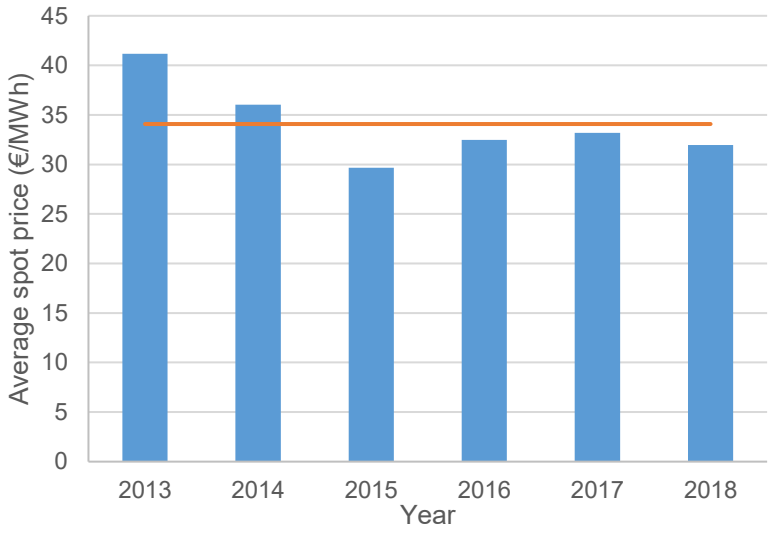

Figure 6: Average spot prices for 2013-2018 (Nord Pool 2019).

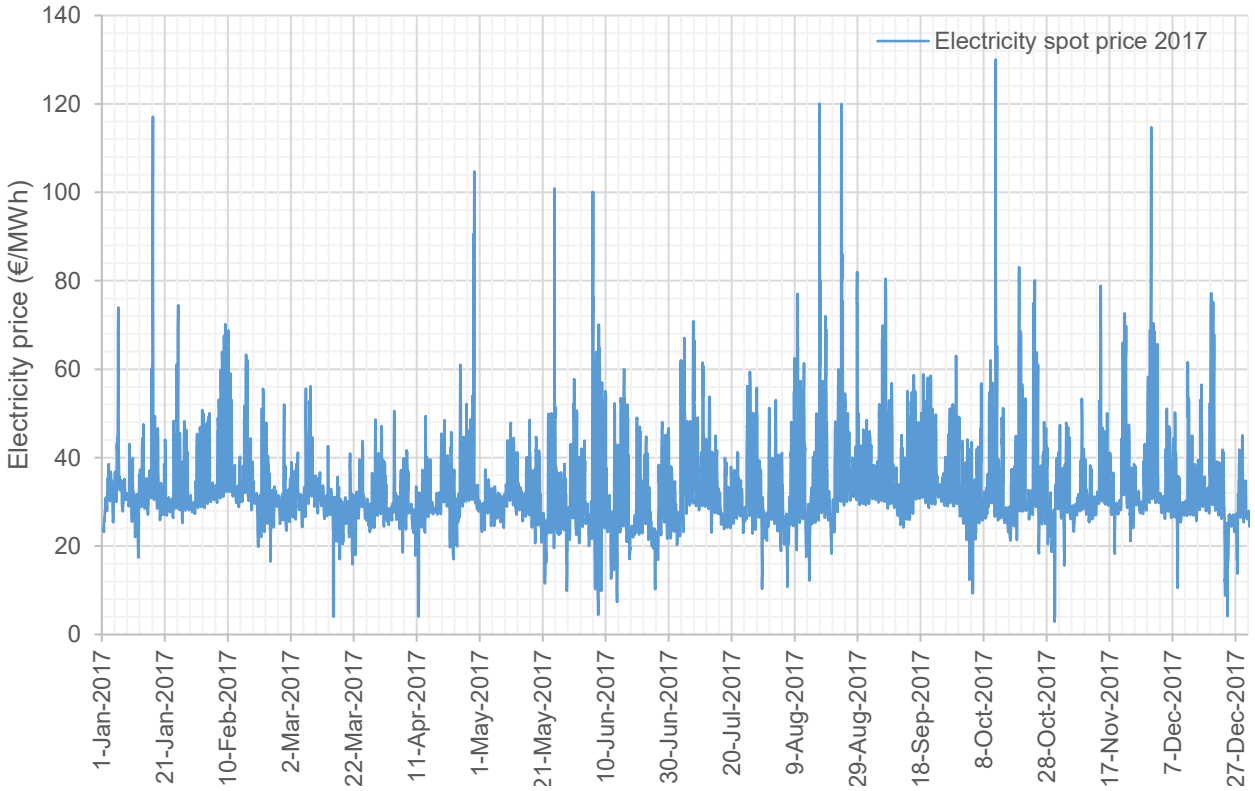

Figure 7: Electricity spot prices for 2017 (Nord Pool 2019).

2.4.2 Future electricity spot prices

Several studies have investigated the effect increased variable generation (such as wind and solar power) has on electricity prices. In 2017 Helistö et al. conducted a study at VTT Technical Research Center of Finland, where estimates of the electricity spot prices for 2030 and 2050 were made by simulating the northern European power system.

A number of simulations were carried out with various variable generation shares and CO_2 prices. The study showed that an increasing share of variable generation will entail more hours of very low electricity spot prices, while increasing CO_2 prices will lead to higher median and maximum electricity prices.

According to Helistö et al., base load power plants will become less profitable if the share of variable generation keeps increasing. Instead there will be a higher demand for flexible power to cover for periods with low energy generation. Thus, base load power plants will be replaced with peak load power plants in the future. During the transition period, when the base load generation still is high and the variable generation is rapidly increasing, there will be temporary overcapacity of power generation, which could lead to very low average electricity prices. This phenomenon can be spotted in the results of the power system simulations for 2030.

When the majority of the non-profitable base load power plants are retired and replaced with peak load power plants, the number of hours with extremely high electricity prices is likely to increase. Hence, the mean electricity spot price is higher for 2050 than for 2030 and 2019, according to the simulation results.

The electricity spot prices, which will be used in this study, are simulated with a 60% variable energy generation share and a CO_2 price of 49 €/t. Two different future price estimates will be used: one for 2030 and one for 2050. The price estimates are shown in the graphs in figure 8 and 9 as a function of time. Figure 10 presents the yearly variation of the spot price in 2017 as well as the yearly variation of the future spot price estimates.

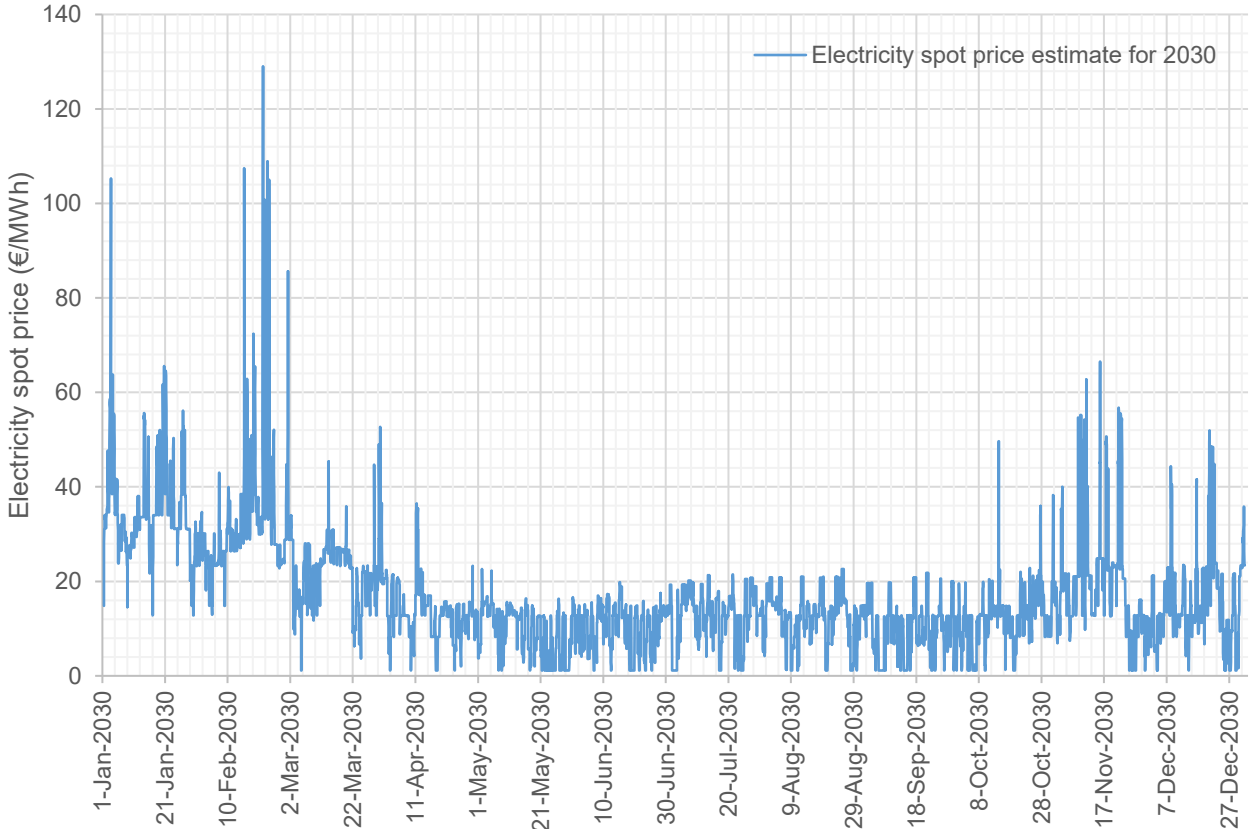

Figure 8: Electricity spot price estimate for 2030 over a one year period.

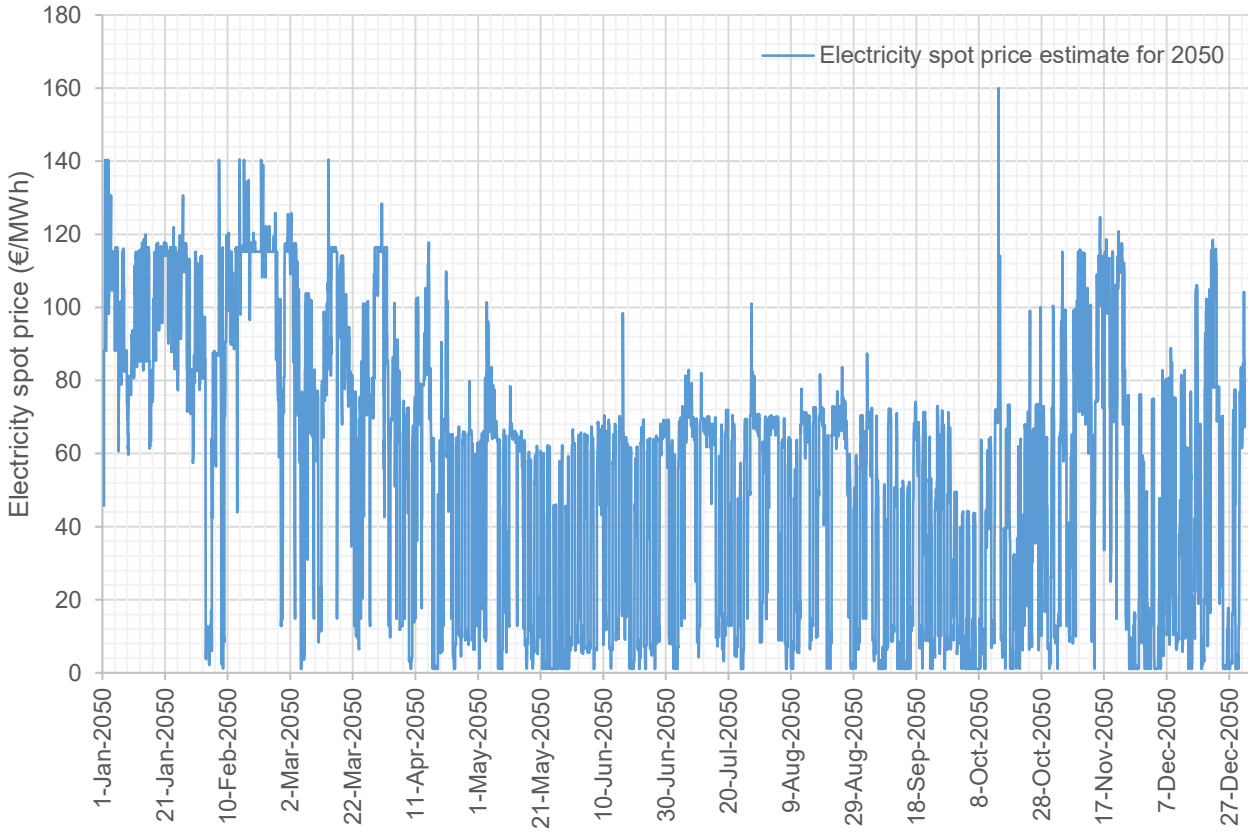

Figure 9: Electricity spot price estimate for 2050 over a one year period.

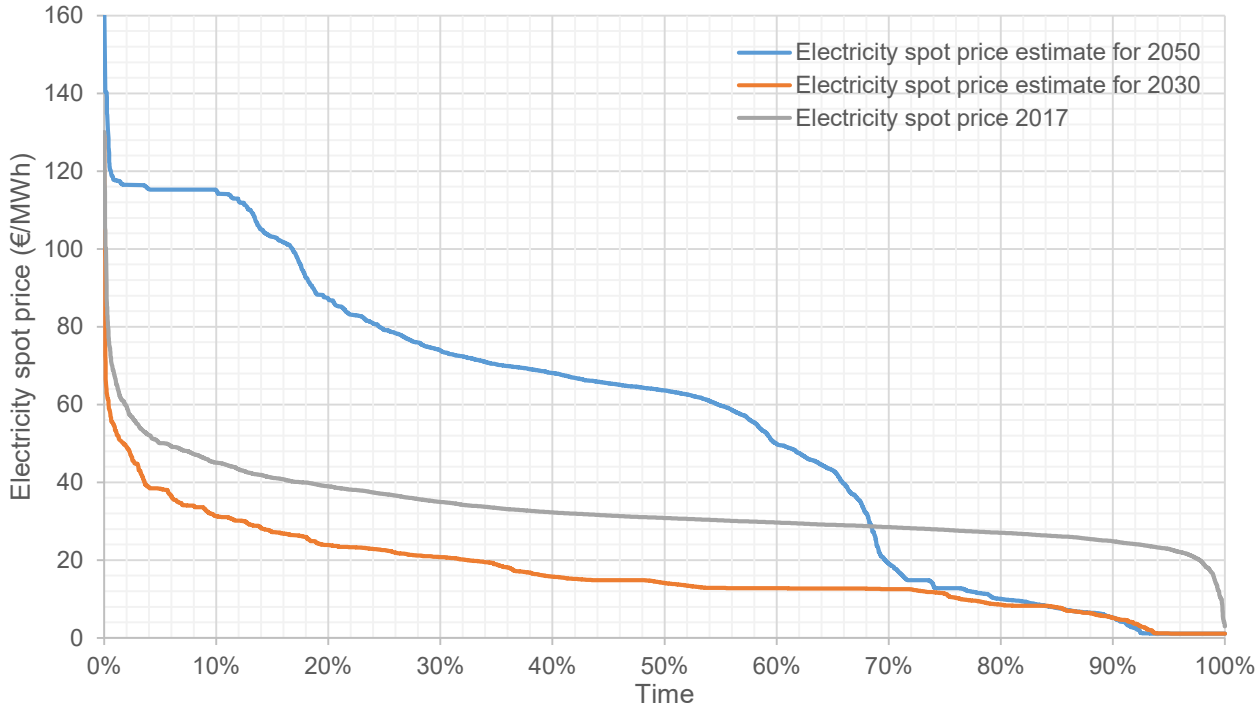

Figure 10: Variation of spot price for 2017 as well as the spot price estimates for 2030 and 2050.

2.5 The office building

The new VTT "FutureHub" building is used as a benchmark office building in this study. The energy demand of the building is based on simulations done by Jari Shemeikka at VTT Technical Research Center of Finland. Figure 11 shows the electrical power and heating demands for the building over a one year time period.

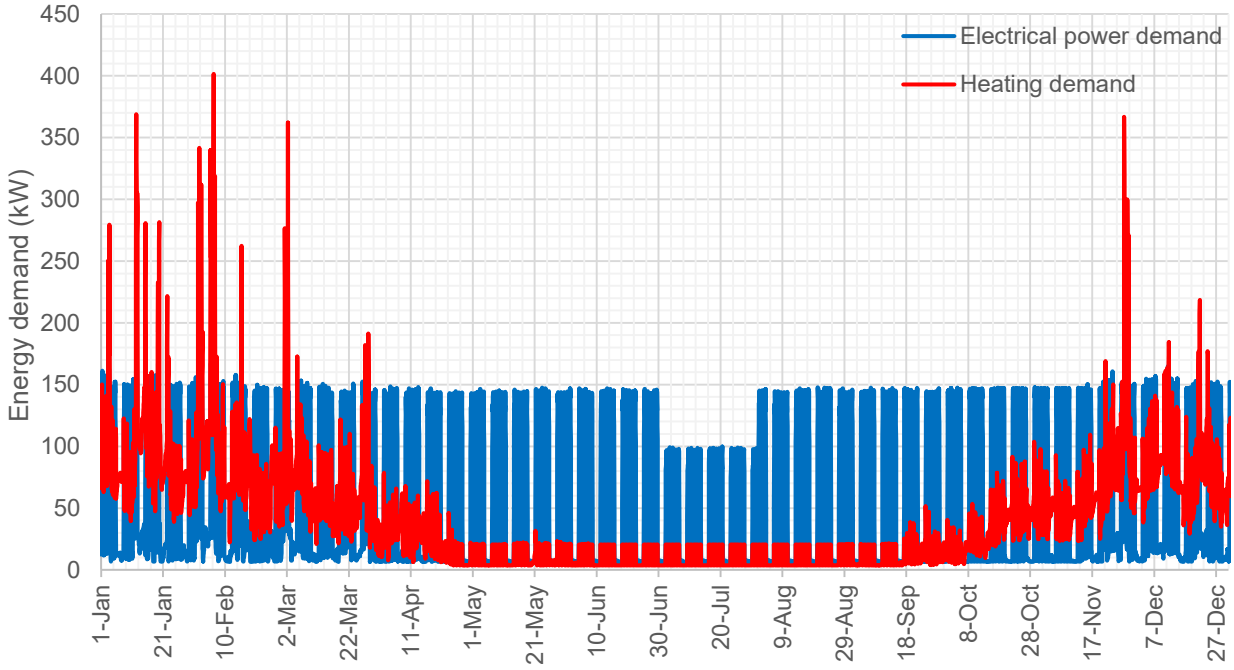

Figure 11: Energy demand of the new VTT office building.

Electrical power is needed for lighting, office appliances, HVAC and snow melting at the door fronts. The percentages of the total electricity demand for each power consumer are depicted in the pie chart in figure 12.

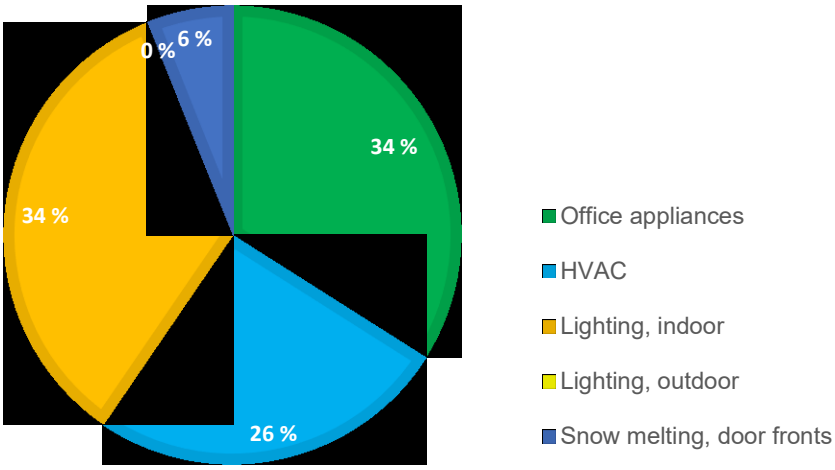

Figure 12: Shares of total electricity demand (Shemeikka 2019).

The office building is equipped with 100 m^2 of photovoltaic panels on the roof. Figure 13 presents the total photovoltaic cell (PV) power output, when half of the photovoltaic panels are facing west and half are facing east. The PV efficiency is assumed to be 17%. (Pfenninger & Staffell 2016)

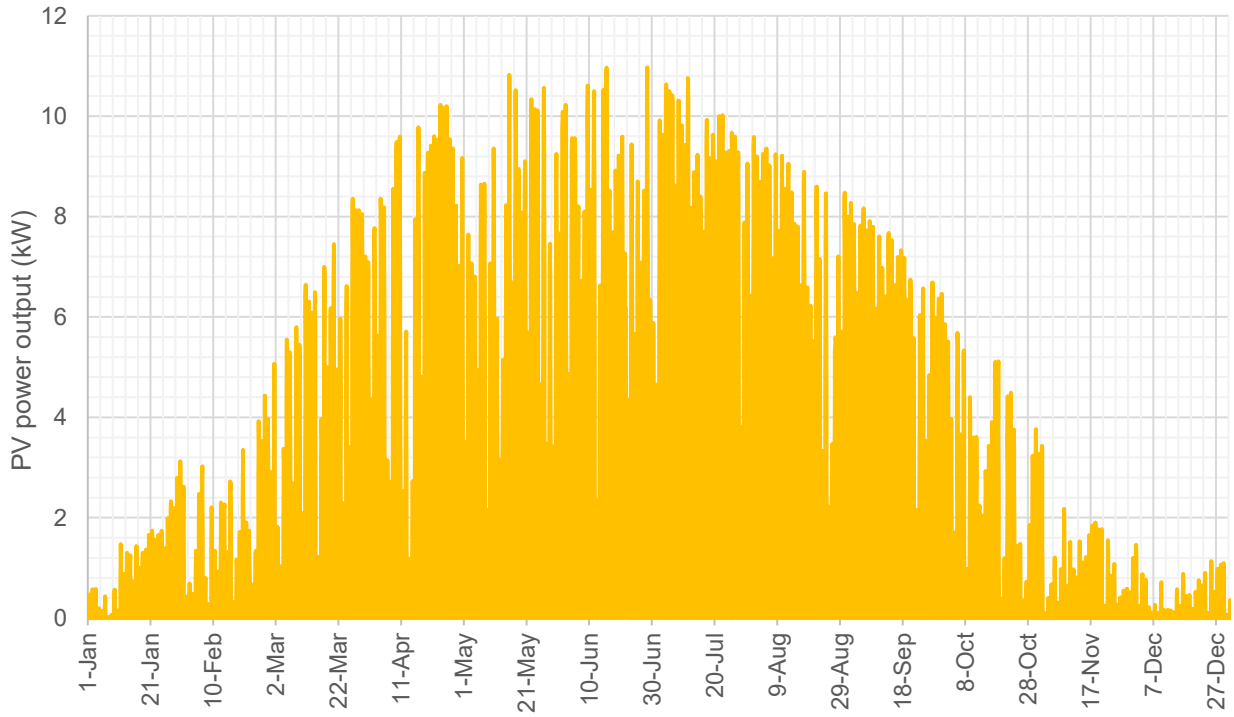

Figure 13: Rooftop PV power output.

2.6 The net present value of the lifecycle cost

There are several ways to evaluate capital investment proposals. Rules like the net present value (NPV) rule, the pay back rule, the internal rate of return (IRR) rule, the profitability index (PI) rule and the average accounting return (AAR) rule are all used to evaluate investments. Out of these rules, the NPV rule is the most consistent with maximization of equity value. Therefore, the NPV rule will be used for investment appraisal in this thesis work. (Hawawini & Viallet 2015)

The NPV rule takes the time value of money into account by adjusting future cash flows with a discount rate. The discounted value of a future cash flow is called the present value (PV). The PV can be calculated with the following equation:

$$\mathrm{PV}_t = \frac{\mathrm{CF}_t}{(1+r)^t} \tag{3}$$

where CF_t is the cash flow at the time t and r is the discount rate. The coefficient $1/(1+r)^t$ is called the discount factor. (Hawawini & Viallet 2015)

The NPV of an investment is calculated by summating the investment cost, I, and the PV of future cash flows:

$$\mathrm{NPV} = -I + \sum_{t=1}^{T} \mathrm{PV}_t \tag{4}$$

T is the point in time when the last cash flow occurs. (Hawawini & Viallet 2015)

According to the NPV rule, an investment shall be undertaken if the NPV is positive (Hawawini & Viallet 2015). In this study, the NPV is most likely negative, since it is unlikely to make a profit by buying and selling energy. The NPV rule is however used, but slightly adjusted. In this study, the NPV of the lifecycle cost ($\mathrm{NPV_{LCC}}$) is calculated. The $\mathrm{NPV_{LCC}}$ for different energy systems can be compared, and the energy system with the lowest $\mathrm{NPV_{LCC}}$ is considered the most economical. The $\mathrm{NPV_{LCC}}$ can be calculated as:

$$\mathrm{NPV_{LCC}} = I + \sum_{t=1}^{T} \frac{C_t}{(1+r)^t} \tag{5}$$

where C_t is the sum of relevant annual costs. (Spickova & Myskova 2015)

2.6.1 Present value of perpetuity and annuity

The PV of an infinite amount of identical periodic cash flows is called the present value of perpetuity (PVP), and can be calculated with the following equation:

$$\mathrm{PVP} = \frac{\mathrm{CF}}{(1+r)^1} + \frac{\mathrm{CF}}{(1+r)^2} + \cdots + \frac{\mathrm{CF}}{(1+r)^\infty} = \frac{\mathrm{CF}}{r} \tag{6}$$

where CF is the periodic cash flow and r is the discount rate.

If the identical periodic cash flows aren't infinite, but instead occur for a certain number of periods, the present value of annuity (PVA) can be calculated. If $\mathrm{PVP}_{1-\infty}$ is the PVP for time step one to infinity and $\mathrm{PVP}_{T-\infty}$ is the PVP for time step T to infinity, the PVA for time step one to time step T is the difference between $\mathrm{PVP}_{1-\infty}$ and $\mathrm{PVP}_{T-\infty}$. The PVA for period one to period T can thereby be expressed as:

$$\mathrm{PVA} = \mathrm{PVP}_{1-\infty} - \mathrm{PVP}_{T-\infty} = \frac{CF}{r} - \frac{CF}{r}\left(\frac{1}{(1+r)^T}\right) = \frac{CF}{r}\left(1 - \frac{1}{(1+r)^T}\right) \tag{7}$$

2.6.2 Weighted average cost of capital as discount rate

The weighted average cost of capital (WACC) is the rate that a company is expected to pay its shareholders and debt holders. Thus, the rate of return (ROR) of a capital investment should be higher than the WACC, in order to meet the expectations of the capital providers (Hawawini & Viallet, 2015).

The WACC can be used as discount rate in the calculation of the $\mathrm{NPV}_{\mathrm{LCC}}$, if the capital investment is financed with shareholder equity and debt (Hawawini & Viallet, 2015).

If E is the market value of the firm's equity and D is the market value of the firm's debt, the WACC is calculated as follows:

$$\mathrm{WACC} = \frac{E}{E+D}k_E + \frac{D}{E+D}k_D \tag{8}$$

where k_E is the cost of capital and k_D are the cost of debt. (Hawawini & Viallet, 2015)

3 OBJECTIVES AND PROBLEM FORMULATION

The emphasis of this thesis work is laid on doing a techno-economic analysis of an RSOC and hydrogen gas storage system for energy storage applications in office buildings. The study involves finding the optimal storage system configuration and operation. This is done by creating an optimization model, which objective is to minimize the life cycle cost (LCC) of the system. The LCC will also be used to apprise the competitiveness of the system, which is the main objective of the study.

In order to apprise the competitiveness of the system, the LCC of the system is compared with the LCC of two alternative energy systems. The first alternative energy system is a ground source HP system, which includes a ground source HP, a grid connection and a district heating connection (for both export and import). The other alternative energy system only consists of a grid connection and a district heating connection.

3.1 System configuration and operation

The basic idea of the RSOC and hydrogen storage system is to balance out energy price and demand peaks. Energy can for example be stored by the system when the electricity prices and demand are low. The stored energy can then be consumed when the energy prices and demand are higher. Excess energy from the solar panels on the roof of the office building can also be stored by the system, instead of being sold cheaply to the electricity provider.

The RSOC and hydrogen gas storage system is composed of an RSOC device, a 200 bar hydrogen storage tank, a hydrogen gas compressor, a hot water TES and an electricity grid connection (for export and import). The following optional components can additionally be integrated into the system framework: a lithium-ion battery, a ground source heat pump (HP) and a district heating connection (for export and import). Combustion of hydrogen for heat generation is also an option in the system.

The LCC minimizing optimization model determines which of the optional components are integrated in the system. Component dimensions and capacities are also determined by the optimization model. The RSOC and hydrogen storage system, including all optional components, is depicted in figure 14.

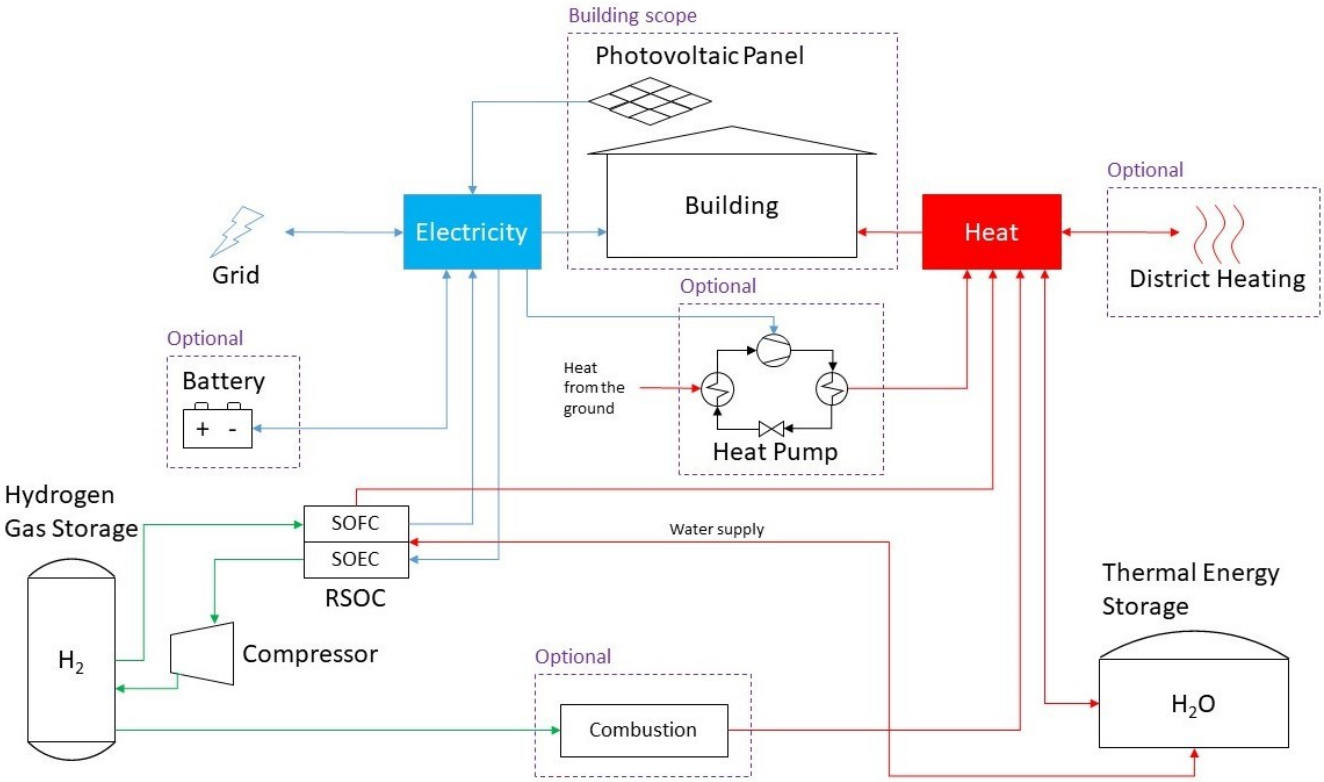

Figure 14: The RSOC and hydrogen storage system with all options included.

3.2 Lifecycle costs of the system

The LCC of the system is dependent on capital expenditures (CAPEX) as well as operating expenditures (OPEX). The CAPEX consists of the capital investment costs of the system components and the OPEX consists of fixed costs (maintenance costs and fees for the grid and district heating network) and variable costs (electricity and district heating costs). The investment costs and the fixed costs are both dependent on the dimensions and capacities of the system components, while the variable costs are dependent on the operation of the system. The operation of the system, in turn, is constrained by the system component dimensions.

3.3 Cases

Three different cases are presented in this study: one case for the situation today (2019) as well as two future cases for the years 2030 and 2050. The assumed electricity spot prices are different in each case. The electricity spot price assumptions are based on the prices presented in chapter 2.4.

Since coal might be replaced by natural gas in the near future, it is possible that district heating prices will increase with up to 25%. Two district heating price scenarios are therefore simulated: one with 25% higher district heating prices in the future cases compared to the 2019 case, and one with the same district heating prices for the future cases as for 2019.

The office energy demand data for the cases is based on simulated hourly energy consumption of the new VTT Technical Research Centre of Finland office building, the “VTT FutureHub”, in Otaniemi, Espoo (see chapter 2.5).

4 METHODS

The minimizing of the system LCC is expressed as a bilevel optimization problem, which is an optimization problem that contains a constraint in the form of another optimization problem. The main optimization problem is referred to as the upper level optimization and the constraint optimization problem is referred to as the lower level optimization. (Sinha et al. 2018).

In this study, the upper level optimization problem minimizes the LCC of the system. The LCC of the system is dependent on the initial investment cost, annual fixed costs and the minimum annual variable costs. In order to find the minimum annual variable costs, the operation of the system must be optimized. Hence, the objective of the lower level optimization problem is to obtain the optimal system operation.

A Matlab algorithm is developed to solve the lower level optimization problem and to calculate the system LCC with the upper level optimization variables as input values (MathWorks 2019a). The upper level optimization is solved by systematically testing different variable combinations and manually generating a solution matrix.

Figure 15 presents a graphical explanation of the bilevel optimization problem. In the figure, D represents the system component dimensions and C_y^v is the annual variable cost. $f_{\mathrm{NPV_{LCC}}}$ and $f_{C_y^v}$ are the upper level and lower level objective functions.

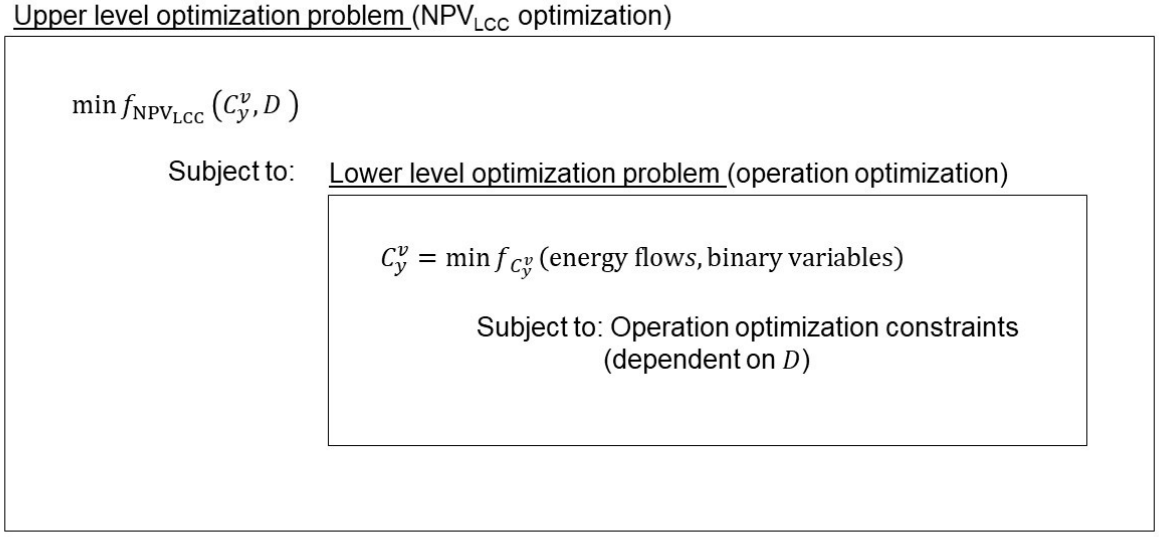

Figure 15: Graphical explanation of the bilevel optimization problem.

4.1 The lower level system operation optimization

The lower level optimization problem is, due to the heavy calculation load, solved as a time series-specific optimization of the system operation, where the annual variable costs are minimized.

The control of the RSOC operational mode (electrolysis or fuel cell mode) requires a binary decision variable in each time step, while the other variables are energy transfer rates, which are considered to be real variables. The RSOC operation functions are non-linear in both electrolysis mode and fuel cell mode. Since the problem is non-linear and contains both binary variables (integers) and real variables, it can be categorized as a mixed integer non-linear programming (MINLP) problem. MINLP problems are, however, in general complicated and time-consuming to solve, and therefore the RSOC functions are linearized, so that the problem can be categorized as a mixed integer linear programming problem (MILP) instead.

4.1.1 Optimization algorithm

Since the system operation optimization problem is an MILP problem, there are both non-integer and integer variables involved. The calculation time of MILP problems tends to increase exponentially with the number of integer variables. In this optimization case, there is an integer variable in binary form for each time step in the annual time series. To be able to optimize an annual time series with comparatively small time steps, within an appropriate calculation time frame, the size of the problem must be reduced.

The reduction of the problem size is done by repeatedly optimizing and bisecting the time interval, using a small constant number of time steps. This way, the time step size will decline for every time interval bisection, until it reaches the desired size (a seven-hour time step size is used in this study).

In the first optimization step, the system operation for the whole time interval (one year) is optimized, using a relatively small number of time steps. Thereafter the energy storage states at the center point, the starting point and the end point of the time interval are set. The storage state at the starting point is the same as the storage state at the end point, since the energy storage state must be the same at the end of the year as at the beginning of the next year. The time interval is then bisected, so that the starting point to the center point forms a new time interval, and the center point to the end point forms another new time interval.

In the following optimization step, new interval center points are generated by re-optimizing the new time intervals separately. The re-optimization is done with the same number of time steps as in the previous optimization, but with a smaller time step size (half of the previous time step size). A new bisection is done after the energy storage states at the new time interval center points are set, and the re-optimization starts again. This process is repeated until the desired step size is reached.

Each time interval optimization problem is solved with Intlinprog, which is a Matlab MILP problem-solving algorithm. The algorithm is based on the branch-and-bound method, but unlike a standard branch-and-bound approach, the algorithm analyzes and adjusts the problem constraints in order to eliminate a part of the futile subproblem candidates (MathWorks[2)] 2019).

Figure 16 presents the first and second optimization steps. $m_{i,j}$ is the energy storage state at the interval center point for optimization step number *i* and time interval number *j*. The energy storage states at the starting point, *a*, and the end point, *b*, are equal and only generated in the first optimization process. The process in the second optimization is repeated *N* number of times, which will result in a decrease in step size and more detailed results.

Figure 17 shows how the size of the time step decreases for every optimization step. The number of time steps used per optimization in figure 17 is eight, which is quite low compared to the 26 to 56 steps that are used in the actual Matlab code.

The time step size used in the study is seven hours. Without using the described interval bisection optimization method (one single problem), the problem contains 1 250 binary variables. By using the bisection optimization method, this number is reduced to 39 binary variables, but the number of subproblems is 819. The number of subproblems and the calculation time do, however, have a linear relationship, while the number of binary variables and the calculation time have an exponential relationship. Hence, the calculation time of the problem can be reduced significantly by using the bisection method.

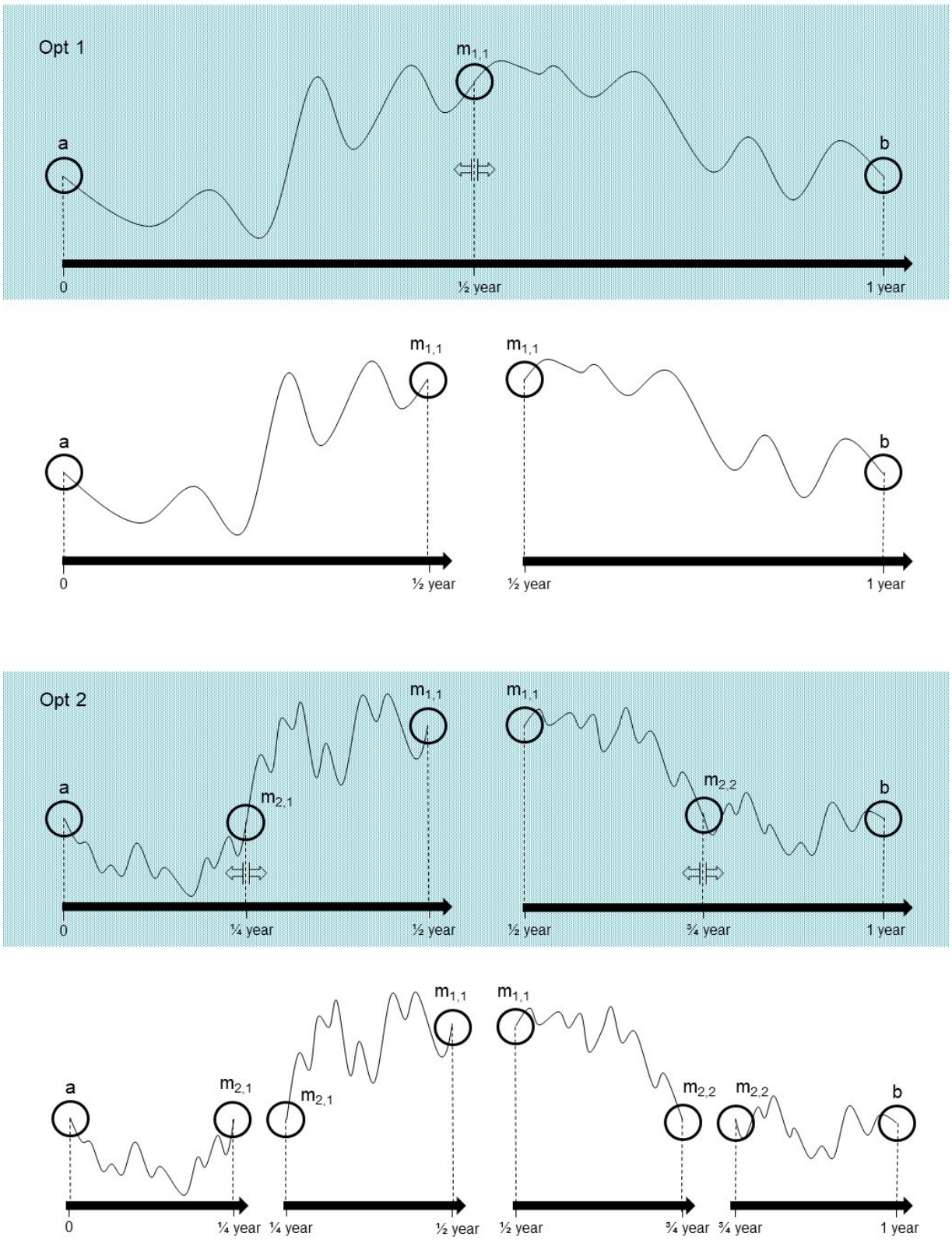

Figure 16: Graphical explanation of the first and second optimization steps.

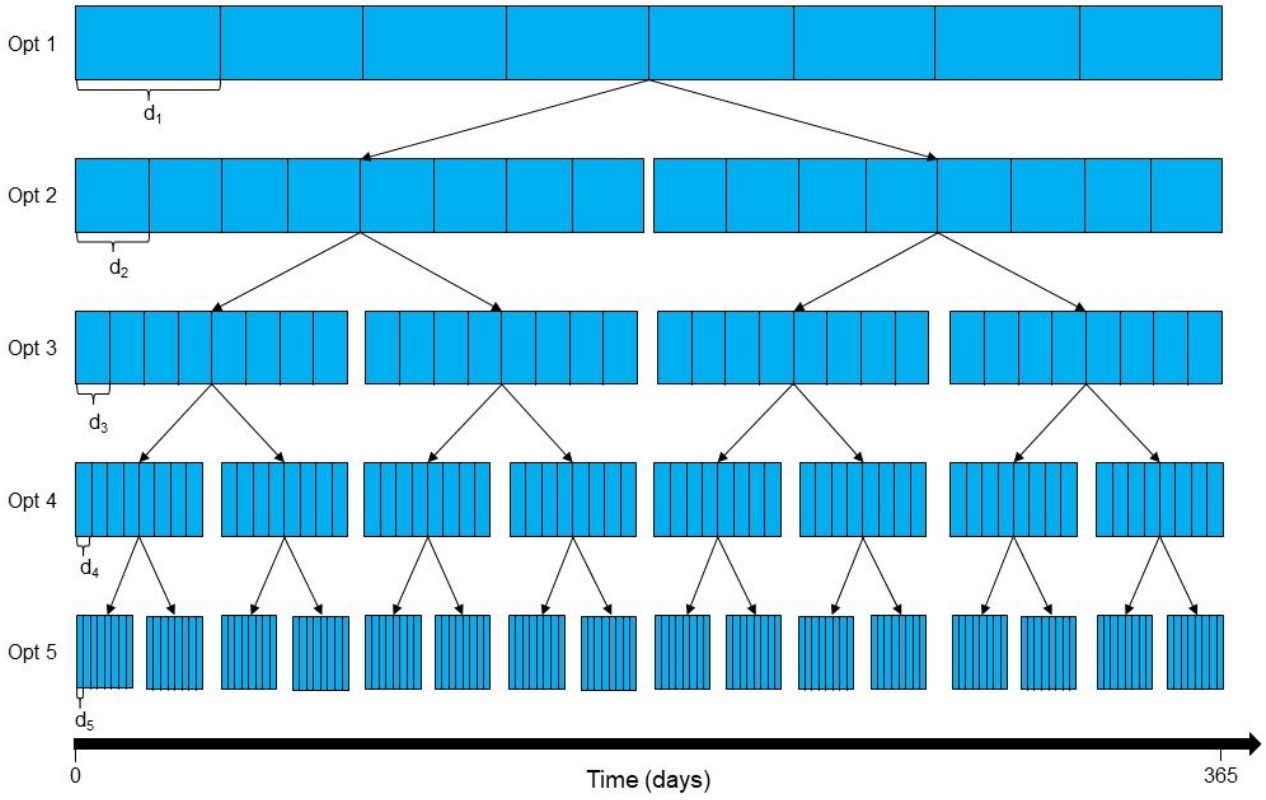

Figure 17: Decrease in time step size for every optimization step.

4.1.2 Variables and parameters

The variables consist of energy transfer rates as well as binary decision variables, which decide if the RSOC runs in electrolysis or fuel cell mode. The parameters consist of energy demand rates, the photovoltaic panel power output and different coefficients as well as storage and energy transfer capacities. The variables and parameters are presented on page 9-10.

4.1.3 RSOC functions

The RSOC is modelled as two different devices, one SOEC device and one SOFC device, which can't operate at the same time. The SOEC device is expressed as one single function, while the SOFC device is expressed as two different functions.

The RSOC functions are based on approximations by members of the VTT's fuel cell solution team. These approximations are also in line with the RSOC efficiencies presented by Reznicek and Brown in figure 5 on page 17 (Reznicek & Brown 2018).

4.1.3.1 SOEC function

It is assumed that the RSOC is only operated above the thermoneutral point of the RSOC device, where the efficiency only varies with a few percentage points (see figure 5 on page 17). Thus,

hydrogen output as a function of the input electrical power can be linearized, without compromising the accuracy of the model. Hydrogen output as a function of electrical power input can be described as:

$$E\left(P_{EC,in,i}, b_i\right) = ba_E + k_E P_{EC,in,i} \tag{9}$$

The electrical input power, $P_{EC,in,i}$, is zero if the binary decision variable, b_i, is zero. If the binary decision variable value is one, the electrical input power is between the minimum electrical input power, $P_{EC,in,min}$, and the maximum electrical input power, $P_{EC,in,max}$. The constants, k_E and a_E, can be calculated with the following equations:

$$k_E = \frac{0.80P_{EC,in,max} - 0.65P_{EC,in,min}}{P_{EC,in,max} - P_{EC,in,min}} \tag{10}$$

$$a_E = 0.65P_{EC,in,min} - k_E P_{EC,in,min} \tag{11}$$

where the 0.65 is the SOEC mode efficiency for the minimum power input, $P_{EC,in,min}$, and 0.80 is the SOEC mode efficiency for the maximum power input, $P_{EC,in,max}$.

4.1.3.2 SOFC functions

There are two different SOFC functions; one that expresses the relation between hydrogen input and electrical power output, and one that expresses the relation between heat output and the electrical power output.

As can be observed in figure 5 on page 17, the hydrogen to electrical power efficiency as a function of electrical output power is nonlinear, and reaches a maximum electrical efficiency somewhere in the middle of the power output interval. It is assumed that the electrical output power of the RSOC doesn't exceed the electrical output power of the maximum efficiency. The maximum electrical output power of the SOFC function, $P_{FC,out,max}$, will thus be in the middle of the actual output power interval of the SOFC mode. This means that $P_{FC,out,max}$ is only half of the real maximum output power.

The maximum load of the SOFC device is lower than the maximum load of the SOEC device, since high loads of the RSOC lead to higher heat generation, and a too high heat generation in SOFC mode is not desirable. The real maximum power output of the SOFC is only ¼ of the maximum power input of the SOEC, and the maximum output power of the SOFC function, $P_{FC,out,max}$, is thus only ⅛ of $P_{EC,in,max}$.

Both of the SOFC functions are linearized between $P_{FC,out,min}$ and $P_{FC,out,max}$. Hydrogen input as a function of electrical output power, F, and heat output as a function of electrical output power, G, can be described as:

$$F\left(P_{FC,out,i}, b\right) = (1 - b_i)a_F + k_F P_{FC,out,i} \tag{12}$$

$$G\left(P_{FC,out,i}, b\right) = (1 - b_i)a_G + k_G P_{FC,out,i} \tag{13}$$

The SOFC functions will operate in the opposite direction of the SOEC function. Hence, the output electrical power, $P_{FC,out,i}$, is between the minimum electrical output power, $P_{FC,out,min}$, and the maximum output electrical power, $P_{FC,out,max}$, if the binary decision variable, b_i, is zero. And if the binary decision variable is one, the output electrical power is zero. The constants, k_F, a_F, k_G and a_G, are calculated using the following equations:

$$k_F = \frac{\frac{P_{FC,out,max}}{0.70} - \frac{P_{FC,out,min}}{0.45}}{P_{FC,out,max} - P_{FC,out,min}} \tag{14}$$

$$a_F = \frac{P_{FC,out,min}}{0.45} - k_F P_{FC,out,min} \tag{15}$$

$$k_G = \frac{\frac{(0.80 - 0.70)P_{FC,out,max}}{0.70} - \frac{(0.80 - 0.45)P_{FC,out,min}}{0.45}}{P_{FC,out,max} - P_{FC,out,min}} \tag{16}$$

$$a_G = \frac{(0.80 - 0.45)P_{FC,out,min}}{0.45} - k_G P_{FC,out,min} \tag{17}$$

where 0.45 is SOFC mode efficiency for the minimum power output, $P_{FC,out,min}$, and the 0.70 is the SOFC mode efficiency for the maximum SOFC function power output, $P_{FC,out,max}$. The 0.80 constant in equation 16 and 17 implies that the RSOC transforms 80% of the hydrogen gas LHV to electricity and heat at all times.

4.1.4 Graphical presentation of the optimization problem

A graphical model of the optimization problem is presented in figure 18, where all energy flows are included. Red lines stand for thermal energy flows, blue lines for electrical power and green lines for hydrogen gas flows.

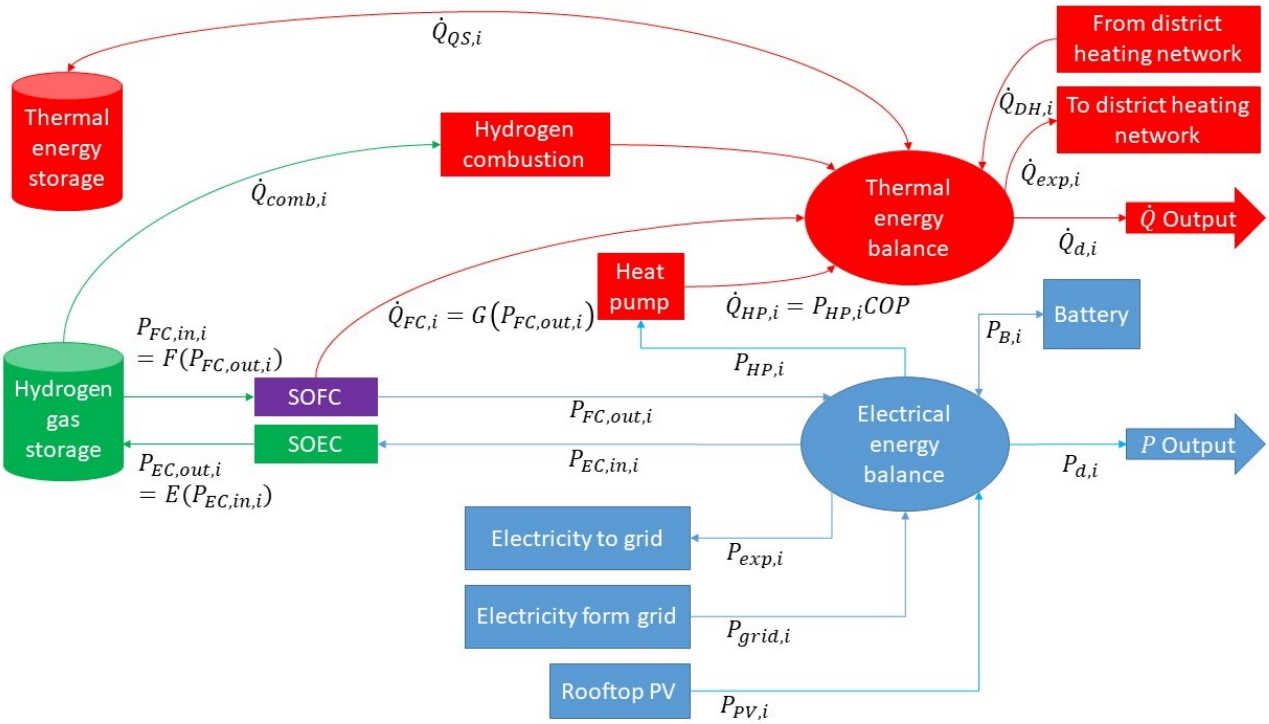

Figure 18: Graphical model of the optimization problem.

4.1.5 Objective function

The objective function minimizes the annual variable costs of the system. The variable costs of the system are defined as the costs of electricity and district heating minus the income generated by energy export to the grid and the district heating network. The objective function is expressed as follows:

$$\min \sum_{i=1}^{N} (\dot{Q}_{DH,i} C_{DH,i} + P_{grid,i} C_{grid,i} - \dot{Q}_{exp,i} C_{Qexp,i} - P_{exp,i} C_{Pexp,i}) t \qquad (18)$$

where $C_{DH,i}$ is the district heating import price and $C_{grid,i}$ is the import electricity price, which is sum of the electricity spot price, the electricity distribution tariff and the grid tax. $C_{Qexp,i}$ and $C_{Pexp,i}$ are the export prices for thermal energy and electricity. Both the export and the import energy prices in the object function are time dependent and vary from hour to hour.

4.1.6 Constraints

The constraints can be divided into equality and inequality constraints. The equality constraints consist of two energy balances; an electrical energy balance and a thermal energy balance. The inequality constraints consist of different energy transfer constraints and storage constraints.

The electrical energy balance (19) comprises all the electrical energy rates for each time step, while the thermal energy balance (20) comprises all the heat transfer rates for each time step. These balances are also depicted in figure 18.

Electrical energy balance:

$$P_{HP,i} + P_{FC,out,i} + P_{B,i}\sqrt{\eta_B} + P_{grid,i} - P_{EC,in,i} - P_{HP,i} - P_{exp,i} - \frac{h_{comp,out} - h_{comp,in}}{\eta_{comp}\mathrm{LHV}} E\left(b, P_{EC,in}\right) = P_{demand,i} - P_{PV,i} \quad \forall i \tag{19}$$

Thermal energy balance:

$$P_{HP,i}\mathrm{COP} + G\left(b, P_{FC,out,i}\right) + \dot{Q}_{comb,i} + \dot{Q}_{QS,i}\sqrt{\eta_{QS}} + \dot{Q}_{DH,i} - \dot{Q}_{exp,i} = \dot{Q}_{demand,i} \quad \forall i \tag{20}$$

The energy transfer constraints 21 to 28 depend on lower and upper limits of the system components. As can be observed in the constraints 21 to 28, every constraint has the same boundaries for each time step, except the RSOC constraints 27 and 28, where the boundaries are dependent on the binary decision variable, b.

District heat constraints:

$$\dot{Q}_{DH,c} \geq \dot{Q}_{DH,i} \geq 0 \quad \forall i \tag{21}$$

$$\dot{Q}_{DH,c} \geq \dot{Q}_{exp,i} \geq 0 \quad \forall i \tag{22}$$

Grid power constraints:

$$P_{grid,c} \geq P_{grid,i} \geq 0 \quad \forall i \tag{23}$$

$$P_{grid,c} \geq P_{exp,i} \geq 0 \quad \forall i \tag{24}$$

HP capacity constraint:

$$\dot{Q}_{HP,c} \geq P_{HP,i}\mathrm{COP} \geq 0 \quad \forall i \tag{25}$$

Hydrogen combustion constraint:

$$\dot{Q}_{comb,i} \geq 0 \quad \forall i \tag{26}$$

RSOC power input and output constraints:

$$P_{EC,in,max} b_i \geq P_{EC,in,i} \geq P_{EC,in,min} b_i \quad \forall i \tag{27}$$

$$P_{FC,out,max}(1 - b_i) \geq P_{FC,out,i} \geq P_{FC,out,min}(1 - b_i) \quad \forall i \tag{28}$$

If b_i is zero, the SOEC input electrical power, $P_{EC,in,i}$, is between the minimum input power, $P_{EC,in,min}$, and the maximum input power, $P_{EC,in,max}$, while the SOFC output power, $P_{FC,out,i}$, is zero. And if b_i is one, $P_{EC,in,i}$ is zero, while $P_{FC,out,i}$ is between the minimum output power, $P_{FC,out,min}$, and the maximum output power, $P_{FC,out,max}$.

The cumulative storage constraints 29 to 34 differ from the earlier constraints, because they are dependent on earlier time steps. The constraints for time step, i, is the cumulative sum of the energy flow rates for the earlier time steps.

In order to keep the model as accurate as possible, the initial amounts of stored energy are expressed as a variables. The constraints also ensure that the stored energy at the end of the time period isn't lower than the initial stored energy.

Hydrogen storage constraint:

$$E_{H2S,c} \geq E_{H2S,0} + t \sum_{ts=1}^{i} \left(E(P_{EC,in,ts}) - F(P_{FC,out,ts}) - Q_{comb,ts} \right) \geq 0 \quad \forall\, i \in \{1 \,..\, (N-1)\} \tag{29}$$

$$E_{H2S,c} \geq E_{H2S,0} + t \sum_{ts=1}^{N} \left(E(P_{EC,in,ts}) - F(P_{FC,out,ts}) - Q_{comb,ts} \right) \geq E_{H2S,0} \tag{30}$$

Heat storage constraint:

$$Q_{QS,c} \geq Q_{QS,0} + t \sum_{ts=1}^{i} \dot{Q}_{QS,ts} \geq 0 \quad \forall\, i \in \{1\,..\,(N-1)\} \tag{31}$$

$$Q_{QS,c} \geq Q_{QS,0} + t \sum_{ts=1}^{N} Q_{QS,ts} \geq Q_{QS,0} \tag{32}$$

Battery storage constraint:

$$E_{B,c} \geq E_{B,0} + t \sum_{ts=1}^{i} P_{B,ts} \geq 0 \quad \forall\, i \in \{1\,..\,(N-1)\} \tag{33}$$

$$E_{B,c} \geq E_{B,0} + t \sum_{ts=1}^{N} P_{B,ts} \geq E_{B,0} \tag{34}$$

4.2 The upper level lifecycle cost minimizing optimization

The upper level optimization problem is solved by manually testing feasible combinations of the variables. Robust adjustments are first done to get an understanding of how different variable combinations affect the solution. Then the variables are fine tuned in order to find the minimum of the object function.

The objective of the upper level optimization problem is to minimize the NPV_{LCC}. The NPV_{LCC} of the whole system can be calculated by summating the capital investments and the present values (PV) of the annual cash flows. The annual cash flows consist of the minimum annual variable costs and annual fixed costs. The objective function of the upper level optimization problem is expressed as follows:

$$min\left[I + (C^{v}_{min,y} + C^{f}_{y})\frac{1}{\mathrm{WACC}}\left(1 - \frac{1}{(1+\mathrm{WACC})^{T}}\right)\right] \tag{35}$$

where $C^{v}_{min,y}$ is the minimum annual variable costs, which is is the same as the object value of the lower level operation optimization. WACC is the weighted average cost of capital rate and T is the point in time when the last annual cash flow takes place. If all system component life spans are roughly the same, T is the value of the system service life or the investment life length. The total initial capital investment, I, is the sum of all system component investment costs and the annual

fixed costs, C_y^f, is the sum of all annual maintenance and service fees. I and C_y^f can be expressed as functions of the component dimension vector, $\vec{D}_{comp}$:

$$I = f_I\left(\vec{D}_{comp}\right) \tag{36}$$

$$C_y^f = f_{C_y^f}\left(\vec{D}_{comp}\right) \tag{37}$$

The vector $\vec{D}_{comp}$ contains all the system component sizes and capacities, and is considered as a variable in the upper level NPV_{LCC} optimization problem.

5 INPUT DATA ASSUMPTIONS

5.1 Technical data

The operation and energy consumption of the RSOC and hydrogen storage system is dependent on the efficiencies of the hydrogen compressor and the energy storages as well as the coefficient of performance (COP) of the HP.

The isentropic efficiency, η_{is}, of a small hydrogen compressor is estimated to be 65% (Department of Energy 2008), while the compressor motor efficiency, η_m, is assumed to be 95%. The total efficiency of the hydrogen compressor can then be calculated as:

$$\eta_{comp} = \eta_{is}\eta_m \approx 62\% \quad (38)$$

The round-trip efficiency of hot water thermal energy storages ranges from 50% to 90% (IAE-ETSAP & IRENA, 2013). In this study, the central value of the efficiency range, 70%, is used as an input value.

According to predictions by the International Renewable Energy Agency, the round-trip efficiency of lithium-ion batteries will increase from between 92% and 96% in 2016 to between 94% and 98% in 2030 (IRENA 2017). Thus, it is assumed that efficiency for the 2019 case is 94% and that the efficiencies for the 2030 and 2050 cases are 96% and 98%, respectively.

The COP for the ground source HP is assumed to be 4.2.

5.2 Investment costs

The investment costs consist of the installation costs of the different system components as well as the grid and district heating connection fees. These costs are dependent on the capacities of the system components, and therefore they are expressed as scalable costs, which can be multiplied with component capacities. The investment cost of the RSOC itself is not taken into account in the study. There is not a market for RSOC devices yet, which makes it hard to evaluate how much it is going to cost.

5.2.1 Hydrogen storage tank installation cost

Three different compressed hydrogen storage investment costs are presented in table 1. The first storage cost is based on a large-scale (ca. 2 GWh capacity) 100 bar underground hydrogen pipe storage in Urdorf, Swizerland (Jauslin Stebler AG 2013). The second storage cost is based on a 700 bar compressed automotive hydrogen storage in 2015 and the third cost is the target cost for automotive hydrogen storage in 2020 (Office of energy efficiency and renewable energy 2015).

The hydrogen storage pressure has to be high enough to ensure that the minimum operating pressure of the RSOC in SOFC mode is reached. Hence, the storage vessel can never be completely emptied during operation. The minimum amount of gas in the storage vessel is called cushion gas (Krieg 2012). The cushion gas is taken into account in the calculation of cost per storage capacity in table 1.

Table 1: Hydrogen storage costs (Jauslin Stebler AG 2013, Office of energy efficiency and renewable energy 2015).

	Underground hydrogen pipe storage in Urdorf, Switzerland	Cost of compressed automotive hydrogen storage systems	2020 target cost of automotive hydrogen storage systems
Year	2013	2015	2020
Volume	720 000 Nm^3	Small-scale	Small-scale
Maximum pressure	100 bar	700 bar	700 bar (assumed)
Cost per kg stored hydrogen[a]	220.59 €/kg	478.68 €/kg	293.04 €/kg
Cost per storage capacity[a,b]	8.28 €/kWh	14.80 €/kWh	9.06 €/kWh
Average cost per storage capacity	10.71 €/kWh		

[a] An annual inflation rate of 1% is assumed.

[b] The cushion gas for a minimum output pressure of 20 bar is taken into account.

In this study, the average cost per storage capacity, 10.71 €/kWh, is used as the input value for the hydrogen system installation cost.

5.2.2 Hydrogen compressor cost

The cost of the hydrogen compressor represents a considerably large share of the total investment cost. The hydrogen compressor investment cost, I_{comp}, as a function of the hydrogen gas mass flow capacity, $\dot{m}_{H_2}$, can be described as (classified source):

$$I_{comp}(\dot{m}_{H_2}) = 121\,908 \left(\frac{\dot{m}_{H_2}}{\left(\frac{\text{kg}}{\text{h}}\right)} \right)^{0.182} \tag{39}$$

The hydrogen compressor investment cost function is depicted in figure 19.

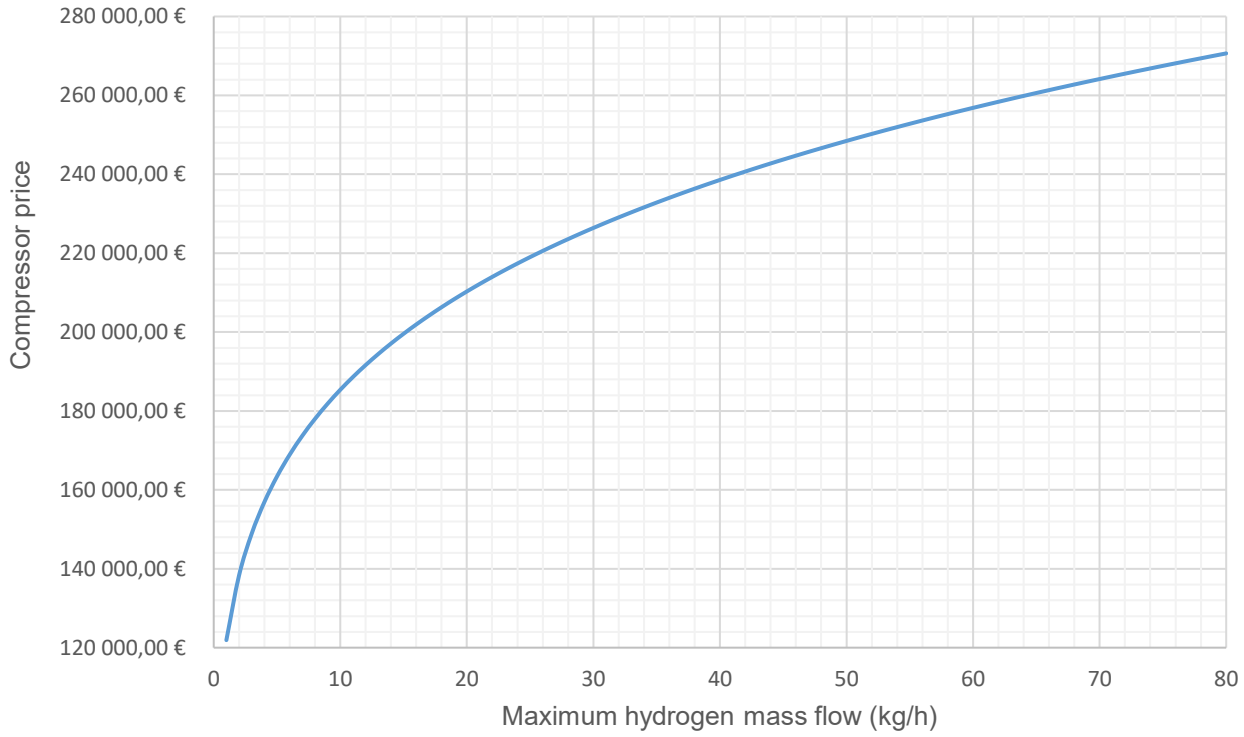

Figure 19: Hydrogen compressor investment cost function.

5.2.3 Thermal energy storage installation cost

The installation cost range for hot water TES in 2013 was 0.1 to 10 €/kWh (IAE-ETSAP & IRENA, 2013). In this study, the central value of the cost range, 5 €/kWh, will be used as the input value for the TES installation cost.

5.2.4 Battery installation cost

According to a market study done by the International Renewable Energy Agency in 2017, battery installation costs are expected to decline drastically in the future. Lithium-ion battery installation costs are expected to decline with over 50% between 2016 and 2030. The central estimate of the installation cost for lithium nickel manganese cobalt batteries (NMC), which are a common choice for stationary applications, is predicted to reach $ 145/kWh (128 €/kWh) by 2030. The central installation cost for NMC batteries in 2016 was about $ 350/kWh, which is equivalent to 347 €/kWh (inflation adjusted). (IRENA 2017)

The central installation cost for NMC batteries in 2016 will be used as an input value in the 2019 case study. In the 2030 and 2050 cases, the central estimate of the installation cost for NMC batteries in 2030 will be used.

5.2.5 Ground source heat pump installation cost

The investment cost for a 50 kW ground source HP is expected to be around 63 000 €, which is equivalent to 1 260 €/kW. Thus, 1 260 €/kW will be used as a scalable installation cost for the ground source HP in the optimization model.

5.2.6 Grid and district heating connection fees

The electricity distribution and district heating companies charge a connection fee for connecting a building to the grid and the district heating network. In Espoo, Finland, the electricity distribution company is Caruna Espoo Oy. Fortum Oyj is assumed to be the district heating provider.

The grid connection fee for connections exceeding 200 A (which applies for the office building) is 60 €/A (vat 24%) (Caruna Espoo Oy 2018), which is 121 €/kWh (vat 0%) if the grid voltage is assumed to be 0.4 kV.

Fortum Oyj's district heating connection fee correlates with the maximum heat transfer rate of the district heating connection. The district heating connection fee for different maximum heating capacities is presented in table 2.

Table 2: District heating connection fee for different maximum heat transfer rates (Fortum Oyj 2019).

Maximum heat transfer rate, $\dot{Q}_{DH,max}$ (kW)	Connection fee, vat 0% (€)
25 - 60	7 300
61 - 190	12 500
191 - 350	20 000
350 -	Case specific

5.3 Annual fixed costs

The annual fixed costs consist of annual grid and district heating fees, as well as annual operations and maintenance costs for the energy storage units and other system components.

5.3.1 Grid network service fees

The electricity distribution company charges network service fees for providing network services, such as electricity distribution, maintenance etc. (Caruna Espoo Oy 2018). The service fees that Caruna Espoo OY charges for a 0.4 kV connection are presented in table 3.

Table 3: Service fees for a 0.4 grid connection (Caruna Espoo OY 2018).

Service fees for 0.4 kV connection	Original fee, vat 0%	Input value in model
Basic fee	42.50 €/month	510 €/year
Power fee	2.09 €/kW, month	25.08 €/kW, year
Reactive power fee, input	4.05 €/kVAR, month	-
Reactive power fee, output	4.05 €/kVAR, month	-

The power fee is dependent on the monthly peak power, but since the optimization model is incapable of optimizing the monthly operation of the system, the power fee is slightly modified so that it is dependent on the maximum annual peak power instead. The reactive power is not taken into account in this thesis work, since it is beyond the scope of the optimization model.

5.3.2 District heating power fee

Fortum Oyj's district heating power fee is an annual fee, which is based on the maximum heat transfer rate of the last 36 months (Fortum Oyj 2019). The power fee for different maximum heat transfer rate ranges are presented in table 4.

Table 4: District heating power fee for different maximum district heating power (Fortum Oyj 2019)

Maximum heat transfer rate, $\dot{Q}_{DH,max}$ (kW)	Power fee, vat 0% (€/year)
3 - 80	$52 \cdot \dot{Q}_{DH,max} - 60$
81 - 300	$37 \cdot \dot{Q}_{DH,max} + 1140$
301 - 600	$21 \cdot \dot{Q}_{DH,max} + 5940$
601 - 1000	$16 \cdot \dot{Q}_{DH,max} + 8940$
1001 - 3500	$11 \cdot \dot{Q}_{DH,max} + 13940$
3500 -	$8 \cdot \dot{Q}_{DH,max} + 24440$

5.3.3 Operations and maintenance costs of system components

The annual operations and maintenance (O&M) cost of the hydrogen gas storage tank is assumed to be 0.5% of the initial investment cost (Zoulias et al. 2006). The same O&M cost is used for the TES. The annual O&M cost considered for the lithium-ion battery is 1% (Zoulias et al. 2006). For the hydrogen compressor and HP, the annual O&M cost is assumed to be 4%.

5.4 Annual variable costs

The annual variable costs are directly dependent on the power imported from the grid and the heat imported from the district heating network. Incomes generated by exporting energy to the grid and district heating network do also affect the variable costs, since they are considered as negative variable costs in this study. Two different scenarios are simulated for the district heating variable

costs: one with a 25% district heating price increase in the future and one with no district heating price increase.

5.4.1 Variable electricity costs

The variable electricity costs are dependent on the amount of imported electricity as well as the electricity spot price, the electricity distribution tariff and the electricity grid tax. The electricity spot prices for each case are more thoroughly presented in chapter 2.4.

The electricity distribution tariff is payed to the electricity distribution company, which in this case is Caruna Espoo Oy. The electricity distribution tariff charged by Caruna Espoo Oy is presented in table 5.

Table 5: Power distribution fee for a 0.4 kV connection (Caruna Espoo OY 2018).

Electricity distribution tariff for 0.4 kV connection	Price, vat 0%
Daytime distribution, winter*	2.42 c/kWh
Other time distribution	1.15 c/kWh
***) Daytime distribution, winter: Mon-Sat 7am-10pm, 1 Nov-31 Mar.**	

The electricity grid tax in Finland is 2.253 c/kWh (vat 0%) for all electricity consumers except for some manufacturing, data center and greenhouse businesses (Helen 2018).

5.4.2 Variable district heating costs

The variable district heating costs are dependent on the district heating prices as well as the amount of imported thermal energy. The district heating prices of Fortum Oyj in 2019 are presented in table 6. The district heating energy tax is included in the prices.

Table 6: District heating price for each month (Fortum Oyj 2019).

Month	District heating price, vat 0% (€/MWh)
January	59.00
February	59.00
March	54.00
April	48.00
May	39.00
June	25.00
July	25.00
August	25.00
September	39.00
October	48.00
November	54.00
December	59.00

Two different district heating price scenarios are simulated in this study. In the first scenario, where coal is replaced by natural gas in the near future, the prices in table 6 are multiplied with a factor of 1.25 in the 2030 and 2050 cases. In the second scenario, the district heating prices are the same as in table 6 for all cases.

5.4.3 Energy export prices

Exporting electricity to the grid has become more common during the last years as a result of the increase in electricity generation by photovoltaic cells. Fortum Oyj pays the spot price minus a 0.24 c/kWh transfer fee for electricity exported to the grid (Fortum Oyj 2019).

The price that Fortum Oyj pays for thermal energy fed to the district heating network depends on the temperature of the outgoing district heating water (if the temperature is suitable for supply or return flow) and time of year. The average thermal energy export prices, which are used in the model are presented in table 7.

Table 7: Average district heating export price for each month (Fortum Oyj 2019).

Month	District heating exportprice, vat 0% (€/MWh)
January	38.50
February	38.50
March	32.50
April	25.50
May	15.00
June	15.00
July	12.00
August	15.00
September	17.00
October	20.50
November	25.50
December	34.00

The export district heating prices are also multiplied with a factor of 1.25 in the 2030 and 2050 cases for the scenario where coal is replaced by natural gas in the near future. In the scenario where there is no price increase, the export prices in table 7 applies for all the cases.

5.5 WACC rate and investment life span

In order to calculate the NPV_{LCC} of the system, a discount rate and the life span of the investment is needed. The WACC rate, which will function as discount rate is assumed to be 7%, which is the average WACC of 276 companies in German-speaking countries participating in a study conducted by KPMG (KPMG 2018). The life span of the RSOC and hydrogen gas storage system is expected

to be 20 years, since the life span of most of the system components is around 20 years (Zoulias et al. 2006, IRENA 2017, IEA-ETSAP 2013).

6 RESULTS AND DICUSSION

In each case (2019, 2030 and 2050), the net present value of the lifecycle cost (NPV_{LCC}) was minimized for three RSOC and hydrogen storage systems with different RSOC device sizes. The smallest RSOC had a maximum input power of 40 kW in electrolysis mode and a maximum output power of 10 kW in fuel cell mode (hereinafter referred to as 40/10 kW). The biggest RSOC had a maximum input power of 240 kW in electrolysis mode and a maximum output power of 60 kW in fuel cell mode (240/60 kW).

Two different district heating price scenarios were simulated for the future cases (i.e. 2030 and 2050); one with the same district heating prices as in the 2019 case and one with a 25% higher district heating prices than in the 2019 case. The last-named scenario is considered more likely to occur, and hence it is used as the standard district heating price scenario in this study.

6.1 Optimal system configuration

The NPV_{LCC} of the different RSOC and hydrogen gas storage systems is depicted in figure 20 as a function of the hydrogen gas storage capacity. A system service life of 20 years was assumed when calculating the NPV_{LCC}. The costs of the RSOC device itself are not included in the NPV_{LCC}.

By examining figure 20, it can be observed that the smaller the RSOC is, the lower the NPV_{LCC} tends to be. Hence, the optimal RSOC and hydrogen gas storage system contains the smallest possible RSOC device, which in this study is assumed to be the 40/10 kW RSOC. This statement holds for every case and every district heating price scenario.

Figure 20 also shows that a 25% increase in district heating prices has a positive effect on the NPV_{LCC} in the 2030 case, since more heat can then be generated by the HP and exported to the district heating network. In the 2050 case, where the HP operation is expensive (due to high electricity prices) and the system is largely dependent on district heating, a 25% increase has mainly negative effects on the NPV_{LCC}.

A couple of remarks can be made by analyzing the optimal capacities of the system components in table 8-10. The capacities presented in the tables indicate that the optimal size of the hydrogen gas storage tank correlates with the size of the RSOC device. Furthermore, the tables show that it is beneficial to install a bigger ground source HP in the RSOC and hydrogen gas storage system if the district heating prices increase with 25%.

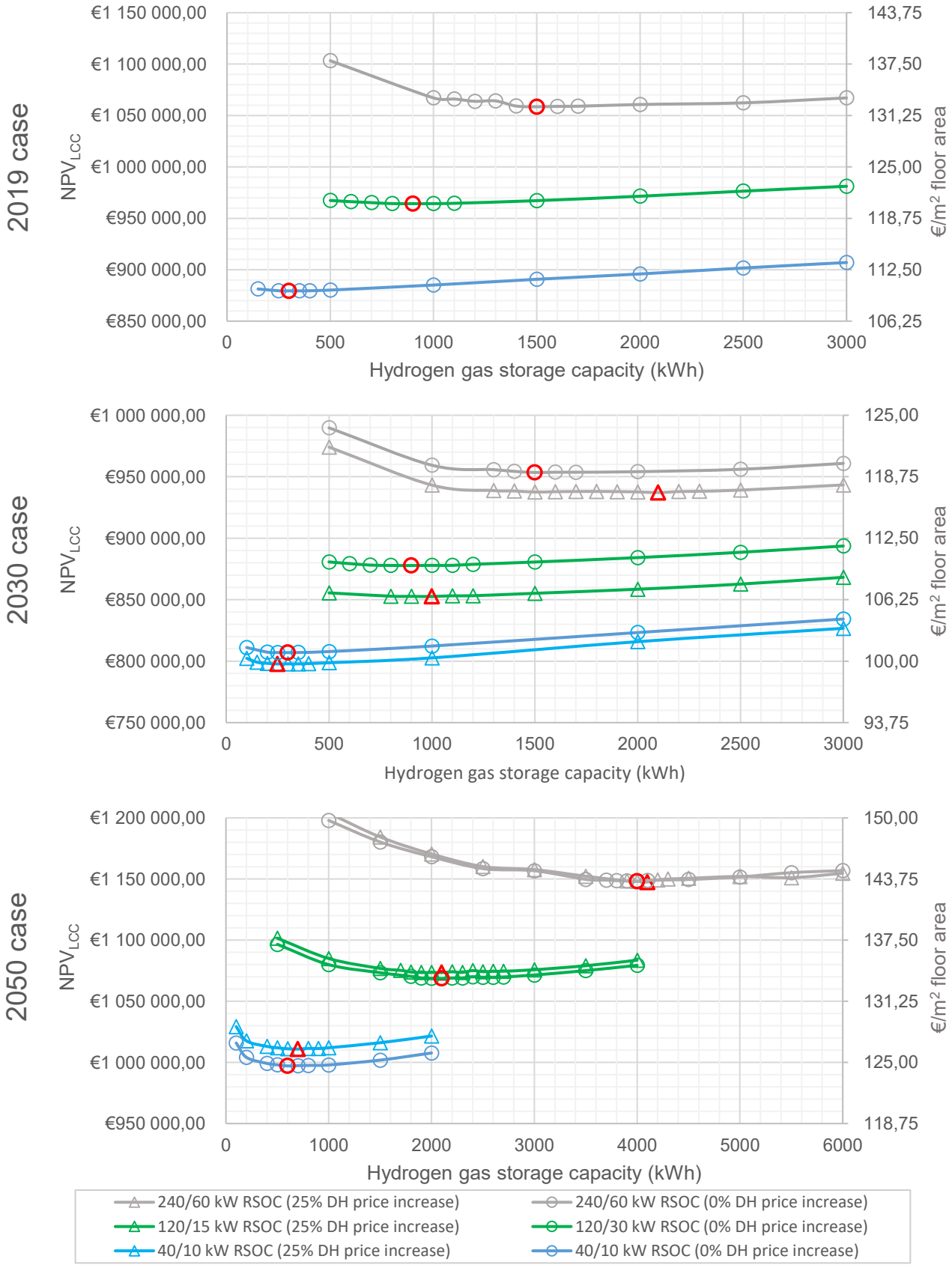

Figure 20: Optimal NPV_{LCC} of a RSOC and hydrogen gas storage system as a function of the hydrogen gas storage capacity. Three different RSOC device sizes and two different district heating price scenarios are presented per case.

Table 8: Optimal system component capacities for each RSOC size in the 2019 case.

RSOC (kW)	40/10	120/30	240/60
Hydrogen gas storage (kWh)	300	900	1 500
Hot water TES (kWh)	70	90	10
Battery (kWh)	0	10	10
Ground source HP (kW)	50	50	50
Grid connection (kW)	200	300	350
District heating connection (kW)	230	160	120

Table 9: Optimal system component capacities for each RSOC size and district heating price scenario in the 2030 case.

RSOC (kW)	40/10		120/30		240/60	
District heating price scenario	0%	25%	0%	25%	0%	25%
Hydrogen gas storage (kWh)	300	250	900	1 000	4 000	4 100
Hot water TES (kWh)	50	50	110	110	10	200
Battery (kWh)	0	1	10	10	10	10
Ground source HP (kW)	50	100	50	100	50	75
Grid connection (kW)	200	200	300	300	300	350
District heating connection (kW)	230	220	160	110	170	100

Table 10: Optimal system component capacities for each RSOC size and district heating price scenario in the 2050 case.

RSOC (kW)	40/10		120/30		240/60	
District heating price scenario	0%	25%	0%	25%	0%	25%
Hydrogen gas storage (kWh)	600	700	2 100	2100	4 000	4 100
Hot water TES (kWh)	50	100	200	250	10	200
Battery (kWh)	10	10	10	10	10	10
Ground source HP (kW)	25	50	50	75	50	75
Grid connection (kW)	200	200	300	300	300	350
District heating connection (kW)	250	230	160	130	170	100

6.2 Optimal operation

Graphs showing the optimal annual operation of the RSOC and hydrogen gas storage system for the standard district heating price scenario are presented in the appendix. These graphs show a time series-specific representation of the hydrogen gas storage and TES states, the ground source HP operation as well as the system interaction with the grid and the district heating network. Positive district heating rates indicate that heat is imported and negative district heating rates indicate that heat is exported to the district heating network.

The graphs indicate that there is a connection between the electricity price and the state of the hydrogen gas storage. According to the graphs the hydrogen gas storage is filled when electricity prices are low and emptied when electricity prices are high. Thus, it can be confirmed that the RSOC and hydrogen gas storage system works as intended.

There are a few other interesting remarks about the optimal operation of the system. By examining the graphs in the appendix, it can be observed that the operating mode of the RSOC is changed nine to twelve times per week in the 2019 and 2030 cases. In the 2050 case, where the hydrogen storage capacity is two times higher than in the 2019 and 2030 cases, the RSOC mode is changed four to six times a week. It can thus be assumed that the hydrogen storage capacity affects how frequent the operating mode is changed.

Variation in electricity spot prices and district heating prices seems to affect the interaction with the district heating network. In the 2019 case, where the electricity prices are at an intermediate level and the district heating prices are low compared to the 2030 and 2050 cases, district heating is utilized from November to March. During the rest of the year, heat is sold to the district heating network. The heat export rate fluctuates between 0 and 50 kW. The same district heating network interaction behavior is observed in the 2050 case, where both district heating and electricity is expensive. The only noticeable difference between the 2050 and 2019 case, is that the heat export rate fluctuates even more in the 2050 case than in the 2019 case.

In the 2030 case, where thermal energy generated by the HP is cheap (as a result of cheap electricity) and district heating prices are high, district heating is only used during the coldest days of the year. As in the 2019 case, heat is exported to the district heating network during the other days of the year. The heat export rate is however less fluctuating than in the other cases and the maximum heat export rate is about twice as high as in the other cases.

In the 2019 and 2050 cases the ground source HP is almost constantly operating at maximum power from October to April. From May to September the output power of the HP varies between zero and maximum output power. In the 2030 case, where it is profitable to export thermal energy generated by the HP, the HP is operating at maximum power all year round.

For the TES operation there is no clear pattern. The TES seems to operate mainly for heat balancing purposes. The battery storage, which is clearly a faster and more flexible electrical energy storage than the hydrogen gas storage, handles the most dramatic demand fluctuations of the office building.

6.3 Competitiveness analysis

The performance of an energy system can be apprised by calculating how much money is saved by investing in the system. This is done by determining the present value (PV) of total cost savings for the energy system. The PV of total cost savings is here the NPV_{LCC} of a reference energy system minus the NPV_{LCC} of the tested system. The reference energy system used in this study is a system consisting of only district heating and grid connections.

Figure 21 presents the PV of total cost savings during a 20 year service life for the RSOC and hydrogen storage system as well as for a system comprised of a ground source HP, a district heating connection and a grid connection (hereinafter referred to as a ground source HP system). The RSOC device costs are not taken into account in the NPV_{LCC} of the RSOC and hydrogen gas storage system.

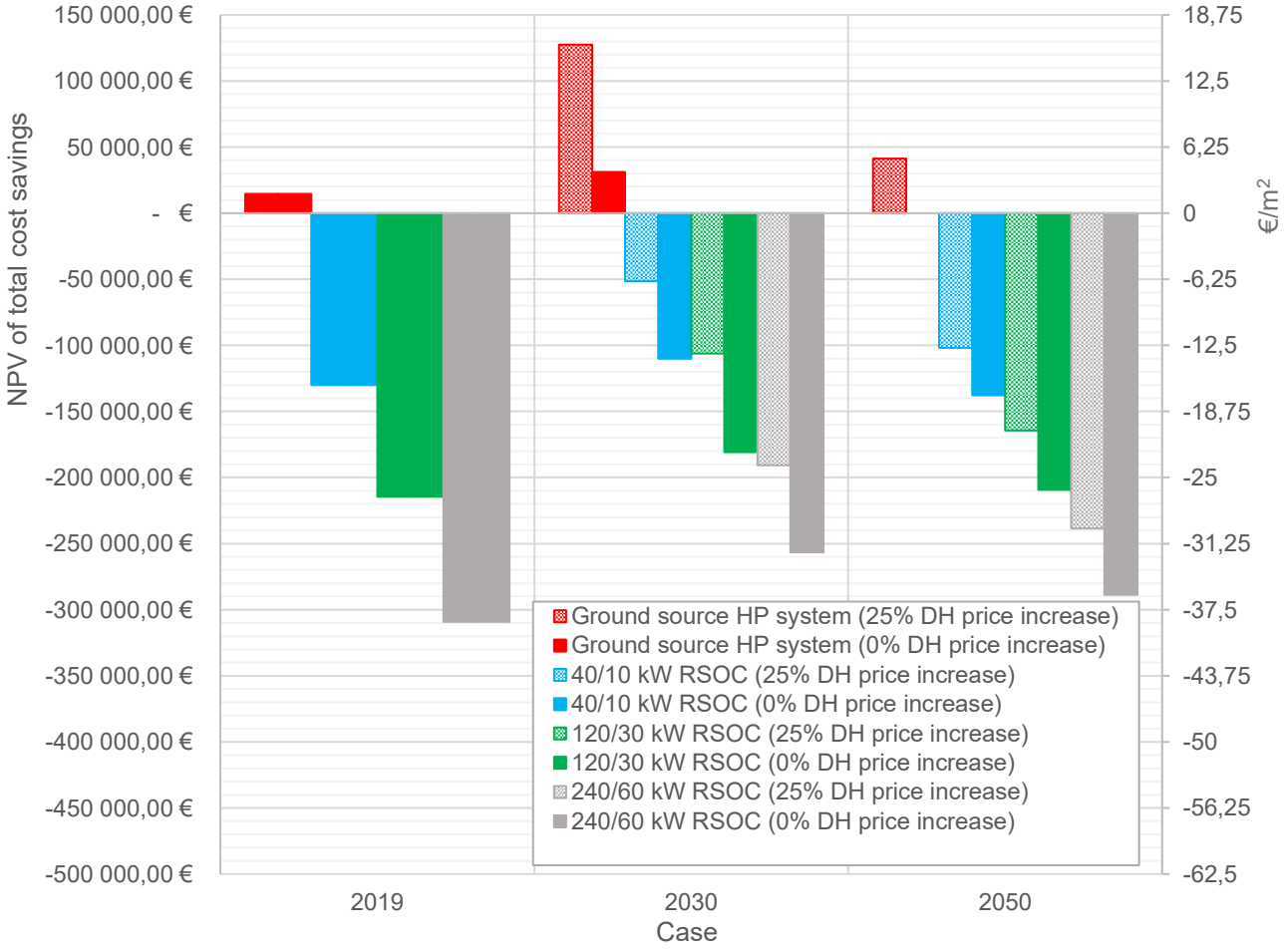

Figure 21: PV of total cost savings (during a 20 year service life) for the RSOC and hydrogen gas storage systems (RSOC costs excluded) as well as for the ground source HP system.

The graphs in figure 21 show that the ground source HP system is clearly the most remunerative energy system. In all cases except for in the 2050 case with a 0% increase in district heating prices, it is possible to save money by installing a ground source HP. The optimal ground source HP dimensions for all cases and district heating scenarios are presented in table 11.

Table 11: Optimal ground source HP capacities for the ground source HP system.

Case	2019	2030		2050	
District heating price scenario	0%	0%	25%	0%	25%
Ground source HP capacity (kW)	75	75	200	0	50

The 25% district heating price increase in the future cases benefits both the ground source HP system and the RSOC and hydrogen gas storage system cost savings. The total cost savings for the RSOC and hydrogen gas storage system are still negative in all cases and for all district heating price scenarios. The RSOC and hydrogen gas storage system is thus outperformed by the system with only district heating and grid connections. This implies that it is not worthwhile investing in an RSOC and hydrogen gas storage system for an office building.

6.3.1 Cost structure comparison

The optimal cost structures of the RSOC and hydrogen gas storage system (excluding the costs of the RSOC device), the ground source HP system and the system with only district heating and grid connections are presented in figure 22 and table 12-14. The optimal cost structure is here expressed as segments of the optimal system NPV_{LCC} for the standard district heating price scenario.

The figure and the tables show that the RSOC and hydrogen storage system has lower OPEX (i.e. annual fixed and variable costs) than the system with only district heating and grid connections. The ground source HP system has the lowest OPEX of the three systems in every case. This is partly caused by the negative district heating costs. Negative district heating costs mean that the revenue of heat sold to the district heating network is higher than the cost of imported heat. Because of the high COP of the HP it is profitable to produce heat with the HP and then sell it to the district heating network.

In the 2030 case the OPEX of the RSOC and hydrogen gas storage system is only 4.6% higher than the OPEX of the ground source HP system. The district heating costs for the RSOC and hydrogen gas storage system is also slightly more negative than for the ground source HP system in the 2030 case.

Of the three energy systems, the RSOC and hydrogen gas storage system has the highest CAPEX (i.e. investment costs) in all cases. The hydrogen gas compressor represents a substantial part of the CAPEX for the RSOC and hydrogen gas storage system. If the hydrogen gas compressor costs

and the RSOC device costs were excluded from the NPV_{LCC}, the RSOC and hydrogen gas storage system would be more remunerative than the district heating and grid connection system in the 2030 and 2050 cases. The RSOC and hydrogen gas storage system would however not be more lucrative than the ground source HP system, even though the hydrogen gas compressor and the RSOC device costs would be neglected.

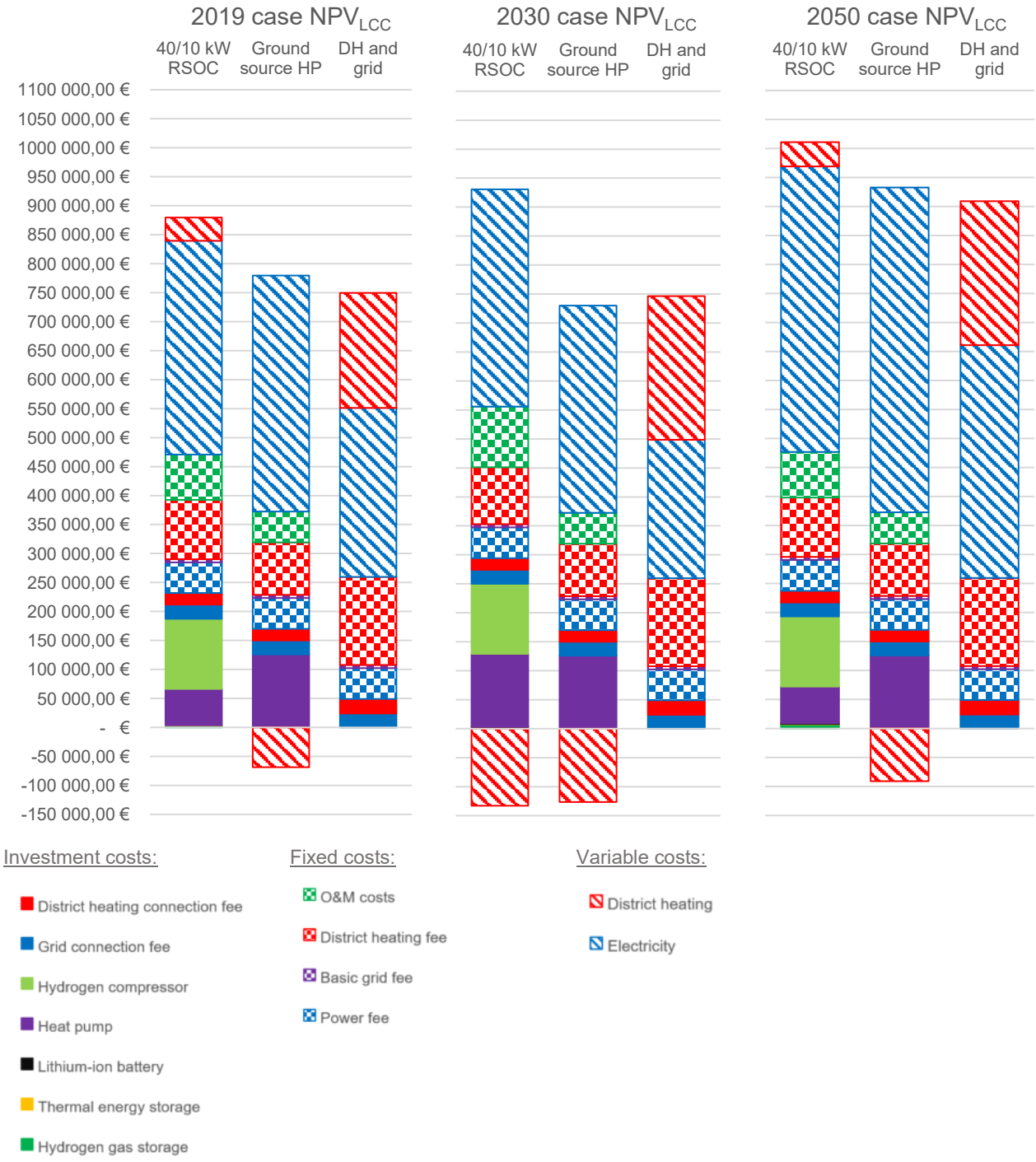

Figure 22: Optimal NPV_{LCC} segments of the 40/10 kW RSOC and hydrogen storage system (excluding the RSOC device cost), the ground source HP system and the system with only district heating (DH) and grid connections. The 25% district heating price increase scenario is applied.

Table 12: NPV_{LCC} segments for 2019.

	Cost	40/10 kW RSOC	Ground source HP	District heating and grid con.
Investment costs	Hydrogen gas storage	3 213 €		
	TES	350 €		
	Lithium-ion battery			
	Ground source HP	63 000 €	126 000 €	
	Hydrogen gas compressor	121 030 €		
	Grid connection	24 200 €	24 200 €	24 200 €
	District heating connection	20 000 €	20 000 €	25 000 €
Annual fixed costs	Power fee	53 140 €	53 140 €	53 140 €
	Basic grid fee	5 403 €	5 403 €	5 403 €
	District heating fee	102 230 €	90 473 €	151 920 €
	O&M costs	78 172 €	53 394 €	
Annual variable costs	Electricity	368 590 €	406 840 €	291 390 €
	District heating	40 042 €	-68 489 €	198 300 €
Total	Total NPV_{LCC}	879 370 €	710 961 €	749 353 €

Table 13: NPV_{LCC} segments for 2030.

	Cost	40/10 kW RSOC	Ground source HP	District heating and grid con.
Investment costs	Hydrogen gas storage	2 678 €		
	TES	250 €		
	Lithium-ion battery	128 €		
	Ground source HP	126 000 €	126 000 €	
	Hydrogen gas compressor	121 030 €		
	Grid connection	24 200 €	24 200 €	24 200 €
	District heating connection	20 000 €	20 000 €	25 000 €
Annual fixed costs	Power fee	53 140 €	53 140 €	53 140 €
	Basic grid fee	5 403 €	5 403 €	5 403 €
	District heating fee	98 312 €	90 473 €	151 920 €
	O&M costs	104 850 €	53 394 €	
Annual variable costs	Electricity	374 680 €	357 610 €	238 890 €
	District heating	-132 930 €	-126 450 €	247 880 €
Total	Total NPV_{LCC}	797 741 €	603 770 €	746 433 €

Table 14: NPV_{LCC} segments for 2050.

	Cost	40/10 kW RSOC	Ground source HP	District heating and grid con.
Investment costs	Hydrogen gas storage	7 497 €		
	TES	500 €		
	Lithium-ion battery	1 280 €		
	Ground source HP	63 000 €	126 000 €	
	Hydrogen gas compressor	121 030 €		
	Grid connection	24 200 €	24 200 €	24 200 €
	District heating connection	20 000 €	20 000 €	25 000 €
Annual fixed costs	Power fee	53 140 €	53 140 €	53 140 €
	Basic grid fee	5 403 €	5 403 €	5 403 €
	District heating fee	102 230 €	90 473 €	151 920 €
	O&M costs	78 543 €	53 394 €	
Annual variable costs	Electricity	492 470 €	560 190 €	401 470 €
	District heating	41 613 €	-90 766 €	247 880 €
Total	Total NPV_{LCC}	1 010 906 €	842 034 €	909 013 €

6.3.2 Payback time

The payback time is the time it takes to pay back the investment costs. In this study however, the payback time is the system life span needed for the NPV_{LCC} for the tested system to be equal to the NPV_{LCC} for the reference system (the system with only district heating and grid connections). The system is more lucrative than the reference system if the life span of the system is longer than the payback time.

The graphs in figure 23 shows the NPV_{LCC} for the different energy systems as a function of the time period of operation. When the graphs are studied it can be observed that payback time for the RSOC and hydrogen gas storage system could be reached in the 2030 case, if the service life of system could be extended with 15 years and if the costs of the RSOC device itself are not taken into account. In the 2019 and 2050 cases, a 15 year longer service life would only close the gap between the NPV_{LCC} for the RSOC and hydrogen gas storage system and the reference system with 9% and 19%, respectively.

The payback time for the ground source HP system is 15 years in the 2019 case, ten years in the 2030 case and eight years in the 2050 case. The payback time for 2030 is longer than the payback time for 2050 because a bigger HP with higher investment costs is installed in the 2030 case. In the 2030 case, the delta NPV_{LCC} (the NPV_{LCC} for the ground source HP system minus the NPV_{LCC} for the reference system) does however decrease faster with time than in the 2050 case. The reason to this behavior is that the NPV_{LCC} of the system is minimized for a time period of 20 years, and not for a time period of eight years.

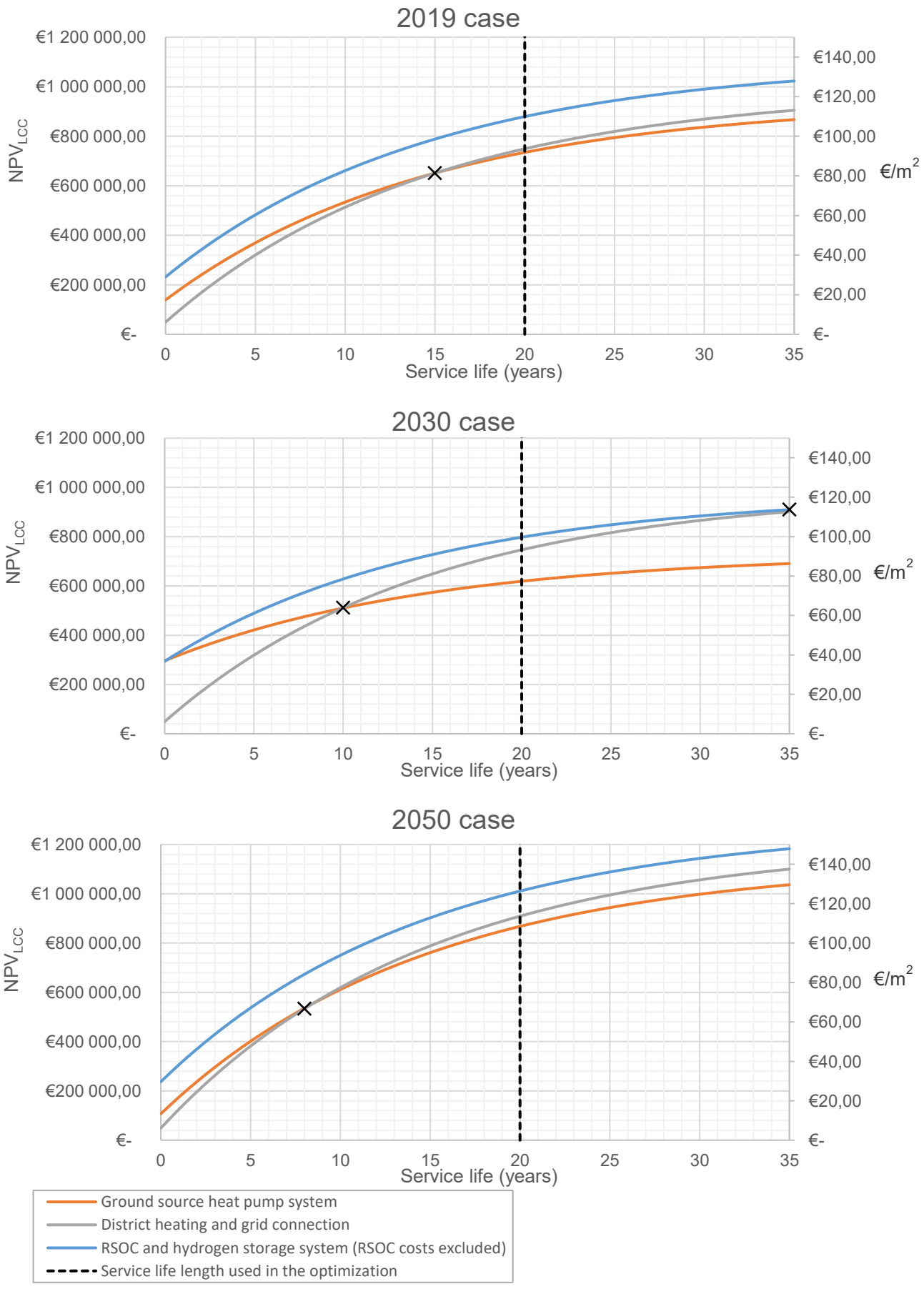

Figure 23: NPV of total costs as a function of the service life length.

7 CONCLUSIONS

The emphasis of this thesis work was to study the competitiveness as well as the optimal operation and configuration of an RSOC and hydrogen gas storage system for office buildings. The optimal operation and configuration was determined by minimizing the net present value of the system lifecycle cost (NPV_{LCC}). The competitiveness of the system was evaluated by comparing the optimal NPV_{LCC} of the RSOC and hydrogen gas storage system with the optimal NPV_{LCC} of alternative energy systems. Three cases with electricity spot prices for 2019, 2030 and 2050 were simulated in the study. Two different district heating price scenarios were also tested.

The NPV_{LCC} minimizing optimization problem was expressed as a bilevel optimization problem, consisting of a NPV_{LCC} minimizing upper level problem and a variable costs minimizing lower level problem. A mixed integer linear programming (MILP) optimization algorithm was written to minimize variable costs in the lower level problem, while the upper level problem was optimized by manually generating a solution matrix.

When the NPV_{LCC} of the RSOC and hydrogen gas storage system was compared with the NPV_{LCC} of a ground source HP system and a standard energy system consisting of only district heating and grid connections, it was shown that the RSOC and hydrogen gas storage system was the least remunerative energy system. Due to its high CAPEX and its poor performance compared to the ground source HP system, the RSOC and hydrogen gas storage system was outperformed by both of the alternative energy systems.

The hydrogen gas compressor represents a significant part of the CAPEX of the RSOC and hydrogen gas storage system. In the 2019 and 2050 cases, the hydrogen gas compressor cost is higher than the investment cost of the 50 kW ground source HP, the district heating connection fee and the grid connection fee combined.

The ground source HP system was shown to be the most lucrative energy system. In the 2030 case, where electricity prices are low and district heating prices are high, up to 16 €/m^2 could be saved per year by installing a ground source HP instead of only relying on district heating. If an RSOC and hydrogen gas storage system would be installed instead, 6.25 €/m^2 would be lost per year (also the 2030 case), if the investment cost of the RSOC device itself is not taken into account.

It should be noted that the results of this study are only approximations based on available price data and predictions. The mathematical assumptions in this study might also not fully correspond to the operation of a real RSOC and hydrogen gas storage system. Changes in prices during the life span of the investments are not taken into account in the model either. Because of the many inaccuracies in the model, the results of this study should only be taken as indicative estimates.

As long as there is an even supply of electricity and no critical need to store electrical energy, it will be difficult to find a market for the RSOC and hydrogen gas storage system as a stationary electricity storage. A recommendation for further research would therefore be to investigate the techno-economic performance of RSOC and hydrogen gas storage systems for off-grid power solutions with high variable energy generation shares and no back-up power generation. The possibility to export oxygen generated by RSOC in SOEC mode would also need further investigation.

8 SVENSK SAMMANFATTNING

8.1 Inledning

I en undersökning av Helistö et al. vid teknologiska forskningscentralen VTT framgår det att en ökning av vind- och solenergi kan leda till större elprisvariationer i framtiden. Om mängden vind- och solenergi ökar, så kommer elpriserna enligt Helistö et al. att sjunka fram till år 2030 p.g.a. överkapacitet. Denna överkapacitet beror på att gamla kraftverk fortfarande är i drift trots att nya vindkraftverk och solpaneler installeras. Allt efter att de gamla kraftverken läggs ner kommer andelen vind- och solenergi i elnätet att öka drastiskt, vilket leder till höga elpriser under en stor del av året. Elpriset för den billigaste 30 procenten av året förblir dock ungefär samma som för år 2030. Detta leder till att det år 2050 kommer att finnas ett större antal timmar med extremt höga elpriser och dessutom ett större antal timmar med väldigt låga elpriser.

Detta fenomen ökar intresset för att utveckla metoder för lagring av elektricitet. Att lagra elektricitet då elpriserna är låga och använda lagret då elpriserna är höga kan ge en ekonomisk fördel. I detta diplomarbete undersöks därför ifall det är lönsamt att i kontorsbyggnader installera ett system som lagrar elektricitet med hjälp av reversibel fast oxid cell- (RSOC) och vätgaslagringsteknologi.

8.2 Teori

8.2.1 Reversibel fast oxid cell

En RSOC är en elektrokemisk apparat som kan fungera antingen som elektrolytisk cell eller som bränslecell. Genom att mata in vatten i apparaten, så kan man producera vätgas (och syrgas) med hjälp av elektricitet och genom att mata in vätgas och syrgas in i apparaten så kan man generera el (och producera vatten). Om man kopplar ihop apparaten med ett vätgaslager, är det möjligt att lagra elektricitet i form av vätgas.

Då RSOC:en fungerar som elektrolytisk cell sker en redoxreaktion. I reduktionsreaktionen donerar en negativt laddad katod elektroner till vattenmolekyler, som i sin tur klyvs så att det bildas vätgasmolekyler och negativt laddade syrejoner. Syrejonerna transporteras sedan genom en fast elektrolyt och donerar elektroner till anoden i en oxidationsreaktion, vilket leder till att syrgas bildas. Vätgasen som bildas i redoxreaktionen kan man lagra i trycksatta vätgastankar.

Även i bränslecellsläget sker en redoxreaktion, men i denna reaktion är det syrgas som tar emot elektroner från katoden och bildar syrejoner. Syrejonerna transporteras genom elektrolyten och reagerar med vätgas och bildar vatten. I samband med denna reaktion doneras elektroner till anoden, vilket ger upphov till en elektrisk ström.

8.2.2 Vätgaslagring

Kostnadseffektiv lagring av vätgas är utmanande, eftersom vätgas har en väldigt låg densitet. Det finns flera olika metoder att öka vätgasens densitet för att uppnå en lönsammare lagring. Trycksatt lagring av vätgas är den metod som i dagens läge är mest lönsam. Fördelarna med att lagra vätgas vid högt tryck är att lagringen kan ske vid omgivningens temperatur och att materialkostnaderna är lägre än för andra vätgaslagringsmetoder.

8.3 Mål och problemställning

Målet med denna studie är att göra en teknisk-ekonomisk analys för ett RSOC och vätgaslagringssystem för kontorsbyggnader. VTT:s nya kontorsbyggnad, "VTT FutureHub", kommer att användas som testobjekt för energilagringssystemet. I den teknisk-ekonomiska analysen ingår att bestämma systemets optimala sammansättning och drift, samt att undersöka systemets konkurrenskraft.

Tre olika fall studeras i detta arbete. Ett fall där dagens elpriser används, samt två framtida fall med elpriser för 2030 och 2050. Dessutom testas två olika fjärrvärmeprisscenarier för de två framtida fallen; ett scenario där fjärrvärmeprisen inte antas stiga och ett scenario där fjärrvärmepriserna för 2030 och 2050 är 25 procent högre än fjärrvärmeprisen för år 2019.

8.4 Optimeringsmetod

För att bestämma systemets optimala sammansättning och drift, bör man minimera nettonuvärdet av systemets livscykelkostnader (NPV_{LCC}). Beräkning av energilagringssystemets NPV_{LCC} förutsätter att systemets investeringskostnader och årliga kostnader är kända. Investeringskostnaderna och de fasta årliga kostnaderna är beroende av de olika systemkomponenternas dimensioner. De årliga rörliga kostnaderna är däremot beroende av hur man driver systemet. Systemets drift begränsas dock av systemkomponenternas dimensioner.

Optimeringen av systemets NPV_{LCC} kommer att bestå av två olika nivåer; en övre nivåns optimering och en undre nivåns optimering. Den övre nivåns optimering är huvudoptimeringen, dvs. optimeringen av systemets NPV_{LCC}, medan den undre nivåns optimering optimerar systemets drift.

Den undre nivåns optimeringsproblem är ett tidsserieproblem med en binär variabel för varje tidssteg. Den binära variabeln bestämmer om RSOC:en drivs som bränslecell eller som elektrolytisk cell. De övriga variablerna består av olika energiöverföringar, som begränsas av systemkomponenternas dimensioner. De matematiska funktionerna för RSOC:en, samt alla övriga matematiska funktioner i problemet linjäriseras för att förenkla optimeringsproblemet. Eftersom optimeringsproblemet då består av endast linjära funktioner och både heltalsvariabler och reella variabler, så kommer klassificeras optimeringsproblemet som ett MILP (mixed integer linear programming) problem.

Eftersom noggrannheten av lösningen till den undre nivåns optimeringsproblem är beroende av antalet tidssteg, så föredras ett stort antal tidssteg. Men då antalet tidssteg ökar så ökar även antalet binära variabler, vilket leder till att beräkningstiden för problemet ökar drastiskt. Därför har en optimeringsalgoritm utvecklats för att minska beräkningstiden. Den övre nivåns optimering sker dock manuellt, genom att systematiskt konstruera en lösningsmatris.

I optimeringsalgoritmen börjar man med att optimera hela tidsintervallet (ett år) och spika fast energilagernivåerna för intervallets ändpunkter och mittpunkt. Efter detta delar man intervallet i två lika stora delintervall och upprepar proceduren genom att optimera delintervallen skilt med samma antal tidssteg som i första optimeringen. Sedan fastställer lagernivåerna för mittpunkten, delar intervallet, optimerar och upprepar processen igen. För varje optimeringssteg kommer då längden på tidsstegen att minska. Processen avbryts då önskad steglängd uppnåtts.

8.5 Resultat

8.5.1 Optimal systemsammansättning

Enligt optimeringsmodellen är RSOC och vätelagringssystemet med den minsta möjliga RSOC-apparaten mest optimal. Den minsta RSOC-apparaten som antas ha en maximal input-effekt på 40 kW i elektrolysläge och en maximal output-effekt på 10 kW i bränslecellsläge. De optimala dimensionerna för de övriga systemkomponenterna presenteras i tabellerna 8-10 på sidan 50. Tabellerna visar bl.a. att vätgaslagrets optimala kapacitet är beroende av RSOC-apparatens storlek.

8.5.2 Optimal drift

Den optimala driften av systemet beskrivs av graferna i appendix. Då man studerar graferna kan man konstatera att vätgaslagret fylls då elpriserna är låga och töms då elpriserna är höga. Hur ofta man byter läge på RSOC-apparaten beror på vätgaslagrets storlek.

Även värmeexporten till fjärrvärmenätet styrs av elpriserna, ty då elpriserna är låga som i 2030 fallet så genererar värmepumpen kontinuerligt maximal värme, som sedan exporteras till fjärrvärmenätet. Då elpriserna är höga eller då fjärrvärmepriserna är låga så exporteras inte lika mycket värme till fjärrvärmenätet.

8.5.3 Lönsamhetsanalys

Då man jämför livscykelkostnaden för RSOC och vätgaslagringssystemet med livscykelkostnaderna för alternativa energisystem så kan man konstatera att det inte lönar sig att investera i ett RSOC och vätgaslagringssystem. På grund av systemets höga investeringskostnader och otillräckliga prestation, så klarar RSOC och vätgaslagringssystemet inte av att konkurrera med de alternativa energisystemen. Det mest lönsamma energisystemet som testades bestod av en jordvärmepump samt koppling till fjärrvärmenätet och elnätet.

8.6 Slutsatser

Då man studerar resultaten kan konstatera att det inte är lönsamt att investera i ett RSOC och vätgaslagringssystem för kontorsbyggnader. Investeringskostnaderna för systemet är för höga i jämförelse med övriga energisystem och systemet presterar dessutom sämre än ett energisystem med jordvärmepump. Så länge det finns kontinuerlig tillgång till elektricitet, så kommer det att vara svårt för RSOC och vätgaslagringssystem att slå igenom på marknaden.

9 REFERENCES

Buttler, A., Spliethoff, H., 2018. Current status of water electrolysis for energy storage, grid balancing and sector coupling via power-to-gas and power-to-liquids: A review. Renewable and Sustainable Energy Reviews. doi:10.1016/j.rser.2017.09.003

Carrette, L., Friedrich, K.A., Stimming, U., 2002. Fuel Cells - Fundamentals and Applications. Fuel Cells 1, 5–39. doi:10.1002/1615-6854(200105)1:1<5::aid-fuce5>3.0.co;2-g

Caruna Espoo Oy, 2018. https://caruna-cms-prod.s3-eu-west-1.amazonaws.com/web_30742941_caruna_espoo_ces_liittymishinnasto_6s_2018_en.pdf?ZtuqaBExO5hr5aralR1ffzEjS29Z4eQb and http://caruna-cms-prod.s3-eu-west-1.amazonaws.com/web_30693845_caruna_ces_verkkopalveluhin_espoo_6s_2018_en.pdf?6dh3iBjwwfRAH2eDp9dCaQrR6DEgnb9b

Department of Energy, 2008. H2A Hydrogen Delivery Infrastructure Analysis Models and Conventional Pathway Options Analysis Results https://www.energy.gov/sites/prod/files/2014/03/f9/nexant_h2a.pdf

Donadei, S., Schneider, G.S., 2016. Compressed Air Energy Storage in Underground Formations, in: Storing Energy: With Special Reference to Renewable Energy Sources. Elsevier Inc., pp. 113–133. doi:10.1016/B978-0-12-803440-8.00006-3

Energiauutiset, 2018. Päästöoikeuden hinta 55 euroon 2030 mennessä. https://www.energiauutiset.fi/uutiset/paastooikeuden-hinta-55-euroon-2030-mennessa.html

Fortum, 2019. https://www.fortum.fi/kotiasiakkaille/sahkoa-kotiin/oman-tuotannon-myynti-lahisahko and https://www.fortum.fi/yrityksille-ja-yhteisoille/lammitys/kaukolampo/avoin-kaukolampo

Gómez, S.Y., Hotza, D., 2016. Current developments in reversible solid oxide fuel cells. Renewable and Sustainable Energy Reviews. doi:10.1016/j.rser.2016.03.005

Götz, M., Lefebvre, J., ... Kolb, T., 2016. Renewable Power-to-Gas: A technological and economic review. Renewable Energy. doi:10.1016/j.renene.2015.07.066

Hauck, M., Herrmann, S., Spliethoff, H., 2017. Simulation of a reversible SOFC with Aspen Plus. International Journal of Hydrogen Energy 42, 10329–10340. doi:10.1016/j.ijhydene.2017.01.189

Hawawini, G., Viallet, C., 2015. Finance for Executives

Helen, 2018. Sähkön siirtohinnasto. https://www.helensahkoverkko.fi/globalassets/hinnastot-ja-sopimusehdot/hsv/sahkon-siirtohinnasto.pdf

Helistö, N., Kiviluoma, J., Holttinen, H., 2017. Sensitivity of electricity prices in energy-only markets with large amounts of zero marginal cost generation, in: International Conference on the European Energy Market, EEM. IEEE Computer Society. doi:10.1109/EEM.2017.7981893

IEA-ETSAP (International Energy Agency - Energy Technology Systems Analysis Programme), IRENA (International Renewable Energy Agency), 2013. Thermal Energy Storage: Technology Brief.

IRENA (International Renewable Energy Agency), 2017. Electricity storage and renewables: costs and markets to 2030.

Jauslin Stebler AG, 2013. Erdgas-Röhrenspeicher Urdorf. http://www.jauslinstebler.ch/VGA/VEM/projekte/erdgas-roehrenspeicher-urdorf.html

KPMG, 2018. Cost of Capital Study 2018 https://assets.kpmg/content/dam/kpmg/ch/pdf/cost-of-capital-study-2018.pdf

Krieg, D., 2012. Forschungszentrum (FZ) Jülich: Konzept und Kosten eines Pipelinesystems zur Versorgung des deutschen Straßenverkehrs mit Wasserstoff

Laguna-Bercero, M.A., Kilner, J.A., Skinner, S.J., 2011. Development of oxygen electrodes for reversible solid oxide fuel cells with scandia stabilized zirconia electrolytes, in: Solid State Ionics. pp. 501–504. doi:10.1016/j.ssi.2010.01.003

Linde AG. 2019. https://www.linde-engineering.com/en/images/P_3_3_e_12_150dpi_tcm19-5774.pdf

Mazloomi, K., Gomes, C., 2012. Hydrogen as an energy carrier: Prospects and challenges. Renewable and Sustainable Energy Reviews. doi:10.1016/j.rser.2012.02.028

Makridis, 2016. Hydrogen storage and compression, in: Methane and Hydrogen for Energy Storage. Institution of Engineering and Technology, pp. 1–28. doi:10.1049/pbpo101e_ch1

MathWorks, 2019a. MATLAB. https://se.mathworks.com/products/matlab.html

MathWorks, 2019b. Mixed-Integer Linear Programming Algorithms https://se.mathworks.com/help/optim/ug/mixed-integer-linear-programming-algorithms.html

Nistor, S., Dave, S., ... Sooriyabandara, M., 2016. Technical and economic analysis of hydrogen refuelling. Applied Energy 167, 211–220. doi:10.1016/j.apenergy.2015.10.094

Nord Pool, 2019. https://www.nordpoolgroup.com/historical-market-data/

Office of energy efficiency and renewable energy, 2015. https://www.energy.gov/eere/fuelcells/physical-hydrogen-storage,

https://www.energy.gov/eere/fuelcells/hydrogen-storagee and https://www.energy.gov/eere/fuelcells/materials-based-hydrogen-storage

O'Callaghan-Gordo, C., Orta-Martínez, M., Kogevinas, M., 2016. Health effects of non-occupational exposure to oil extraction. Environmental Health: A Global Access Science Source. doi:10.1186/s12940-016-0140-1

Ozarslan, A., 2012. Large-scale hydrogen energy storage in salt caverns. International Journal of Hydrogen Energy 37, 14265–14277. doi:10.1016/j.ijhydene.2012.07.111

Pfenninger, S., Staffell, I., 2016. Long-term patterns of European PV output using 30 years of validated hourly reanalysis and satellite data. Energy 114, 1251–1265. doi:10.1016/j.energy.2016.08.060

Reznicek, E., Braun, R.J., 2018. Techno-economic and off-design analysis of stand-alone, distributed-scale reversible solid oxide cell energy storage systems. Energy Conversion and Management 175, 263–277. doi:10.1016/j.enconman.2018.08.087

Schaber, C., Mazza, P., Hammerschlag, R., 2004. Utility-scale storage of renewable energy. Electricity Journal 17, 21–29. doi:10.1016/j.tej.2004.05.005

Schoenung, S., 2011. Economic Analysis of Large-Scale Hydrogen Storage for Renewable Utility Applications, U.S. Department of Commerce.

Shemeikka, J., 2019. Energy demand simulation for the new VTT building.

Sinha, A., Malo, P., Deb, K., 2018. A Review on Bilevel Optimization: From Classical to Evolutionary Approaches and Applications. IEEE Transactions on Evolutionary Computation. doi:10.1109/TEVC.2017.2712906

Spickova, M., Myskova, R., 2015. Costs Efficiency Evaluation using Life Cycle Costing as Strategic Method. Procedia Economics and Finance 34, 337–343. doi:10.1016/s2212-5671(15)01638-x

Tilastokeskus, 2018. Uusiutuvien energialähteiden käyttö kasvoi sähkön ja lämmön tuotannossa 2017. http://www.stat.fi/til/salatuo/2017/salatuo_2017_2018-11-01_tie_001_fi.html

Wendel, C.H., Kazempoor, P., Braun, R.J., 2015. Novel electrical energy storage system based on reversible solid oxide cells: System design and operating conditions. Journal of Power Sources 276, 133–144. doi:10.1016/j.jpowsour.2014.10.205

World Energy Council, 2019. New Hydrogen Economy - Hope or Hype. https://www.worldenergy.org/wp-content/uploads/2019/06/WEInnovation-Insights-Brief-New-Hydrogen-Economy-Hype-or-Hope.pdf

Xu, J., Wang, R.Z., Li, Y., 2014. A review of available technologies for seasonal thermal energy storage. Solar Energy 103, 610–638. doi:10.1016/j.solener.2013.06.006

Zakeri, B., Syri, S., 2015. Electrical energy storage systems: A comparative life cycle cost analysis. Renewable and Sustainable Energy Reviews. doi:10.1016/j.rser.2014.10.011

Zoulias, E.I., Glockner, R., ... Taylor, P., 2006. Integration of hydrogen energy technologies in stand-alone power systems analysis of the current potential for applications. Renewable and Sustainable Energy Reviews. doi:10.1016/j.rser.2004.10.001

Züttel, A., 2004. Hydrogen storage methods. Naturwissenschaften. doi:10.1007/s00114-004-0516-x

APPENDIX

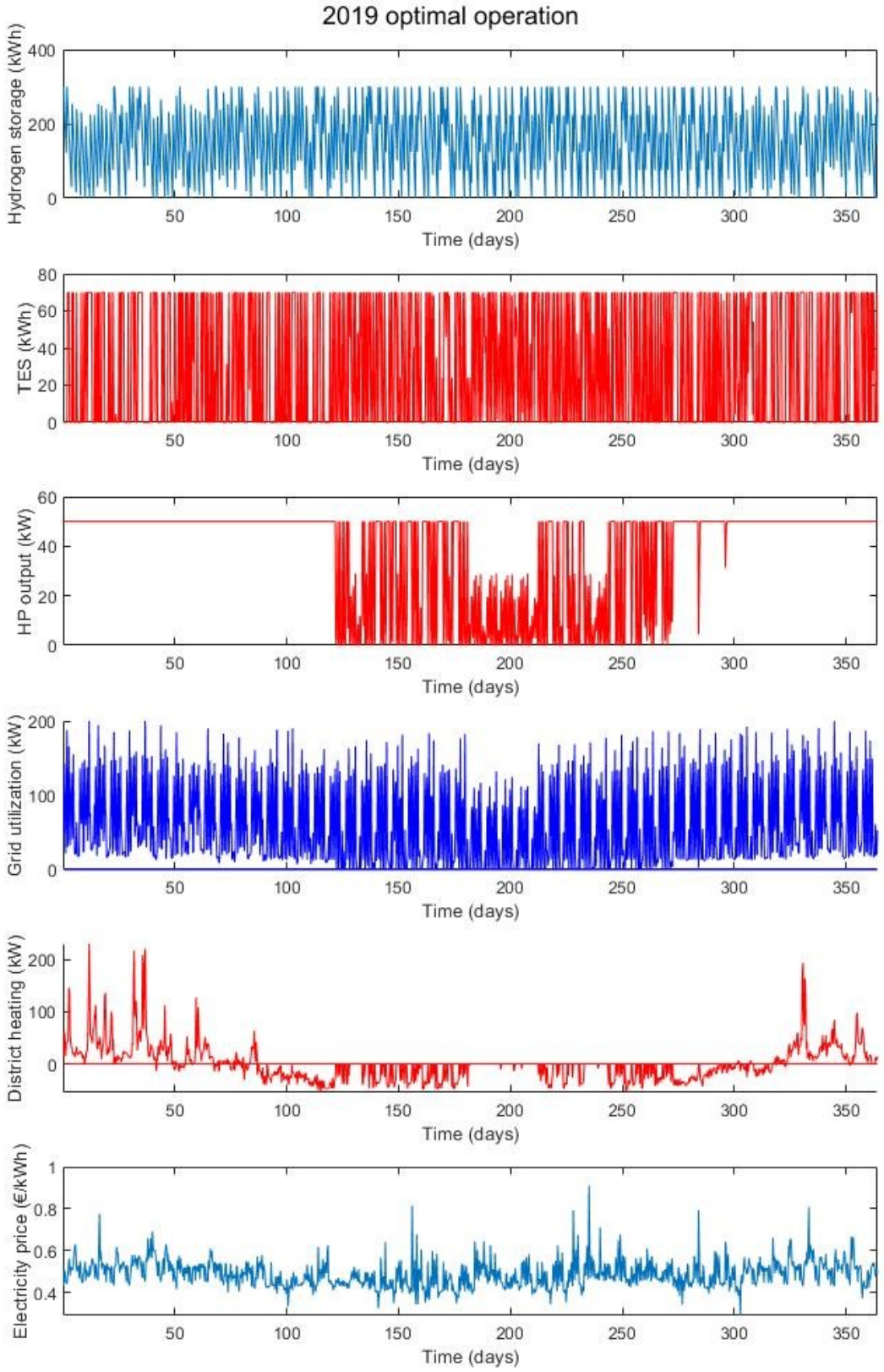
2019 optimal operation
Hydrogen storage (kWh)
TES (kWh)
HP output (kW)
Grid utilization (kW)
District heating (kW)
Electricity price (€/kWh)
Time (days)

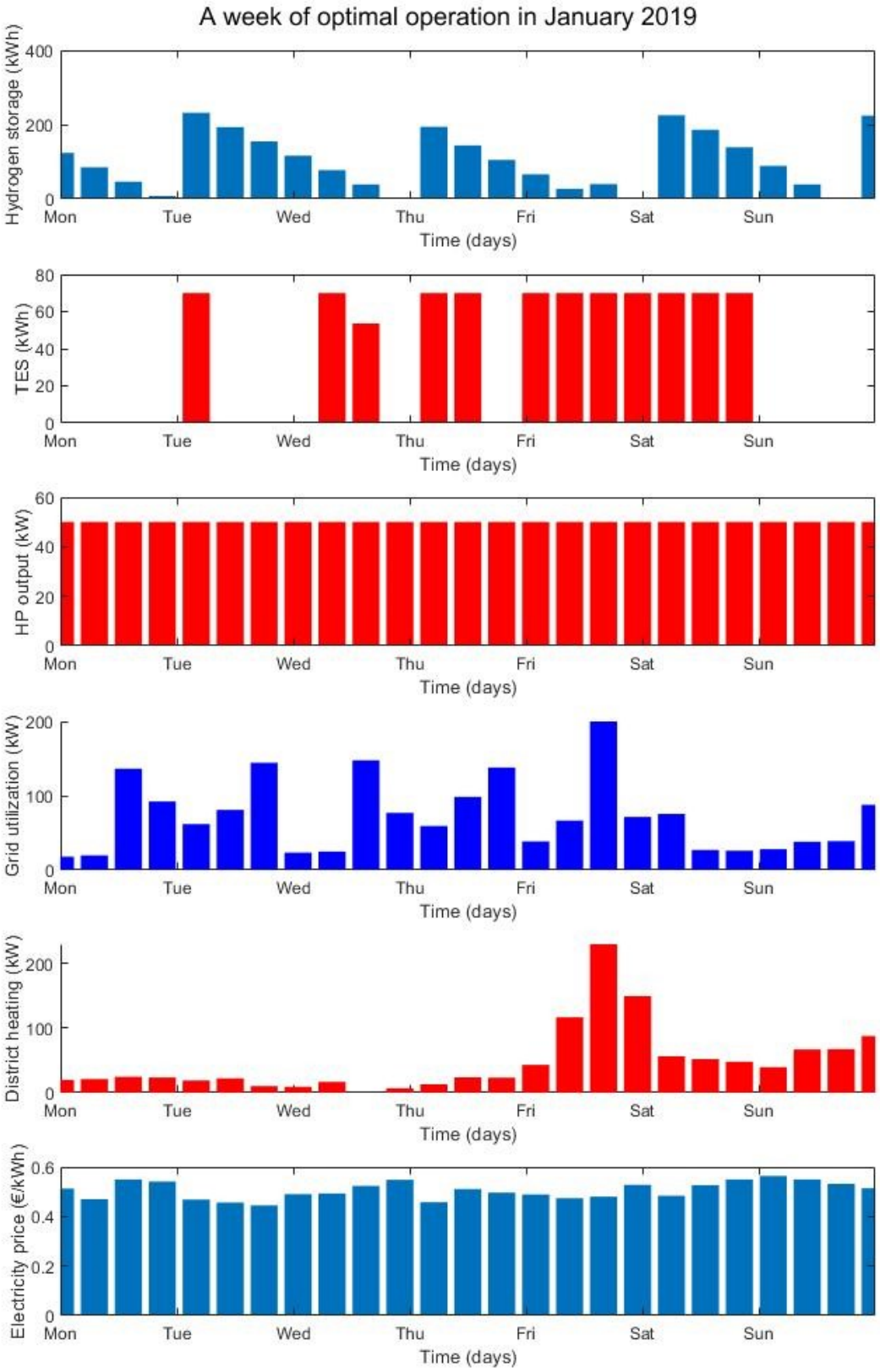
A week of optimal operation in January 2019
Hydrogen storage (kWh)
400
200
0
Mon
Tue
Wed
Thu
Fri
Sat
Sun
Time (days)
TES (kWh)
80
60
40
20
0
Mon
Tue
Wed
Thu
Fri
Sat
Sun
Time (days)
HP output (kW)
60
40
20
0
Mon
Tue
Wed
Thu
Fri
Sat
Sun
Time (days)
Grid utilization (kW)
200
100
0
Mon
Tue
Wed
Thu
Fri
Sat
Sun
Time (days)
District heating (kW)
200
100
0
Mon
Tue
Wed
Thu
Fri
Sat
Sun
Time (days)
Electricity price (€/kWh)
0.6
0.4
0.2
0
Mon
Tue
Wed
Thu
Fri
Sat
Sun
Time (days)

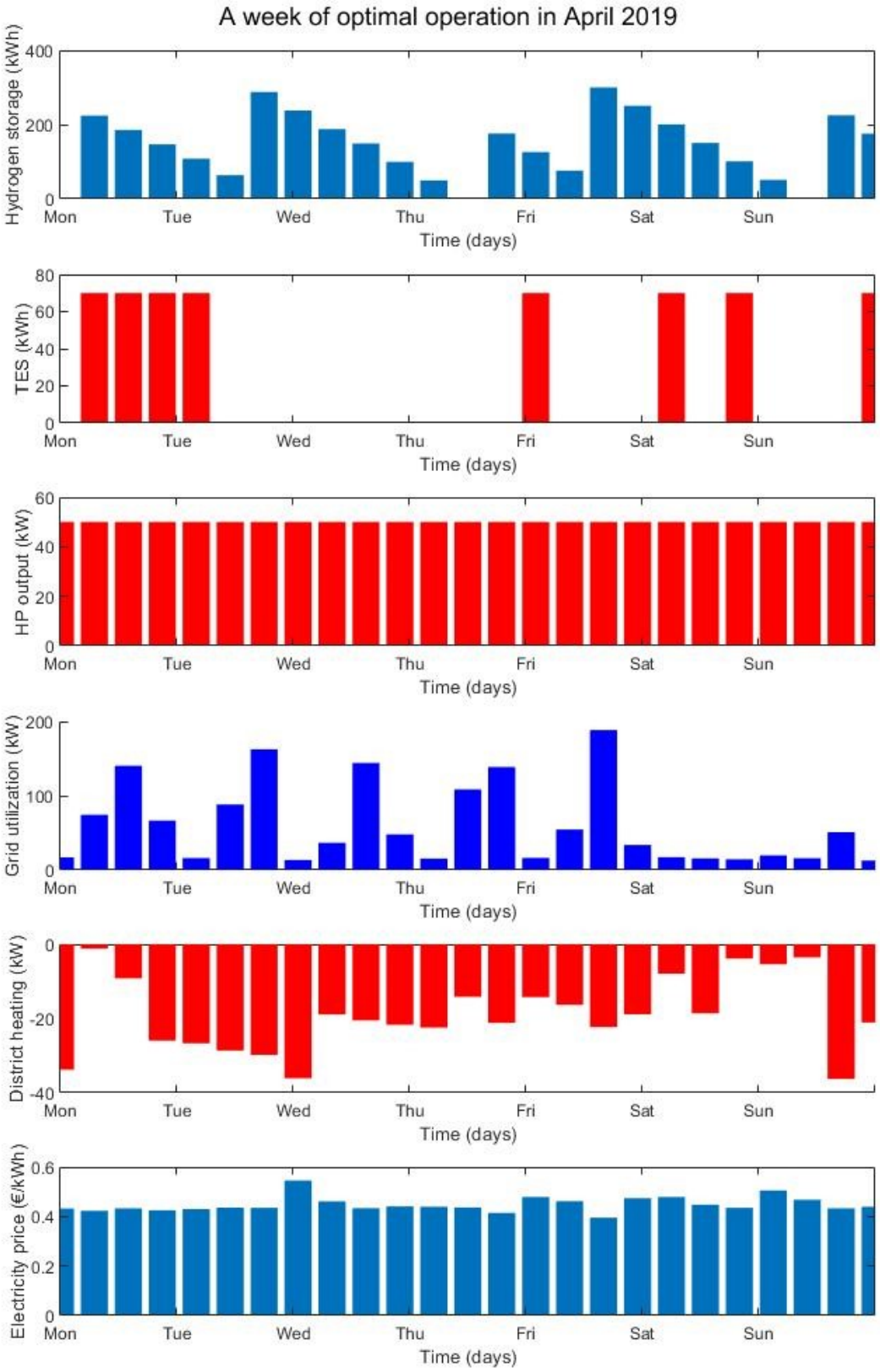
A week of optimal operation in April 2019
Hydrogen storage (kWh)
400
200
0
Mon
Tue
Wed
Thu
Fri
Sat
Sun
Time (days)
TES (kWh)
80
60
40
20
0
Mon
Tue
Wed
Thu
Fri
Sat
Sun
Time (days)
HP output (kW)
60
40
20
0
Mon
Tue
Wed
Thu
Fri
Sat
Sun
Time (days)
Grid utilization (kW)
200
100
0
Mon
Tue
Wed
Thu
Fri
Sat
Sun
Time (days)
District heating (kW)
0
-20
-40
Mon
Tue
Wed
Thu
Fri
Sat
Sun
Time (days)
Electricity price (€/kWh)
0.6
0.4
0.2
0
Mon
Tue
Wed
Thu
Fri
Sat
Sun
Time (days)

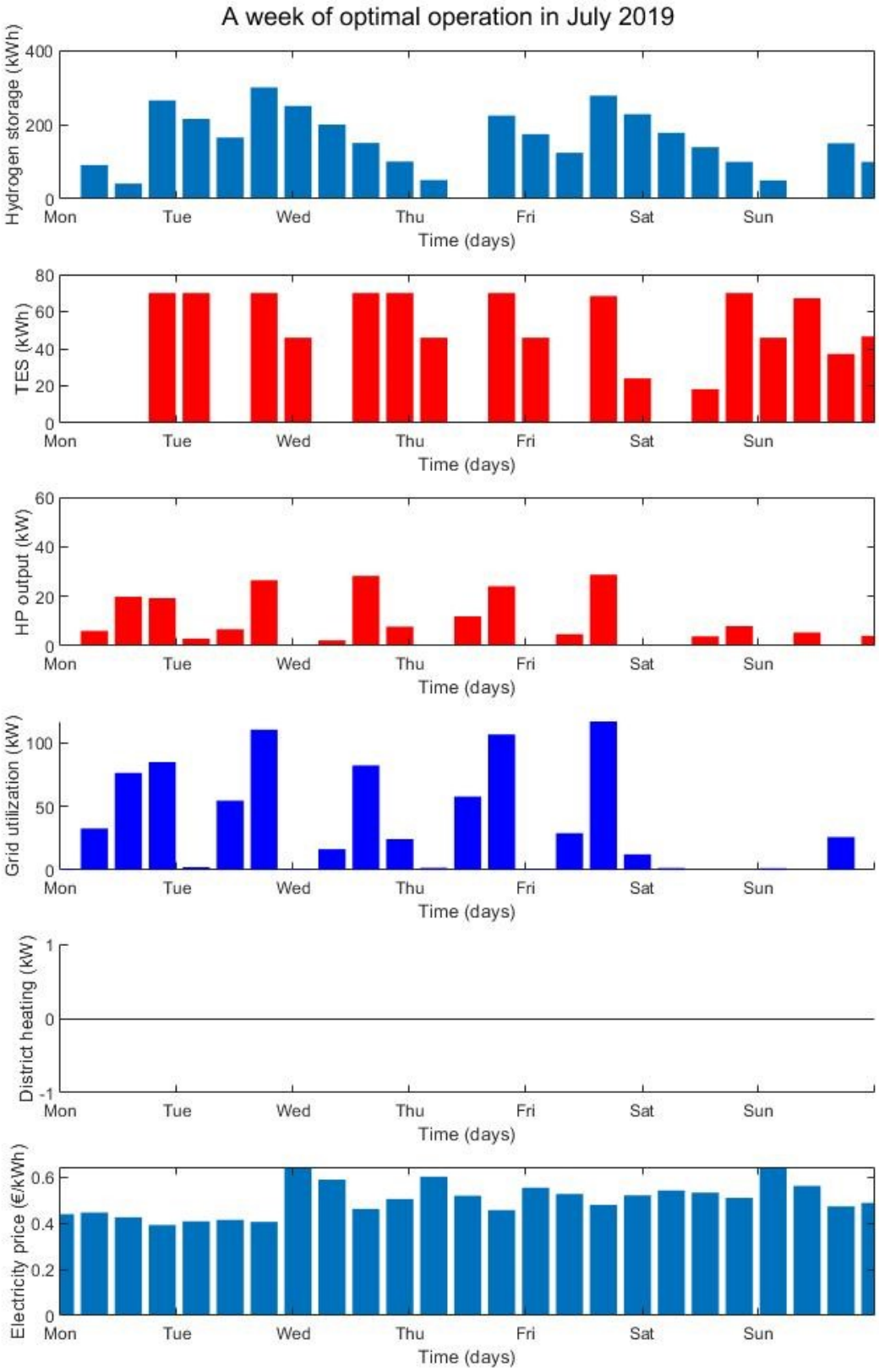
A week of optimal operation in July 2019
Hydrogen storage (kWh)
400
200
0
Mon
Tue
Wed
Thu
Fri
Sat
Sun
Time (days)
TES (kWh)
80
60
40
20
0
Mon
Tue
Wed
Thu
Fri
Sat
Sun
Time (days)
HP output (kW)
60
40
20
0
Mon
Tue
Wed
Thu
Fri
Sat
Sun
Time (days)
Grid utilization (kW)
100
50
0
Mon
Tue
Wed
Thu
Fri
Sat
Sun
Time (days)
District heating (kW)
1
0
-1
Mon
Tue
Wed
Thu
Fri
Sat
Sun
Time (days)
Electricity price (€/kWh)
0.6
0.4
0.2
0
Mon
Tue
Wed
Thu
Fri
Sat
Sun
Time (days)

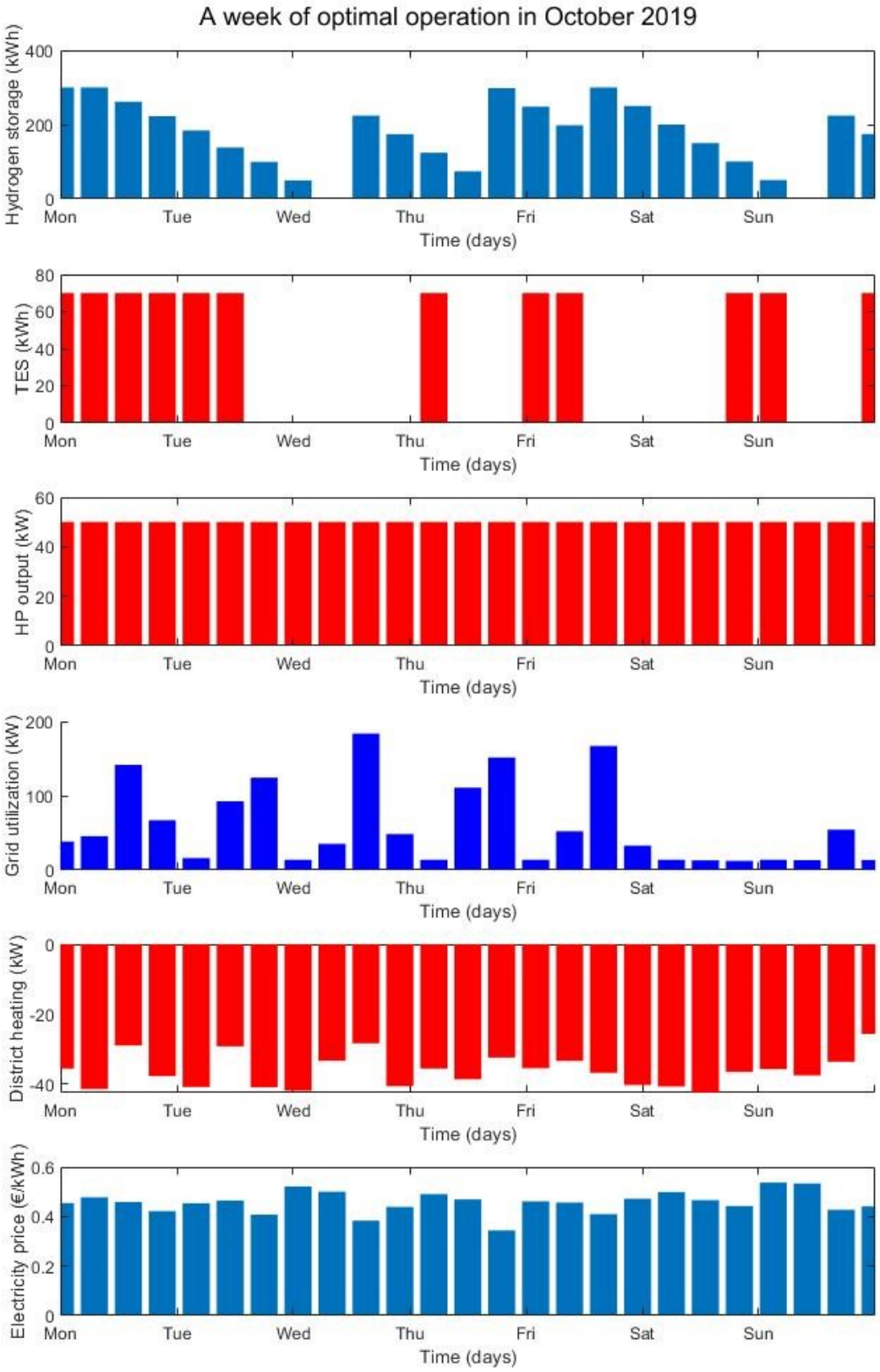
A week of optimal operation in October 2019
Hydrogen storage (kWh)
400
200
0
Mon
Tue
Wed
Thu
Fri
Sat
Sun
Time (days)
TES (kWh)
80
60
40
20
0
Mon
Tue
Wed
Thu
Fri
Sat
Sun
Time (days)
HP output (kW)
60
40
20
0
Mon
Tue
Wed
Thu
Fri
Sat
Sun
Time (days)
Grid utilization (kW)
200
100
0
Mon
Tue
Wed
Thu
Fri
Sat
Sun
Time (days)
District heating (kW)
0
-20
-40
Mon
Tue
Wed
Thu
Fri
Sat
Sun
Time (days)
Electricity price (€/kWh)
0.6
0.4
0.2
0
Mon
Tue
Wed
Thu
Fri
Sat
Sun
Time (days)

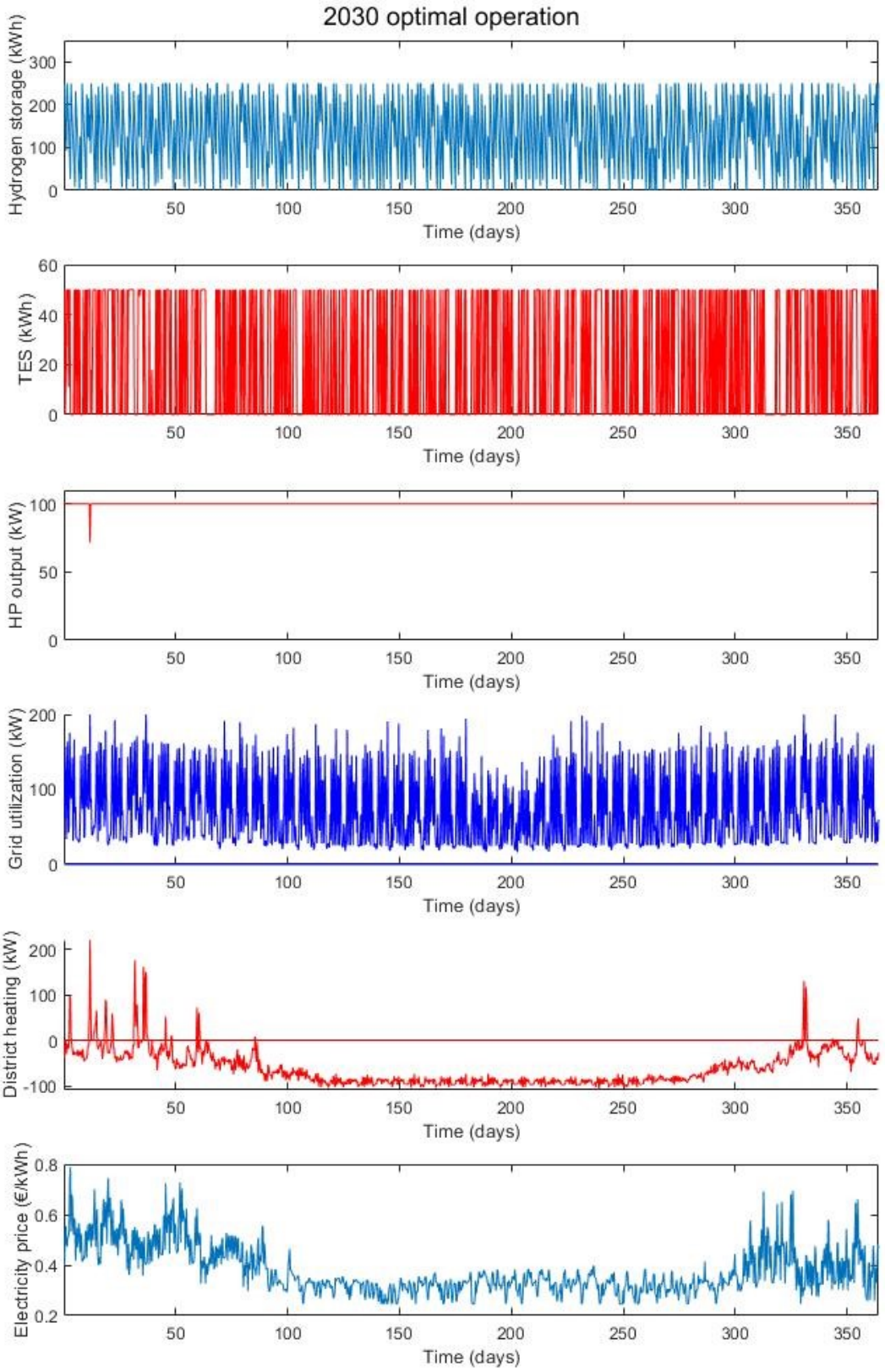
2030 optimal operation
Hydrogen storage (kWh)
TES (kWh)
HP output (kW)
Grid utilization (kW)
District heating (kW)
Electricity price (€/kWh)
Time (days)

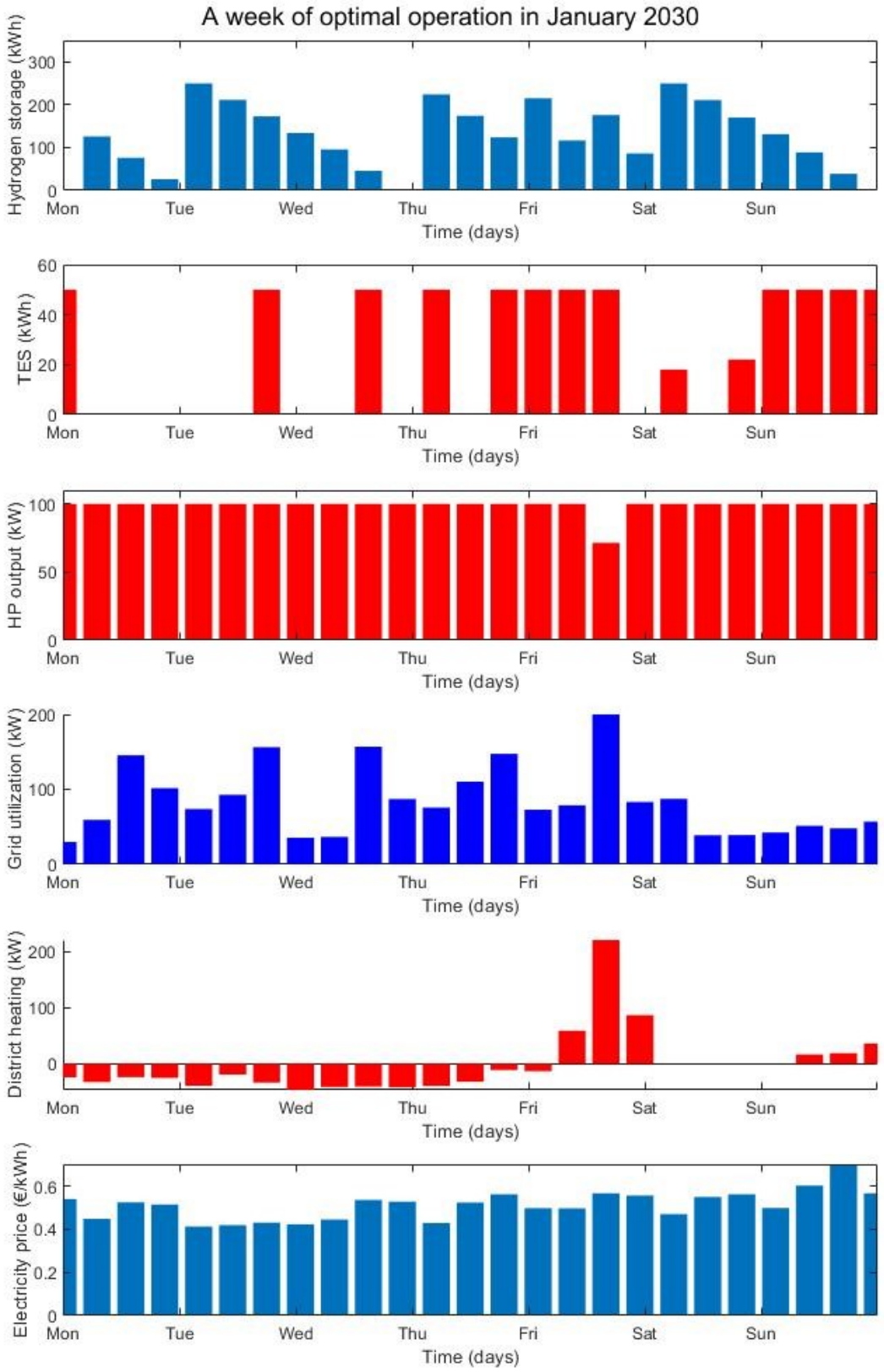
A week of optimal operation in January 2030
Hydrogen storage (kWh)
0
100
200
300
Mon
Tue
Wed
Thu
Fri
Sat
Sun
Time (days)
TES (kWh)
0
20
40
60
Mon
Tue
Wed
Thu
Fri
Sat
Sun
Time (days)
HP output (kW)
0
50
100
Mon
Tue
Wed
Thu
Fri
Sat
Sun
Time (days)
Grid utilization (kW)
0
100
200
Mon
Tue
Wed
Thu
Fri
Sat
Sun
Time (days)
District heating (kW)
0
100
200
Mon
Tue
Wed
Thu
Fri
Sat
Sun
Time (days)
Electricity price (€/kWh)
0
0.2
0.4
0.6
Mon
Tue
Wed
Thu
Fri
Sat
Sun
Time (days)

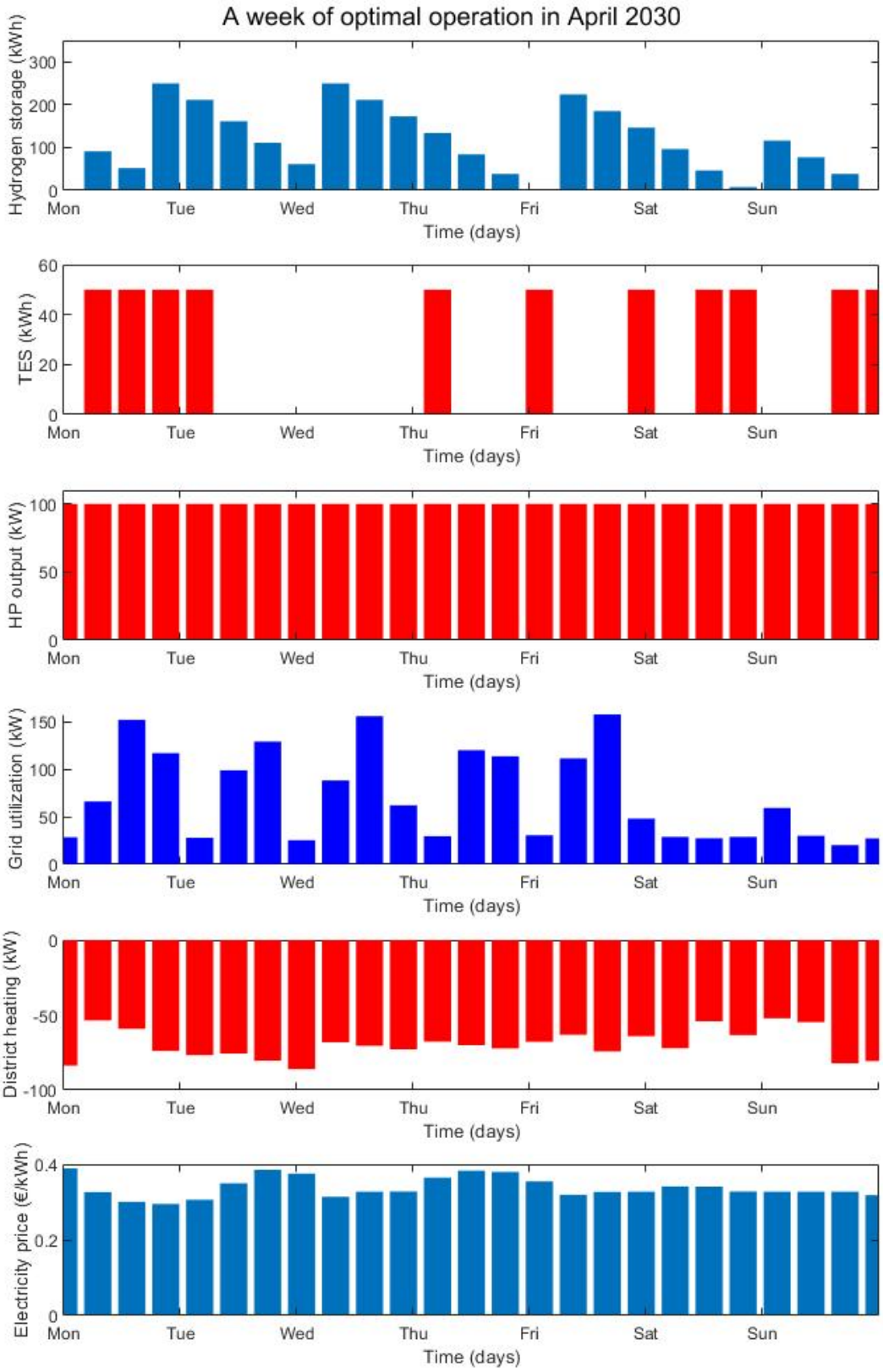
A week of optimal operation in April 2030
Hydrogen storage (kWh)
0
100
200
300
Mon
Tue
Wed
Thu
Fri
Sat
Sun
Time (days)
TES (kWh)
0
20
40
60
Mon
Tue
Wed
Thu
Fri
Sat
Sun
Time (days)
HP output (kW)
0
50
100
Mon
Tue
Wed
Thu
Fri
Sat
Sun
Time (days)
Grid utilization (kW)
0
50
100
150
Mon
Tue
Wed
Thu
Fri
Sat
Sun
Time (days)
District heating (kW)
0
-50
-100
Mon
Tue
Wed
Thu
Fri
Sat
Sun
Time (days)
Electricity price (€/kWh)
0
0.2
0.4
Mon
Tue
Wed
Thu
Fri
Sat
Sun
Time (days)

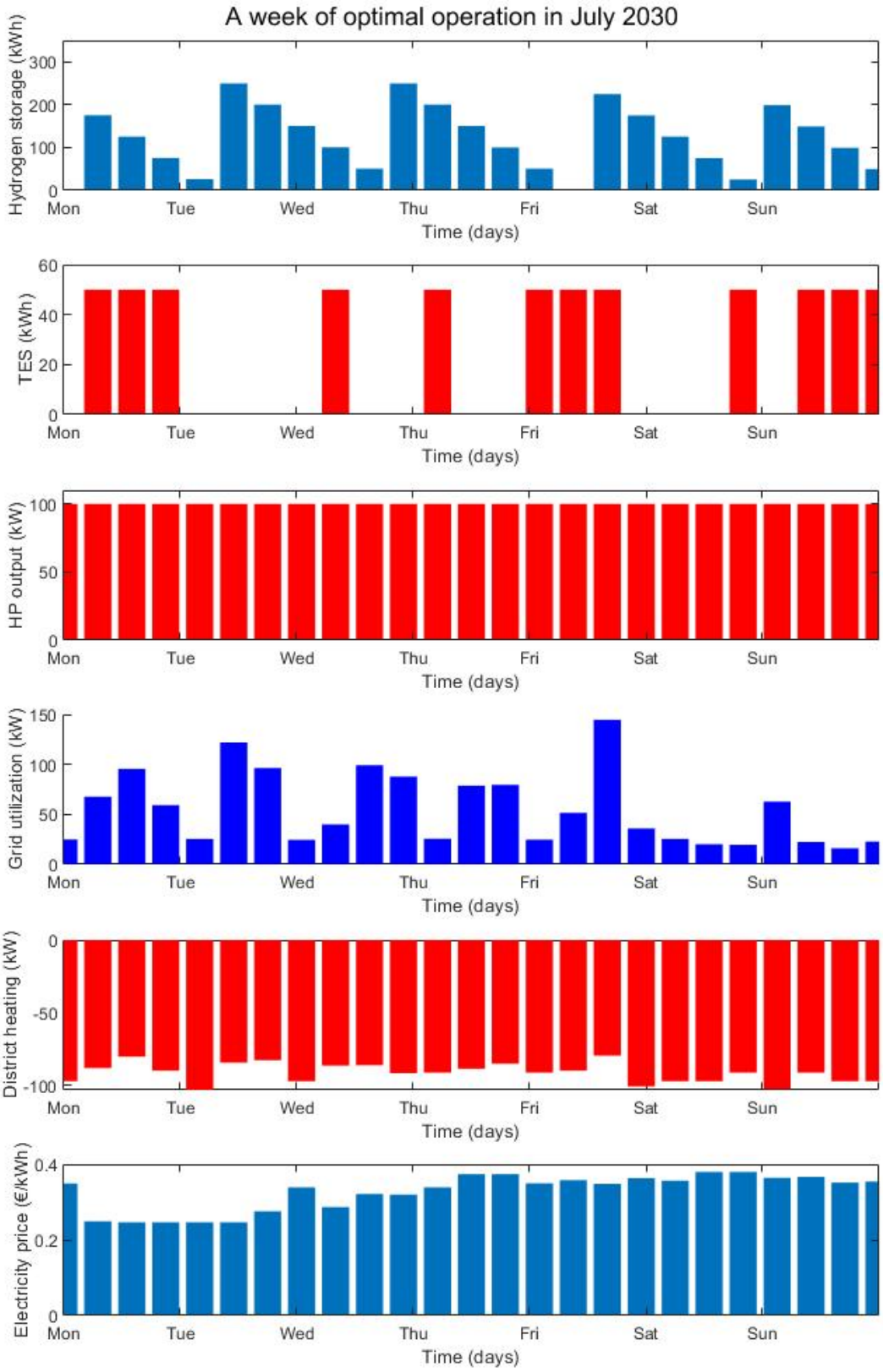
A week of optimal operation in July 2030
Hydrogen storage (kWh)
0
100
200
300
Mon
Tue
Wed
Thu
Fri
Sat
Sun
Time (days)
TES (kWh)
0
20
40
60
Mon
Tue
Wed
Thu
Fri
Sat
Sun
Time (days)
HP output (kW)
0
50
100
Mon
Tue
Wed
Thu
Fri
Sat
Sun
Time (days)
Grid utilization (kW)
0
50
100
150
Mon
Tue
Wed
Thu
Fri
Sat
Sun
Time (days)
District heating (kW)
0
-50
-100
Mon
Tue
Wed
Thu
Fri
Sat
Sun
Time (days)
Electricity price (€/kWh)
0
0.2
0.4
Mon
Tue
Wed
Thu
Fri
Sat
Sun
Time (days)

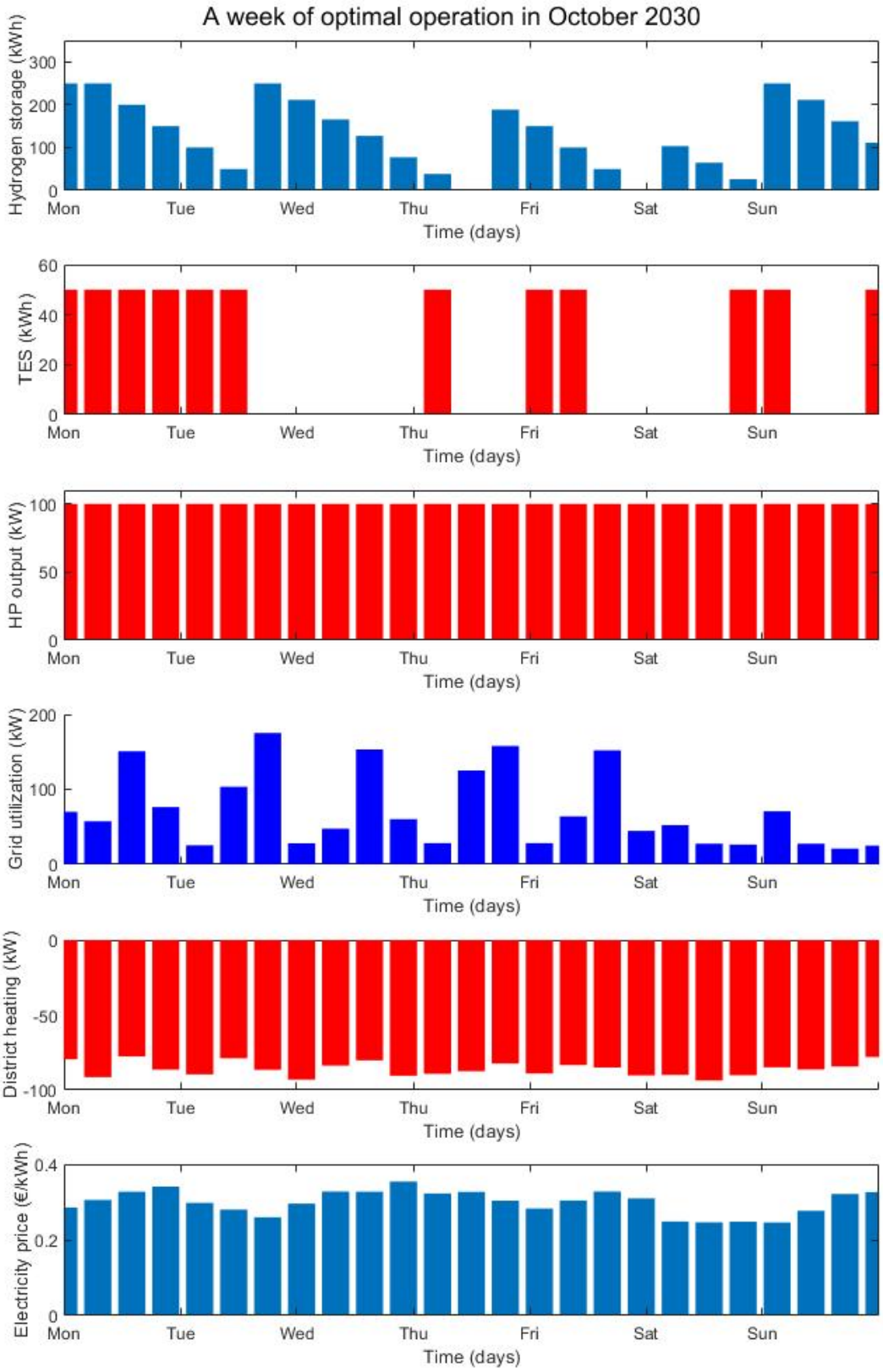
A week of optimal operation in October 2030
Hydrogen storage (kWh)
300
200
100
0
Mon
Tue
Wed
Thu
Fri
Sat
Sun
Time (days)
TES (kWh)
60
40
20
0
Mon
Tue
Wed
Thu
Fri
Sat
Sun
Time (days)
HP output (kW)
100
50
0
Mon
Tue
Wed
Thu
Fri
Sat
Sun
Time (days)
Grid utilization (kW)
200
100
0
Mon
Tue
Wed
Thu
Fri
Sat
Sun
Time (days)
District heating (kW)
0
-50
-100
Mon
Tue
Wed
Thu
Fri
Sat
Sun
Time (days)
Electricity price (€/kWh)
0.4
0.2
0
Mon
Tue
Wed
Thu
Fri
Sat
Sun
Time (days)

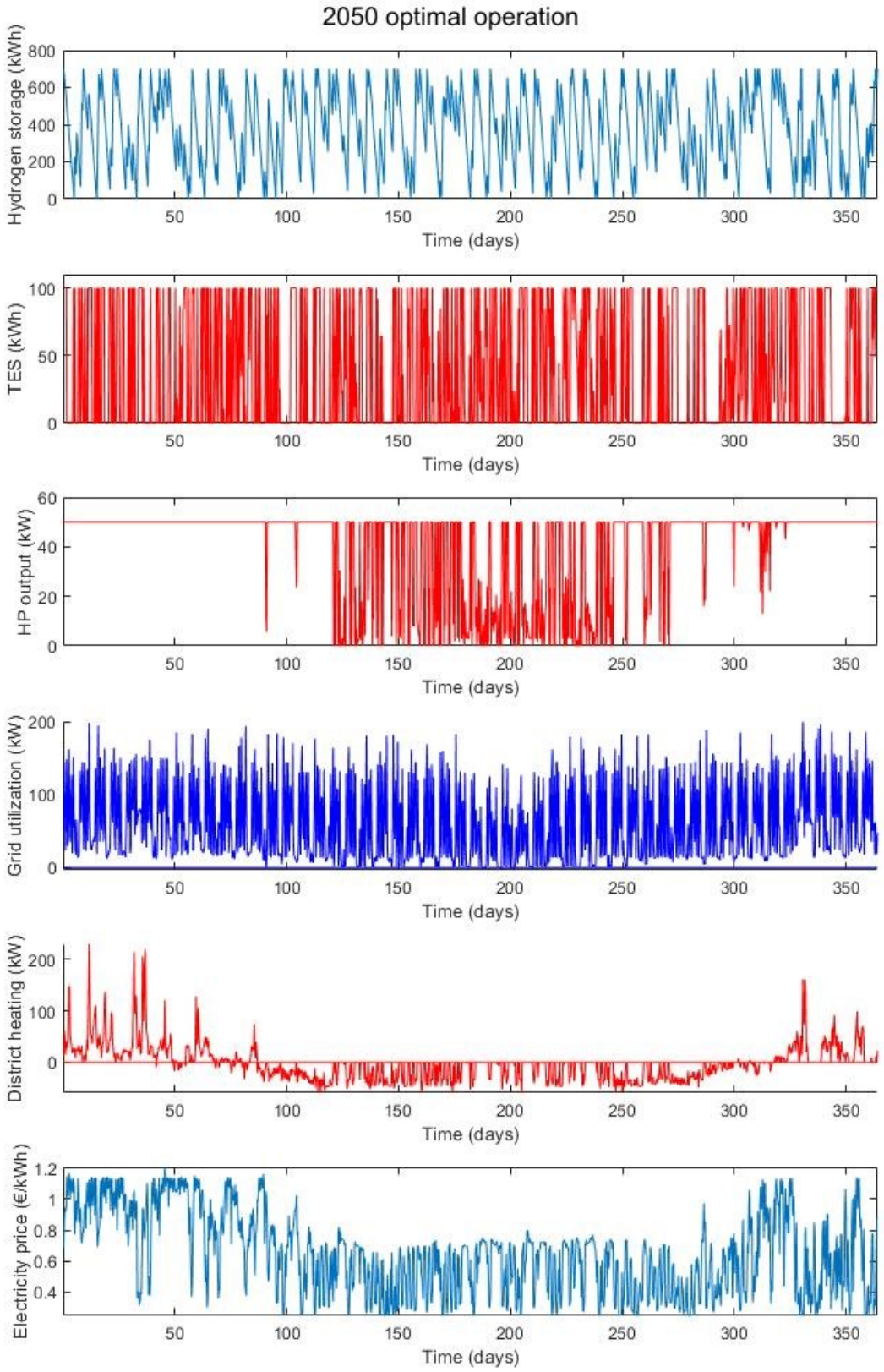
2050 optimal operation
Hydrogen storage (kWh)
0
200
400
600
800
50
100
150
200
250
300
350
Time (days)
TES (kWh)
0
50
100
Time (days)
HP output (kW)
0
20
40
60
Time (days)
Grid utilization (kW)
0
100
200
Time (days)
District heating (kW)
0
100
200
Time (days)
Electricity price (€/kWh)
0.4
0.6
0.8
1
1.2
Time (days)

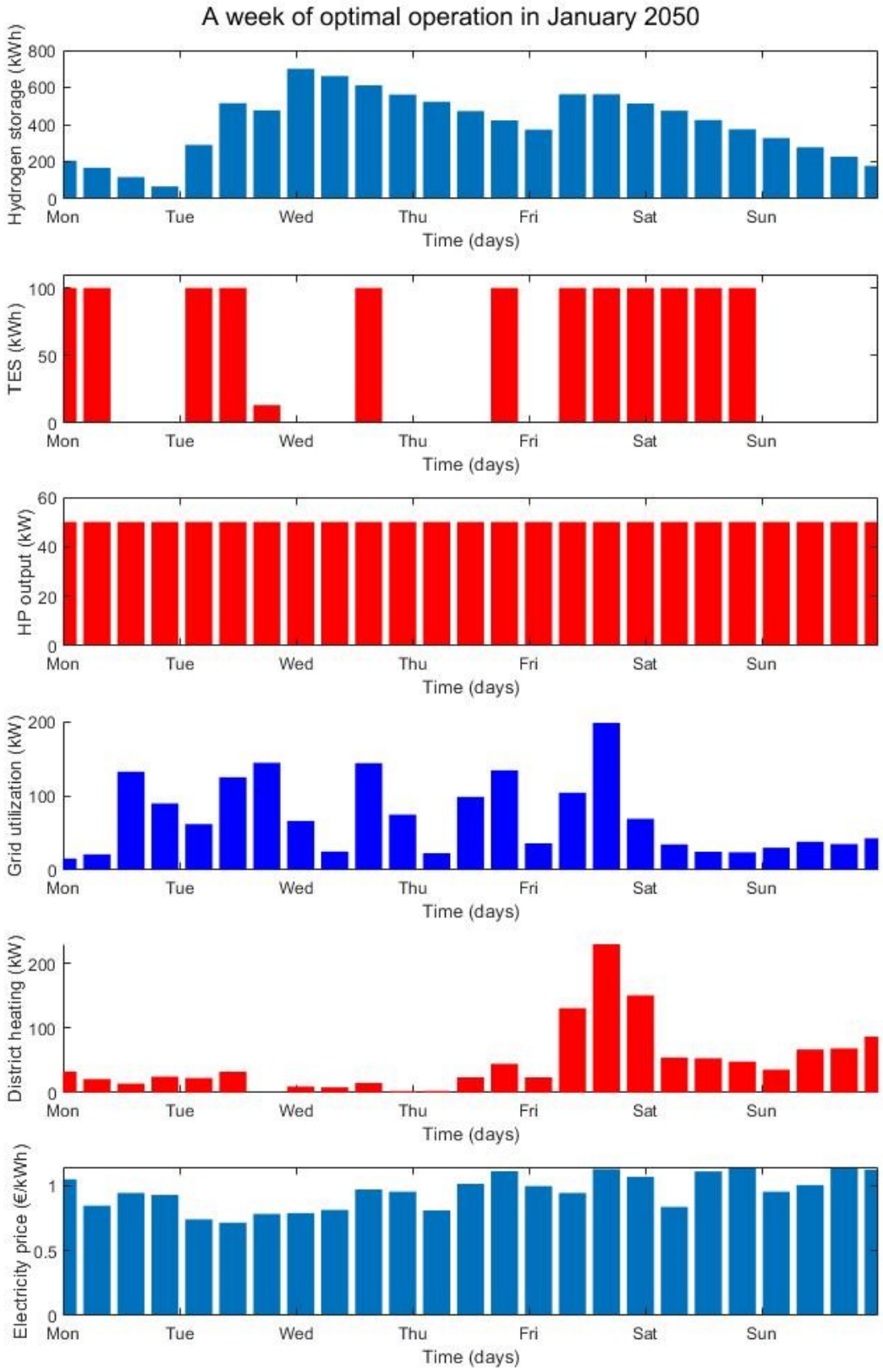
A week of optimal operation in January 2050
Hydrogen storage (kWh)
0
200
400
600
800
Mon
Tue
Wed
Thu
Fri
Sat
Sun
Time (days)
TES (kWh)
0
50
100
Mon
Tue
Wed
Thu
Fri
Sat
Sun
Time (days)
HP output (kW)
0
20
40
60
Mon
Tue
Wed
Thu
Fri
Sat
Sun
Time (days)
Grid utilization (kW)
0
100
200
Mon
Tue
Wed
Thu
Fri
Sat
Sun
Time (days)
District heating (kW)
0
100
200
Mon
Tue
Wed
Thu
Fri
Sat
Sun
Time (days)
Electricity price (€/kWh)
0
0.5
1
Mon
Tue
Wed
Thu
Fri
Sat
Sun
Time (days)

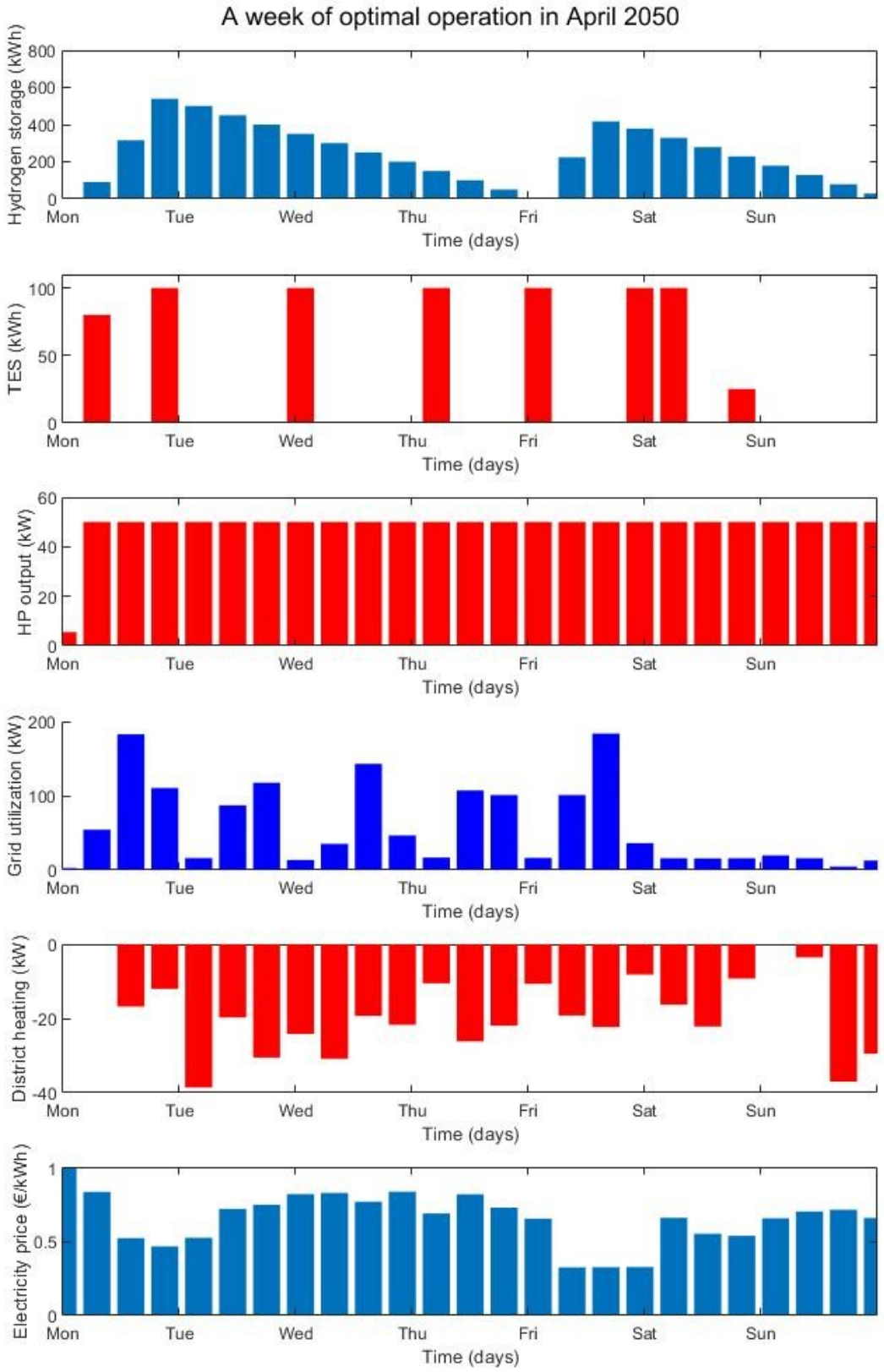
A week of optimal operation in April 2050
Hydrogen storage (kWh)
800
600
400
200
0
Mon
Tue
Wed
Thu
Fri
Sat
Sun
Time (days)
TES (kWh)
100
50
0
Mon
Tue
Wed
Thu
Fri
Sat
Sun
Time (days)
HP output (kW)
60
40
20
0
Mon
Tue
Wed
Thu
Fri
Sat
Sun
Time (days)
Grid utilization (kW)
200
100
0
Mon
Tue
Wed
Thu
Fri
Sat
Sun
Time (days)
District heating (kW)
0
-20
-40
Mon
Tue
Wed
Thu
Fri
Sat
Sun
Time (days)
Electricity price (€/kWh)
1
0.5
0
Mon
Tue
Wed
Thu
Fri
Sat
Sun
Time (days)

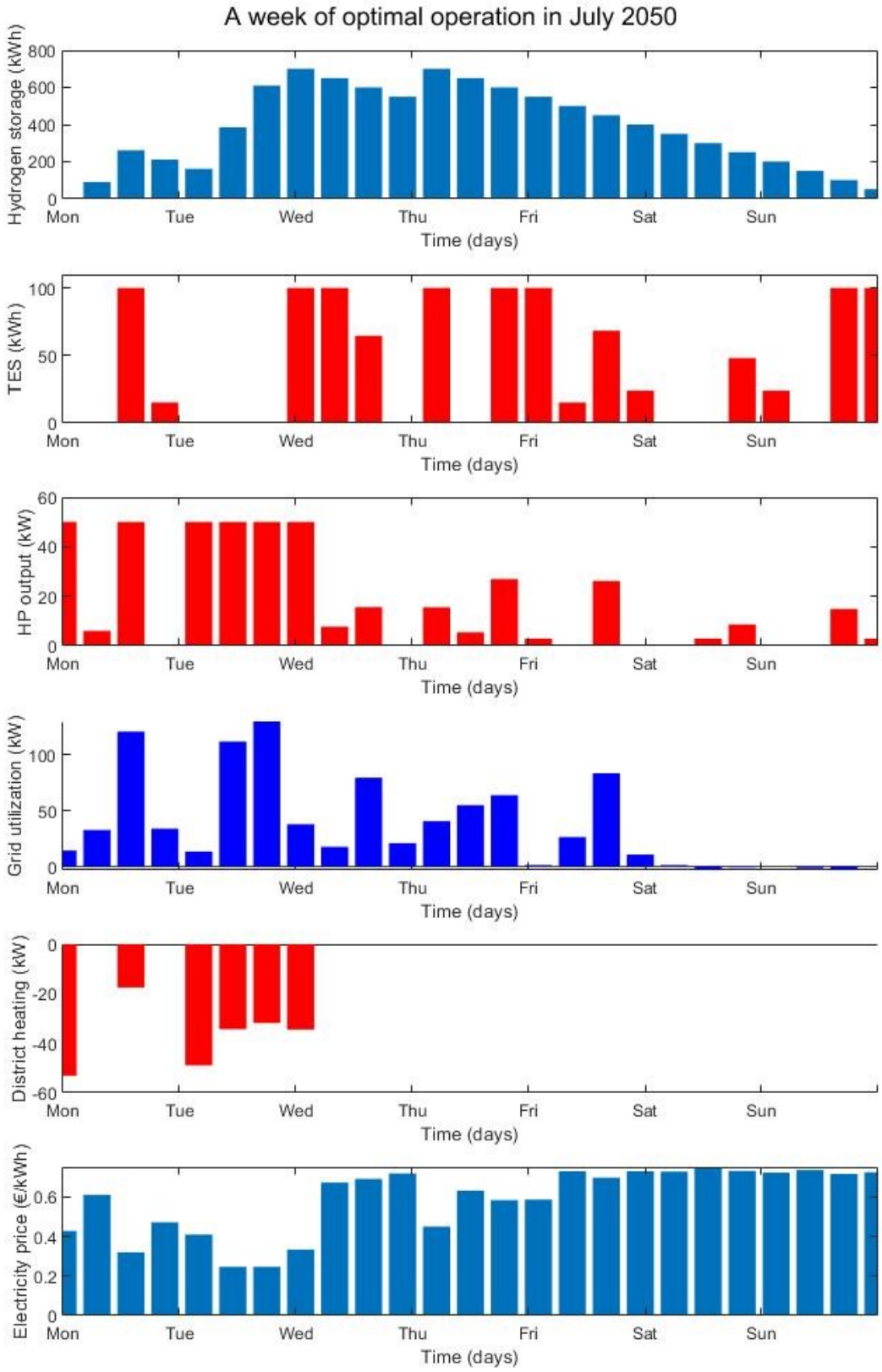
A week of optimal operation in July 2050
Hydrogen storage (kWh)
800
600
400
200
0
Mon
Tue
Wed
Thu
Fri
Sat
Sun
Time (days)
TES (kWh)
100
50
0
Mon
Tue
Wed
Thu
Fri
Sat
Sun
Time (days)
HP output (kW)
60
40
20
0
Mon
Tue
Wed
Thu
Fri
Sat
Sun
Time (days)
Grid utilization (kW)
100
50
0
Mon
Tue
Wed
Thu
Fri
Sat
Sun
Time (days)
District heating (kW)
0
-20
-40
-60
Mon
Tue
Wed
Thu
Fri
Sat
Sun
Time (days)
Electricity price (€/kWh)
0.6
0.4
0.2
0
Mon
Tue
Wed
Thu
Fri
Sat
Sun
Time (days)

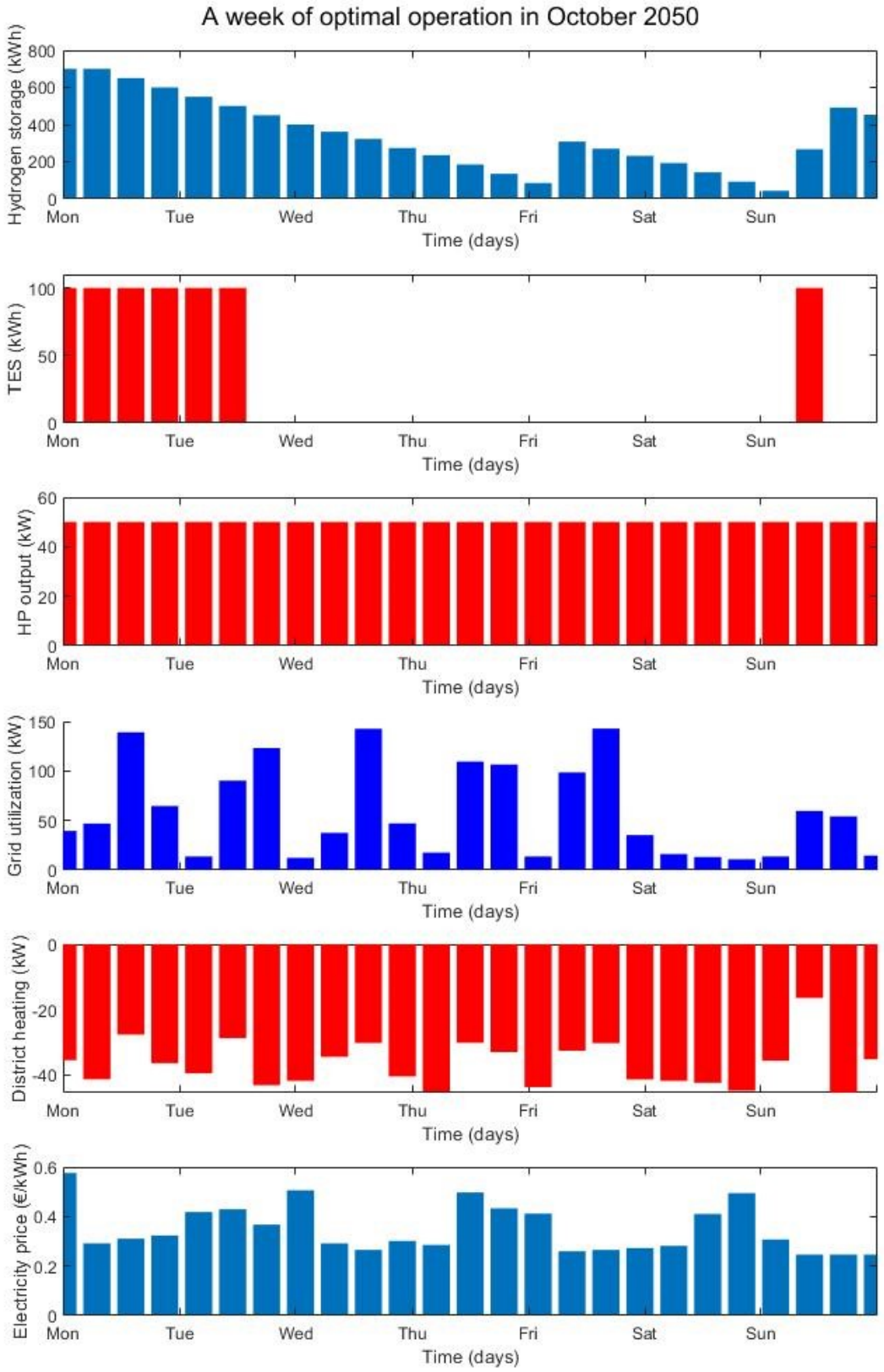
A week of optimal operation in October 2050
Hydrogen storage (kWh)
800
600
400
200
0
Mon
Tue
Wed
Thu
Fri
Sat
Sun
Time (days)
TES (kWh)
100
50
0
Mon
Tue
Wed
Thu
Fri
Sat
Sun
Time (days)
HP output (kW)
60
40
20
0
Mon
Tue
Wed
Thu
Fri
Sat
Sun
Time (days)
Grid utilization (kW)
150
100
50
0
Mon
Tue
Wed
Thu
Fri
Sat
Sun
Time (days)
District heating (kW)
0
-20
-40
Mon
Tue
Wed
Thu
Fri
Sat
Sun
Time (days)
Electricity price (€/kWh)
0.6
0.4
0.2
0
Mon
Tue
Wed
Thu
Fri
Sat
Sun
Time (days)